Republic of Iraq
Ministry of Higher Education
and Scientific Research
University of Babylon
College of Engineering
Mechanical Engineering Department

Static and Free Vibration Analysis of Functionally Graded Materials using Modified Couple Stress Theory

A Thesis

Submitted to the College of Engineering / University of Babylon

in Partial Fulfillment of the Requirements for the Degree of

Master of Science in Engineering/ Mechanical Engineering / Applied

By

Duaa Mohammed Ridha Mohsin

Supervised by

Asst. Prof. Dr. Mohammed Ali Saihood

2021 A.D. **1442 A.H.**

بسم الله الرحمن الرحيم

اقْرَأْ بِاسْمِ رَبِّكَ الَّذِي خَلَقَ ﴿١﴾ خَلَقَ الْإِنسَانَ مِنْ عَلَقٍ
﴿٢﴾ اقْرَأْ وَرَبُّكَ الْأَكْرَمُ ﴿٣﴾ الَّذِي عَلَّمَ بِالْقَلَمِ ﴿٤﴾
عَلَّمَ الْإِنسَانَ مَا لَمْ يَعْلَمْ ﴿٥﴾

صدق الله العلي العظيم

سورة العلق

Supervisor Certification

I certify that this thesis entitled "**Static and Free Vibration Analysis of Functionally Graded Materials using Modified Couple Stress Theory"** was prepared by **Duaa Mohammed Ridha ….** Under my supervision at the University of Babylon in partial fulfillment of the requirements for the degree of Master of Science in Mechanical Engineering -Applied.

I recommend that this thesis be forwarded for examination following the regulation of the University of Babylon.

Signature:

Supervisor Name: Asst. Prof. Dr. Mohammed Ali Saihood Al-Shujairi

Date: / /2022

Dedication

To my dear family

The reason for what I become today

Thanks for your great support and continuous care

Duaa

Acknowledgement

Praise is to Almighty God who has been helped me in completing this dissertation, and prayers and peace be upon his beloved Mustafa Mohammad and pure family.

I want to express my deep thanks and gratitude to my supervisor Asst. Prof. Dr. Mohammed Ali Al-Shujairi, for his valuable guidance and encouragement during the development of my work.

I want to thank the dean of the College of Engineering, Prof. Dr. Hatim Al-Tai, and the boss of the Mechanical Department, Asst. Prof. Dr. Samer Mohammed, for their attention through the study period.

I want to thank all of my teachers at the College of Mechanical Engineering, whom I have taken from them the sciences engineering via all the stages of studying.

I want to thank all the employees who worked to provide the best services for the college.

I want to thank all of my colleagues for their help during my graduate studies.

Finally, I would like to thank my family for their support and encouragement to me at every moment when I felt frustrated and weak. Their love for me was the energy that shipped me throughout the study.

Duaa

Abstract

Functionally gradient materials are a promising new class of microstructures. The mechanical properties of functionally graded microstructures change depending on a change in the spatial dimension of the structure. Recent advances in manufacturing techniques, such as powder metallurgy, have made it possible to adapt the mechanical properties of structures on a small scale by making them from a multilayer functional mixture of two or more materials.

The governing equations and boundary conditions are simplified by Hamilton's principle, the Euler-Bernoulli beam theory, and the first-order shear deformation theory. It is solved numerically by the method of Lagrangian multiples. The Matlab program was relied on to find the results. The mechanical properties of the functionally graded structures were studied by the ruling mixture method and the Mori Tanaka technique.

Several factors influence the three models of microbeam functional grading, namely: rule of mixtures index, porosity volume fraction, porosity distribution types (FGM-I, and FGM-II), carbon nanotube volume fraction, and types of nanotube functional grading distributions. These are (FG-X), (UD), (FG-V), and (FG-O), aspect ratio, and different boundary conditions. In general, when the concept of functional grading is used in the design of the microstructure of composite materials, it has shown an improvement in mechanical performance.

The following points were reached from the study of the three models as follows: Increasing the index of the rule of mixtures will decrease the

rigidity of the functionally graded fine beam composed of ceramic and metal, which leads to an increase in the deflection and a decrease in the natural frequency. whereas the static deflection and normal frequency of the second model of functionally graded porosity materials have different behaviors that depend on the rule index of mixtures. Moreover, the microbeam of functionally graded type carbon nanotubes (FG-X) has the maximum natural frequency, while FG-O has the lowest natural frequency. The modified couple stress theory (MCST) can predict the smallest static deflection and the largest free vibration of the functionally graded microbeam depending on the material length scale parameter when compared to the classical beam theory (CBT) prediction. Comparative results with previous studies were acceptable. The results of this investigation can be used to design and improve precision machines and microsystems.

Contents

List of Abbreviations

A Symbol	Description
AFGM	Axially Functionally graded material
CBT	Classical beam theory
EBBT	Euler–Bernoulli beam theory
FGM	Functionally graded material
FGPM	Functionally graded porosity material
FSDT	First-order shear deformation beam theory
HSDT	Higher-order shear deformation beam theory
LMM	Lagrange multiplier method
MCST	Modified couple stress theory
SWCNTRC	Single-walled carbon nanotubes reinforced composited
SWCNTs	Single-walled carbon nanotubes.
TBT	Timoshenko beam theory

List of Symbols

a. Alphabet Symbols

Symbol	Meaning	Unit
V_c	Ceramic constituent	%
V_m	Metal constituent	
V_{CNT}, V_m	The volume fraction of carbon nanotube and polymer matrix, respectively.	
E	"Young's modulus"; modulus of elasticity	pa,
G	Shear modulus	
K_e	Effective Bulk Modulus	
G_e	Effective Shear Modulus	
E_{11}^{CNT}, E^m	Elastic moduli for CNT and matrix (polymer), respectively.	
σ_{xx}	Classical stress	
σ_{xz}	Shear stress	
E_k	Kinetic energy	J,N.m
E_s	Strain energy	
E_w	Work done of externally applied forces.	
u,w	Axial displacement and transverse	m
b	Width	
h	Hight, Thickness	
l_m	The material length scale parameter	
L/h	Slenderness ratio, aspect ratio,	-
f	Power law index	-
N	Number of a grid point	

b. Greek Symbols

Symbol	Meaning	Unit
ν	Poisson's ratio	/
ν^{CNT}, ν^{m}	Poisson's ratios of carbon nanotube and polymer matrix, respectively.	
ρ^{CNT}, ρ^{m}	mass densities of carbon nanotube and matrix, respectively.	Kg/m^3
η_i	efficiency parameters of carbon nanotube	/
α	porosity volume fraction index	
ϕ	Total bending rotation of the cross-sections	/
$\boldsymbol{\Theta}$	components of the rotation vector.	/

c. Super subscript

Symbol	Meaning
m	Metal, Matrix
c	Ceramic
cnt	Carbon nanotube

INTRODUCTION

1.1 Functionally graded materials (FGMs)

Functionally graded materials (FGMs) are non-homogeneous composite materials made up of two or more elements; the composition varies continuously and smoothly along a specific direction (length or thickness). The mechanical properties of FGM are more effective in structural design compared to pure homogeneous materials or traditional composite materials. Functionally graded materials have been found in nature (flora and fauna) as bamboo stems, shells, bones, and teeth. As shown in Figure (1.1) [1].

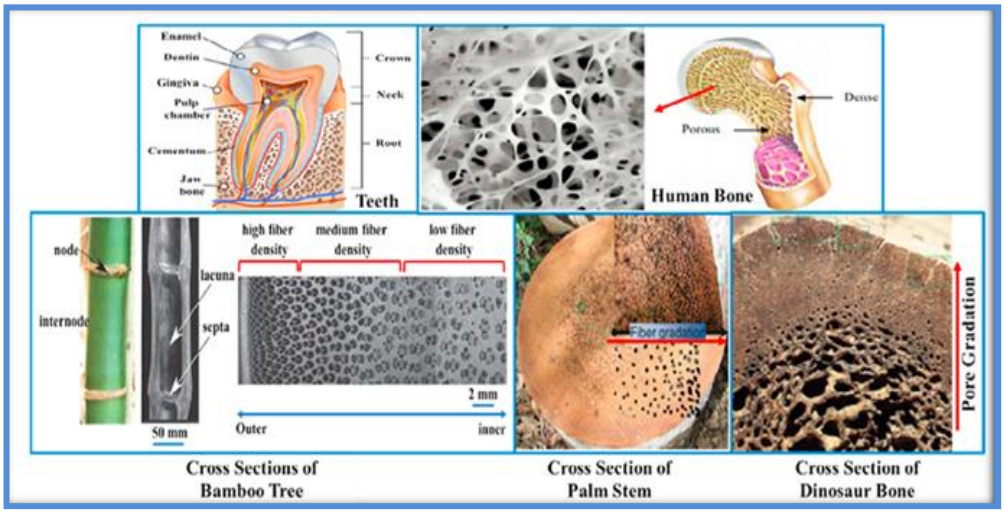

Figure 1. 1: Several examples of FGMs in natural [1]

The traditional composite materials are separated into their original elements due to the thermal expansion coefficients of the original elements by a phenomenon known as delamination. Thus scientists are interested in finding a solution to the poor performance of composite materials for industrial applications under extreme conditions.

In 1984 researchers in Japan made a thermal barrier represented by a coating made of a composite material with a thickness of 10 mm that reduces the temperature from 2000 Kelvin to 1000 Kelvin. This adaptation is replacing sharp interfaces with a gradient interface that smooth's the transition from one material to another and eliminates stress concentrations compared to composite materials.[2]

The majority of the studies used FG ceramic-metal materials to investigate the mechanical and thermal characteristics of graded constructions; ceramic decreases high heat and corrosion, while metal protects materials from cracking when subjected to heat stress. [3]. The behavior of both conventional composites and FGM composites is illustrated in Figure (1.2).

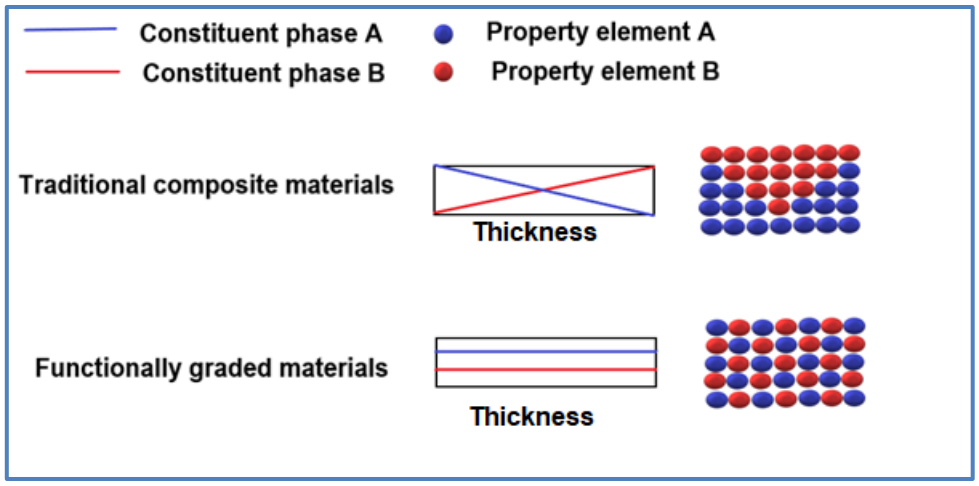

Figure 1. 2: Variation of FGMs and traditional composites, - *Ref **[3]** modified*

1.2 Applications of Functionally Graded Materials

Thirty years later, FGMs have garnered significant attention due to their new thermo mechanical properties that enable them to be used in a wide variety of applications across a variety of sectors as shown below. With the advancement of material science, a new field of application for FGMs

has emerged: micro–electro–mechanical systems**[1]**.

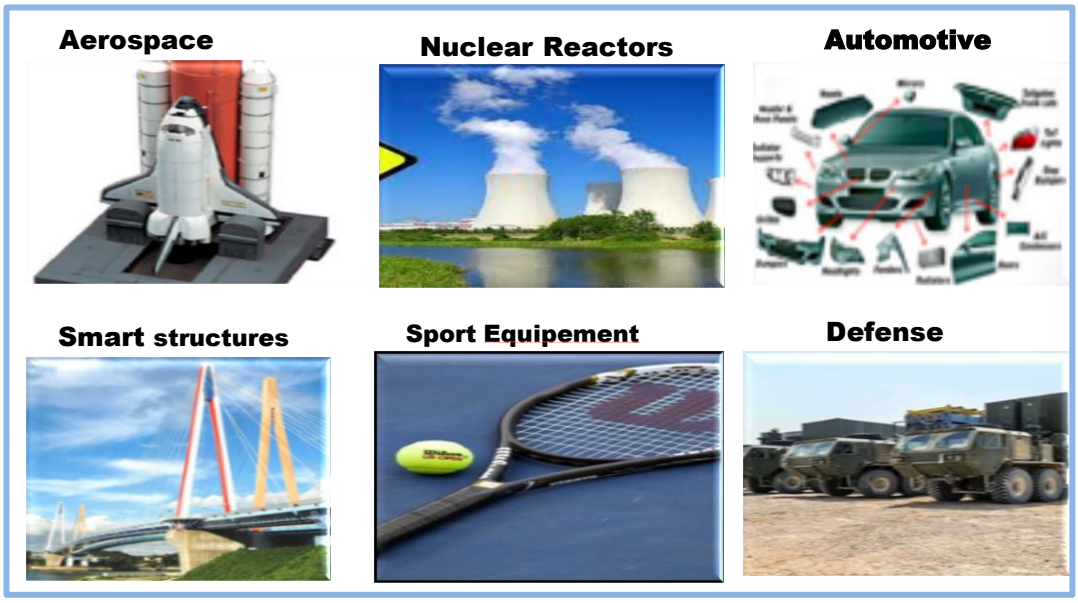

*Figure 1. 3: Application of FGM- Ref **[3]** modified*

Also, in biomedicine, a return to mimicry of nature is observed in the design of artificial neural networks through human brain simulation. **[2]** Also, parts of the human body such as muscle tendons and a gradient design of the prosthetic arm and intervertebral disc [4] are shown in Figure**(1.4).**

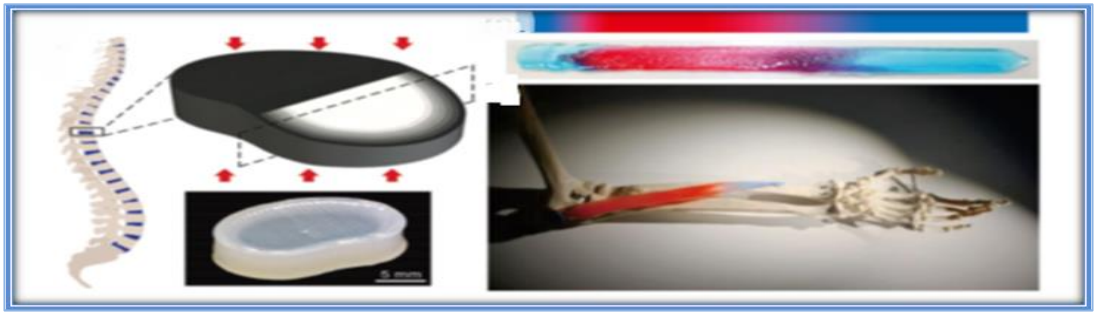

Figure 1. 4: Application fields of functionally graded material-Ref. **[4]** *modified.*

1.3 Manufacture of Functionally Graded Materials (FGM)

FGM manufacturing techniques: powder metallurgy is an example of FGM preparations. Figure (1.5) summarizes the stages involved in prepping FGM for various production methods.

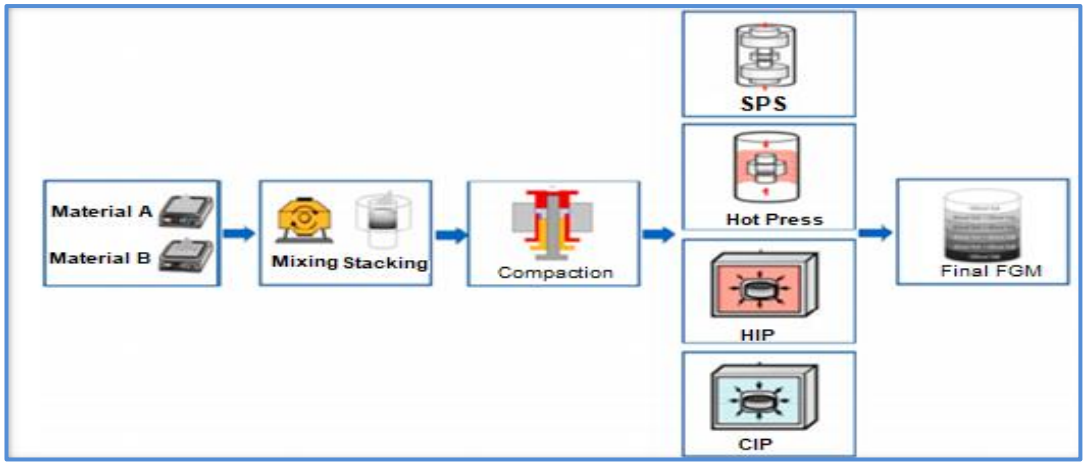

(a) Powder metallurgy (PM) [1]

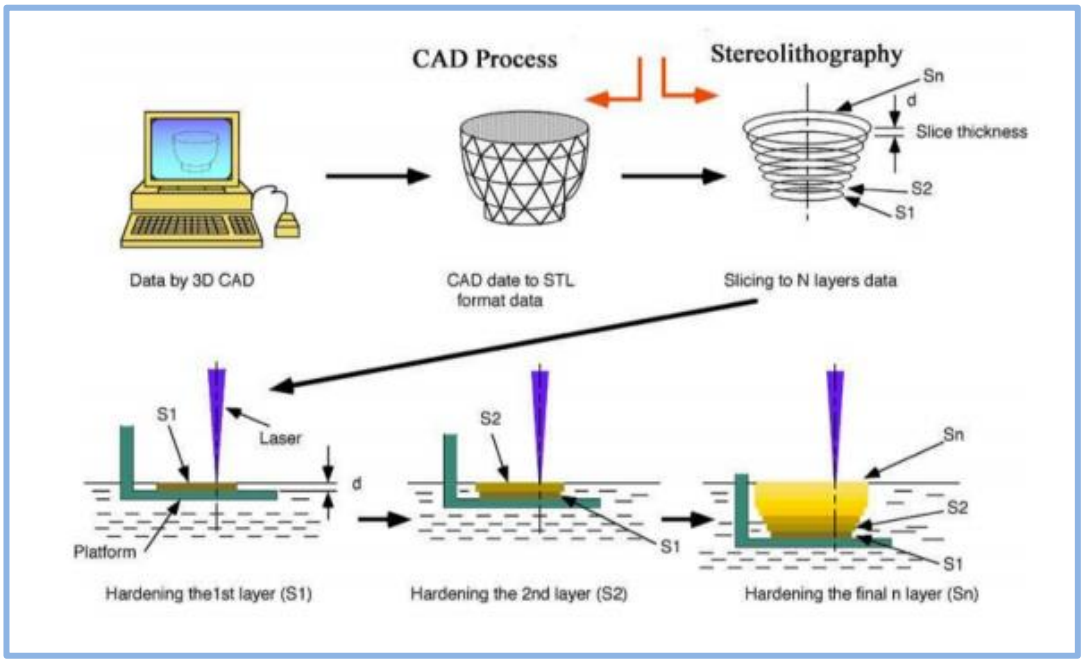

(b) Fused deposition modeling (FDM) [3].

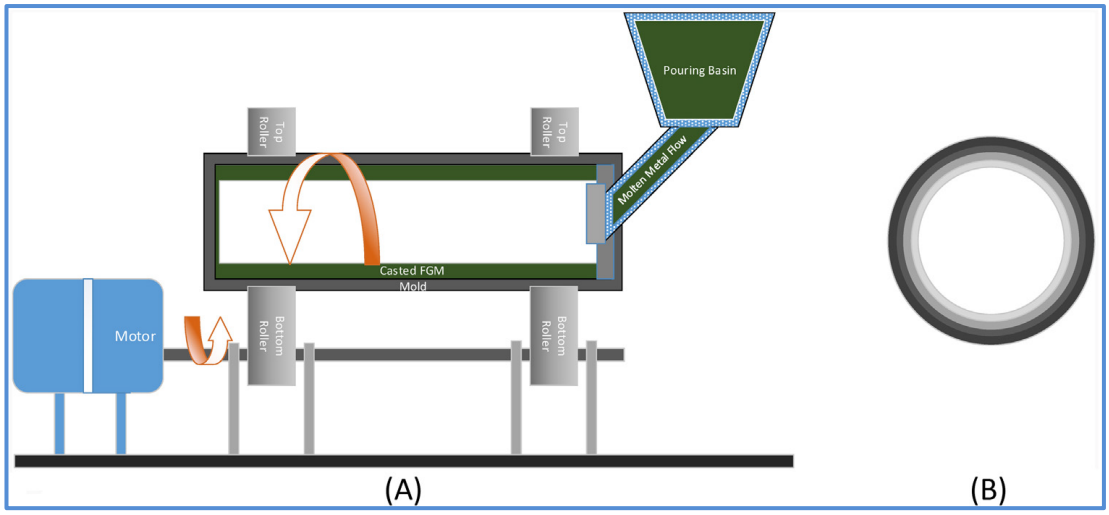

(c) Centrifugal casting method[5]

Figure 1. 5: Multiple Methods of Producing FGM

1.4 The porosity of functionally graded materials

Porosity is defined as the ratio of pore volume to total volume [6]. Porosity is found in structural materials (beam and shells) as the result of faulty manufacturing, Porosity has represented a challenge in as widespread structural design for many years.[7]

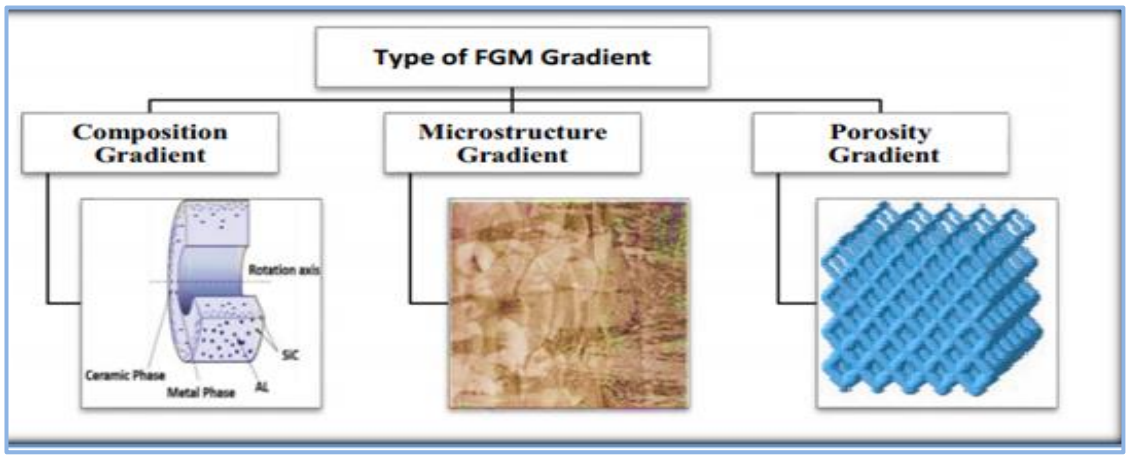

Figure 1. 6: Classification of FGM -Ref.[3], modified

The porosity exists as a result of an error accompanying the production of FGM. There are small voids or pores inside the FG-material, resulting from the significant temperature difference during sintering. Porosity exists as air bubbles during the dissolution of a matrix or water vapor concentrated on the surface of the body structure. [8]

Recently, constructions have included porosity using the concept of functional gradation of the pores. Researchers are interested in developing a porous material that maintains a high level of strength; porous materials have several desirable qualities, including high impact energy absorption capacity and a lightweight structure. As a result, it is an excellent option for a wide variety of current engineering applications in aerospace, automotive, and civil engineering, including innovative energy absorption systems, thermal barrier systems, and lightweight construction. [8][9]

The functionally graded of pores can be investigated in the **two models** as in figure (1.7): The **first** is a modified rule of mixture, which porosity as sub-function added to the rule of mixture. The addition of graded materials and porosity affects the mechanical properties of the structure, which is represented by Young's modulus, mass density, Poisson's ratio, and volume fractions. [10]**.**The **second model** is to study the mechanical behavior of porous materials according to a specific continuous function changing with the structure's thickness. In general, the pore distribution is either uniform (symmetric) or asymmetric. The thesis examines the porosity based on the first model**.** [11]

(a) First model

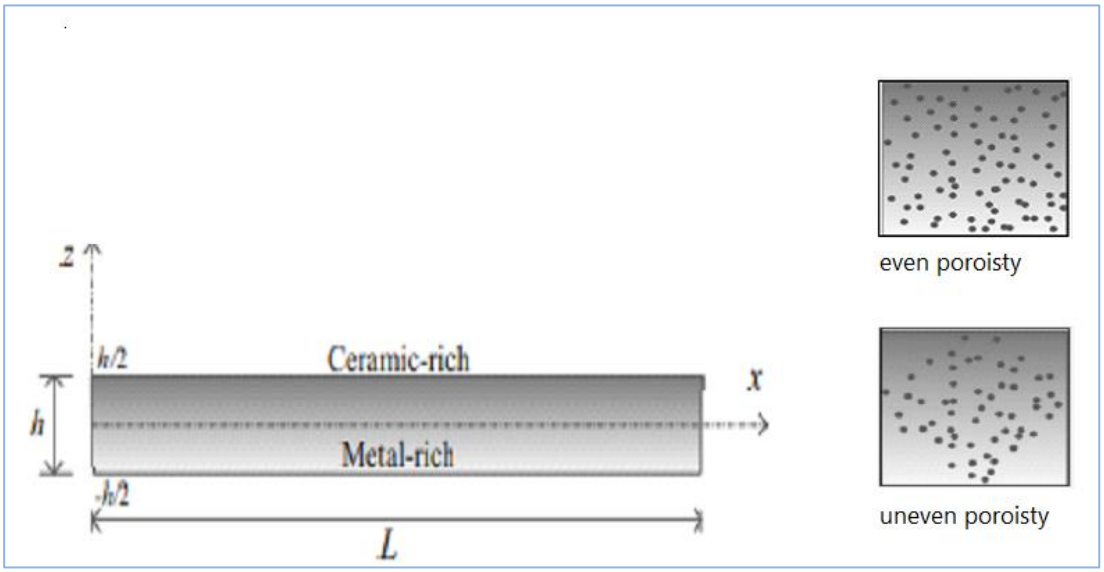

(b) *the Second model*

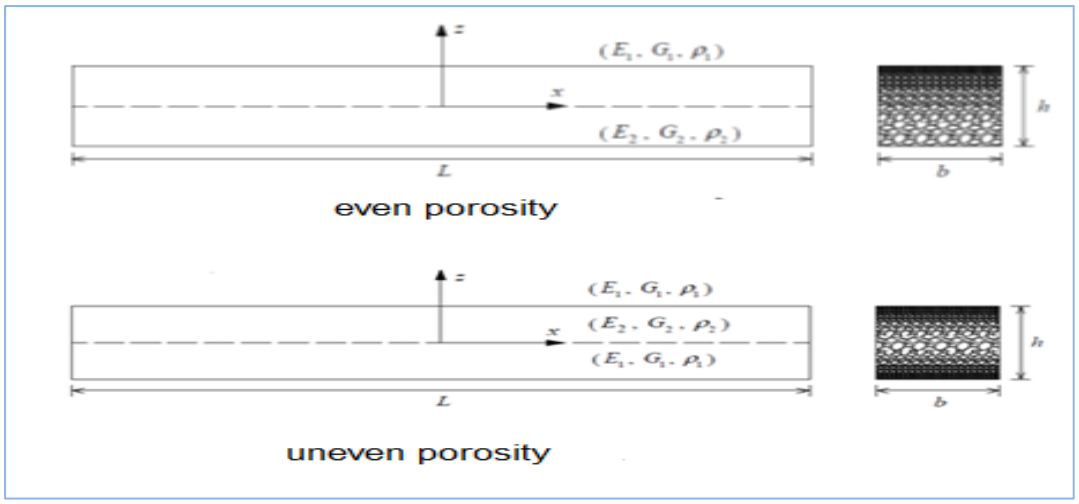

Figure 1. 7: models of functionally graded porous(Ref. [10],[11] modified)

1.5 Application of Functionally Graded Single-Walled Carbon nanotube-reinforced beam.

Iijima has been suggested a single-walled carbon nanotube (SWCNT) in 1993[12]. Characterize as has high compressive strength and toughness, as well as their high tensile stress, modulus of elasticity, light weight, resistance to torsion and sectional deformations, and slenderness ratio is

greater than 1000 .where micro- and nano-sized particles could be used to improve the characteristics of polymer composites. [13].

Shen[14] firstly has been proposed the usage of functionally graded of CNTs in the polymer. The performance of the polymer is increased by adding carbon nanotubes as reinforcements' structure. Consequently, their natural frequency and electrical conductivity are enhanced[15].

The performance of both micro-sensors and micro-actuators is an effective design when it is improved the lightweight micro-polymer by a reinforced carbon nanotube so it can measure high-frequency vibrations of machine structures. The applications of micro electromechanical system devices are shown in Figure (1.8). [16],[17]

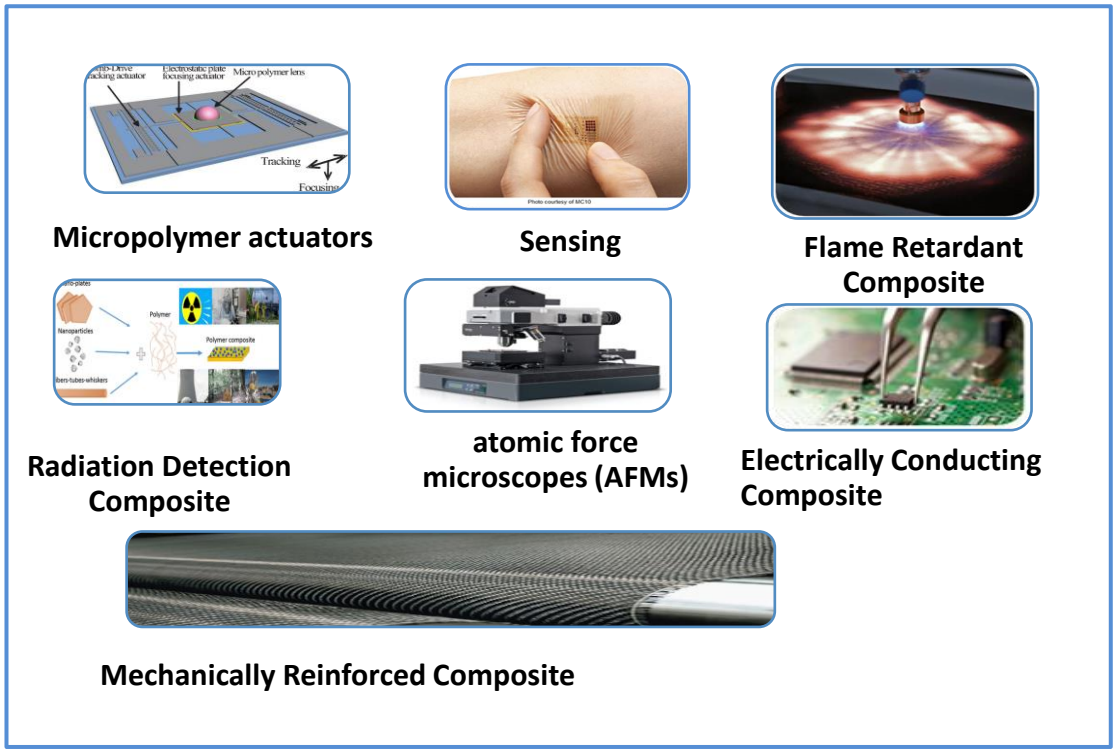

Figure 1. 8: application of CNT reinforcement in polymer composites

1.6 Objectives of the Present Work

The primary objective of this work is to investigate the static analysis and free vibration of three models of (functionally graded material), (functionally graded porosity), and (functionally graded single-walled carbon nanotubes) microbeams when subjected to uniform distribution load by using a modified couple stress theory based on the First-order shear deformation theory and the Euler Bernoulli beam theory. The objectives of the thesis will be:

1- Analyzing static bending and free vibration of a functionally graded material microbeam for three FG models.

2- Examining many parameters such as material length scale parameter ratio (h/lm), aspect ratio (L/h), power-law index (f), porosity index (α), CNT volume fraction index (V_{CNT}) and CNT distribution model $(FG-X, -UD, FG-V and, FG-O.)$ with various boundary conditions (i.e. C-C, C-S, S-S and, C-S) for three FG models.

3- Studying the effect of using Mori-Tanaka's technique on the first model of FG - microbeam beam.

4- Studying the effect of using Poisson's ratio technique on the three models of FG - microbeam beam.

1.7 Structure of the thesis

The thesis is divided into five chapters. **Chapter one** provides a general introduction to functionally graded materials, the porosity, and microstructures of FG-SWCNT reinforced polymer, and lists the main objectives of the thesis. The **second chapter** provides a literature review of previous research according to the categories investigated. In this work, previous research on FG beam, FG microbeam, porous FG microbeam, FG-SWCNT micro, and modified couple stress theory is explained, including a brief explanation of the results of the literary works. The **third chapter** includes details of the governing equations and their associated BCs for the FG microbeam and methods for their solution. The **fourth chapter** presents and discusses the results obtained from the numerical solutions. **Chapter Five** provides a summary and conclusions of the work and some recommendations for future work.

.

CHAPTER Two

LITERATURE REVIEW

The static and free analysis of three models a micro FG composite microbeam subjected to a distributed load with different boundary conditions are investigated in this thesis employing Modified Couple Stress Theory (MCST) in conjunction with EBBT and TBT.

Several studies have published articles on the mechanical behavior of the functionally graded structures and the porosity effect, investigations of functionally graded micro beams based on modified couple stress theory and, Studies of FG structures reinforced by CNT using various ideas the articles listed below.

2.1 Functionally Graded Material beam

Kadoli R.et al,(2008)[18] studied the transverse deflection, axial, and shear stresses in a thick FG beam (C-C, S-S). Higher-order shear deformation theory was used to solve this problem. The static equilibrium equation for the FGM beam was calculated using stationary potential energy and the finite element approach. The volume fraction of metal or ceramic was studied using power-law exponents. The static deflection and static stresses change when the FG beam surface is ceramic or metal-rich.

Şimşek M. et al.,(2009) [19] examined bending vibration of a functionally graded (FG) beam utilizing the Ritz approach's First shear deformation theory (FSDT) and Higher-order shear deformation beam theories (HOSDT). Following the law of mixture, the beam's material properties altered with thickness. The Ritz method trigonometric functions are required to study transverse, axial, and rotating deflections

of cross-sections of FG-supported beams under uniform load. It shows that the stress distribution of the FG beam is different from the beam's isotropic properties.

Thai H. and Vo. T.p (2012) [20] studied the FG-free beam's bending and vibration by the Euler-Bernoulli and first shear deformation beam theories. The shear correction component of FSDT can be omitted by using high-order theorems. Euler-Bernoulli beam theory is a specific instance of High-order theory. The metal-ceramic beam is investigated using finite elements. The power-law index has a significant impact on the bending and free vibration results of functionally graded beams.

Vo T. et al, (2015) [21] is presented a quasi-3D theory with the finite element model and the Navier technique to find the solution of lowest and largest displacement occurs at the mid-plane of the beam, and maximum shear stress occurs at the mid-plane of the beam for both symmetric and non-symmetric sandwich beams. The numerical results are predicted by many beam theories, including EBBT, FSDT, and HSDT. The following parameters as a power-law exponent, boundary conditions, and skin-core-skin thickness ratios are considered.

The static and free vibration of functionally graded beams is studied by **Jing L. et al,(2016)** [22], using the cell-center finite volume method (C-C FVM) and Timoshenko beam theory due to the general resultant equilibrium equations with strong form. which no effect shear locking as compared to Finite Element Method that a numerical phenomenon produced by increasing strain energy terms. In static analysis, The material qualities supposed to change in a power-law index along with the thickness. The natural frequencies are proportional to the value of L/h but the values of natural frequencies are inversely proportional to the

power-law exponents. the ideal shear correction factor is found when no shear locking.

M. Şimşek and M. Al-shujairi**,(2017)**[23] studied static bending and forced vibration induced by two successive harmonic loads on FG sandwich girders. Based on the Timoshenko beam theory. The effective material property of the FG sandwich beam gradually changes through the thickness according to the power law, and three sandwich beam models used. Lagrange equations are used with Newmark methods to solve the governing equation. The unknown displacement functions expressed using simple polynomial, and auxiliary variables functions represent the boundary conditions The normalized dynamic deflection increases as the distance between the loads decreases, and the power-low index drops as the sandwich beam become more flexible due to the higher metal content.

Khafaji S. et al,(2020)[24] studied transient and modal analysis of functionally graded ceramic-metal with both simple support and cantilever beams by Timoshenko beam theory (TBT) and the Finite element method. The characteristics vary smoothly along the transverse direction of the beam. The effect of numerous parameters, including power index, boundary conditions, and modulus ratio. Lower levels of the gradient index had a considerable effect on the transient response of both simple support and cantilever beams. While the power-law index and slenderness ratio has an impact on the peak response, the beam constraint type has the greatest impact.

2.2 Functionally Graded microbeam based on (MCST)

S. K. Park and X. L. Gao, **(2006)** [25]**.** studied bending rigidity a cantilever beam problem by using modified couple stress theory and an Euler-Bernoulli beam to generate the strain energy density function. applied the principle of minimum total potential energy to derive the beam's governing equation and boundary conditions. found the resulting beam model has an internal material length scale parameter that capable of capturing the size effect. the quantitative differences, it illustrated between the new beam model and the classical Bernoulli–Euler beam theory.

A modified couple stress theory combined with Hamilton's principle is used to build a microstructure-dependent model for the Timoshenko beam, which was published by **Gao, X et al. (2008)** [26]. The numerical results for the static bending of the simply-simply beam are smaller than the classic Timoshenko beam model predicts. Furthermore, the differences in deflection and rotation anticipated by the two models are very high when the beam thickness is small, but they lessen as the beam thickness increases.

Şimşek, M. and J.N.Reedy,(2012) [27] studied the static bending and free vibration FG- microbeams by utilizing unified beam theory, including various higher-order beam theories, The Euler–Bernoulli and Timoshenko beam theory based on modified couple stress theory. The Mori–Tanaka scheme assumed material properties of the FG- microbeams vary in the thickness direction. Hamilton's principles associated with a simply-supported FG- microbeam gave the governing equation of vibration. The Navier-type method simplifies the governing equation. The results showed that the non-classical beam models effect

by the size effect when the thickness of the micro beams approaches the parameter of the material length scale. It was also shown that classical beam models overestimate (understate) the static responses (the free vibration responses). The addition of the Poisson effect reduces static deflections and increases vibration frequencies.

Şimşek, M. et al,(2012) [28] illustrated static bending of the small size of FG beams depending on the modified couple stress theory with EBBT and TBT. According to the Mori–Tanaka homogenization, the properties of the material for FG- microbeam changed smoothly across the thickness in the z-direction. The minimum total potential energy principle derived the governing equation of motion of functionally graded simply. Many parameters affected on the static, bending of small scale FG- microbeam with material length scale parameter, slenderness ratio, and Poisson effect investigated. Results showed that the deflections of the classical beam theory of FG-microbeam always be greater than those predicted by the modified couple stress theory.

Şimşek, M. et al.,(2013)[29] investigated the buckling of small-scale FG- embedded microbeam subject to an axial compressive load in elastic Pasternak medium using the modified couple stress theory (MCST) and a unified higher-order beam theory. According to the Mori–Tanaka homogenization technique, the effective material properties have resulted from the mechanical properties. The minimum total potential energy concepts are dependent on deriving the equations of motion and related B.C.s. The Navier method solution was dependent on the critical buckling load. Many parameters that influence the buckling load of small size FG- microbeams, including the material length scale parameter,

aspect ratio, different material properties, and elastic medium parameters on the critical buckling load effect discussed. It found that all higher-order beam theories produce the same results with a few differences.

Şimşek M.,(2014) [30] Have investigated the nonlinear static and vibration analysis FG- microbeam to a triple-layered nonlinear elastic foundation with the EBBT and the von-Kármán's geometric nonlinearity based on the modified couple stress (MCST). The governing equations and B.C.(SS) and (CC) are derived by Hamilton's principle. The Galerkin technique is used to solve the nonlinear partial differential governing equation. The nonlinear frequency can be obtained analytically by He's vibrational method. The numerical results showed that the nonlinear frequency ratio decreased with the increase of the dimensionless scale parameter and the nonlinear basis coefficient according to Winkler and Pasternak's parameter. It has an inverse effect on the nonlinear frequency.

Aydın, M. et al,(2015) [31]studied the dynamic stability subjected to a moving load with the modified couple stress theory combined with the Kirchhoff – Love plate theory. A Lagrange's equation and associated with five sets of B.C.s used to drive the equations of motion solved by implicit time integration Newmark-β method. The effect of the following parameter, the material length scale parameter, aspect ratio of the plate, different boundary conditions, and the moving load velocity on the dynamic response of the microplate explored. It reached that the dynamic deflections are affected by the material length scale parameter and the moving load velocity.

2.3 Functionally Graded beams with porosities

Chen, D. et al.,(2015) [32] have presented elastic buckling and static bending of various FG- porous beams based on the first-order shear beam theory. In comparison, utilized two symmetric and unsymmetric porosity distributions. The Hamilton principle concludes the total energy of the porous beam and various boundary conditions into governing equation of vibration solved by the Ritz technique. porosity distribution influences critical buckling load, maximum deflection, and related stress distribution. Compared to the unsymmetrical distribution pattern, the symmetric distribution pattern has a higher buckling potential and bending resistance.

Yousef S. et al,(2016) [33] used the transfer matrix method to investigate the dynamic behavior of porous FG for ceramic-metal classical beams, EBBT and TBT include the effects of shear deformation with different boundary conditions. On the non-dimensional natural frequencies, the impacts of porosity, slenderness ratio, material parameters, boundary conditions, different beam theories, and volume fraction index are described. It has been discovered the non-dimensional natural frequencies decrease as the volume fraction index increases

Shafiei N. et al,2016 [34] analyzed the nonlinear vibration response of porous tapered FG- microbeams based on modified couple stress conjunction with Euler–Bernoulli theories. A modified power-law determined the variation in material properties with porosity as two models of porous distributions. Hamilton's principle with Von-Kármán's nonlinear strain is used to drive the equations of motion and the corresponding B.C.s. The direct iterative model and the generalized differential quadrature method (GDQM) obtained solutions. The

influence parameters on fundamental frequency discussed, such as nonlinear amplitude, material length scale, rate of thickness, FG- index, and porosity volume fraction.

Şimşek M. et al,(2017)[35] studied the static bending and forced vibration leading from moving load on imperfect FG-micro-plate founded on the MCST. The displacement field of the FG- micro plate is based on the Mindlin plate theory. According to a simple power law, the neutral surface concept determines effective material property with porosities that gradually change through the thickness. The Lagrange equations with the Newmark- method are used to solve the governing equations of FG-micro plate behaviors solved in the time domain by Newmark's way. Many factors are including porosity volume fraction and porosity type, length material scale parameter, and moving load velocity that affected dynamic behaviors. Results showed the existence of the porosities causes an increase in the dynamic responses of the FG microplate. The influence of the uniformly distributed porosities on the responses is more noticeable than the effect of the functionally distributed porosities.

Fouda N. et al.,(2017) [36] suggested two models of porosity study mechanical behaviors such as the static bending, buckling, and functionally graded free vibrations of a porous beam. The first model is linear functions of the modulus of porosity. The second is a modified model, that varying elasticity as an implicit function of porosity with an explicit density function. The governing equation for motions was obtained by applying the Euler-Bernoulli beam theory and solving the finite element method. It was found that the static deflection increased in both models by increasing the porosity and the material distribution

parameter, on the contrary, with the critical buckling load. The researcher showed that the second model is good to be used in an experimental expression for porosity.

Bachiri A. et al,(2019) [37] investigated the bending and free vibration of functionally graded porous beams sitting on elastic foundations. 3variable shear deformation and no requirement for shear factor correction. The material properties were computed using a modified power-law with even porosities. The Navier method is used to solve the governing differential equations and boundary conditions of a porous FG- beam. increasing the Pasternak and Winkler, the fundamental frequency increase. Reverse with increase volume fraction porosity.

2.4 Functionally graded CNT Reinforced Composite Beams

Adding minimal amounts of CNT to polymeric composites has been shown to increase mechanical properties, making it a prominent topic in the field.

H. S. Shen and C. L. Zhang**,(2010)** [38] proposed that the concept of FGMs be applied to nanocomposite plates reinforced by SWCNTs with low nanotube volume fractions and showed how it affects the nonlinear bending response of functionally graded carbon nanotube-reinforced composite (FG-CNTCR) plates subjected to a transverse uniform or sinusoidal load under various environmental conditions. The results show that functionally graded reinforcing can greatly boost the load-bending moment curves of the plate.

Ke L. et al. (2010) [39] investigated nonlinear free vibration analysis of functionally graded nanocomposite beams reinforced by SWCNTs using Timoshenko beam theory with von Kármán geometric

nonlinearity. The mixing technique based on continuously modifying the material properties of FG microbeams over thickness. Hamilton's concept with B.Cs was used to calculate the motion equations. The governing eigenvalue equation solved using the Ritz technique, and the nonlinear vibration frequencies of FG-CNTRC beams with varied end support determined. Carbon nanotube volume fraction, vibration amplitude, slenderness ratio, end supports, and CNT distribution are all affected by the nonlinear free vibration characteristics of FG-CNTRC beams. Numerical results demonstrated that increasing the CNT volume fraction leads to greater linear and nonlinear frequencies for both UD- and FG-ACNTRC beams, and Functionally graded symmetrical CNT distribution had higher linear and nonlinear frequencies than beams with uniform CNT distribution.

Samadi N. et al,2012 [40] The elastic-free vibrations and buckling of FG-SWCNTRC. With or without an elastic foundation, Spreading of carbon nanotubes (UD) in the composite beam thickness direction (FGe-X, FG-A, and FGeX-O) of carbon nanotubes. The natural frequency and critical buckling load of CNTRC beams were computed. The effect of CNT volume fraction, foundation stiffness, and distribution on natural frequencies and critical buckling load of CNTRC beams was examined. The beam of FG-X has a higher fundamental frequency and critical buckling load than other beams –UN, FG-A and, FG-O. while boundary condition, C-C follows C-S, S-S, and C-F.

Heshmati M. et al,(2013) [41] The impact of CNT agglomeration on the dynamic behavior of functionally graded nanocomposite beams reinforced by randomly oriented carbon nanotubes for various CNTs were investigated. Finite element analysis is used to

numerically analyze distributions. method. A two-parameter agglomeration model is used to material characteristics were determined It is very evident that the CNT aggregation has a severe weakening impact in carbon nanotube-reinforced composites. The result observed the efficient Young's modulus has the highest value when all carbon nanotubes in the cluster and matrix must be homogeneously dispersed.

F. Lin and Y. Xiang,(2014) [42] investigated an FG-CNT beam reinforced with single-walled carbon nanotubes using the First (FSDT) and Third (TSDT) shear deformation theories (SWCNT). The governing equation associated boundary conditions for the FG-CNT beam, namely hard clamped (H.C.) and soft clamped (S.C.), are produced using Hamilton's principle and variation scheme, and then resolved by the p-Ritz. The effects of CNT volume fraction and CNT distribution model examined. There was a distinction between hard and soft clamped solutions for first and third-order beam theories. The FGX-CNT beams have the highest frequency, while the FGA-CNT beams have the lowest frequency. The frequency characteristics of the beams improved significantly when the CNT volume percentage is increased from 0.12 to 0.17.

Pourasghar A.,(2015)[43] investigated the free vibration of the FG-CNTR non-uniform column resting on an elastic foundation for the FGM beam. the normal frequency was founded by solving the governing equation using the generalized differential square (GDQ) technique. distribution types of CNT reinforcement of column were selected such FG-V, FG-X, and UD .the factors are effective on the FG-CNTRC column's normal frequencies and critical load such distribution type and CNT volume fraction. Result reached the critical

load lowers with increasing parameters of CNT efficiency and independent on the elastic foundation.

Rokni H. et al,(2015) [17] examined the vibration behavior of FG-CNT Reinforced Polymer microcantilevers beam. Achieving this by maximizing the volume fraction of the CNT profile represented as a function of micro-beam length. The micro-beam model is based on the Bernoulli–Euler theory and Modified couple stress theory. It had been discovered that by using the optimal CNT distribution profile in the longitudinal direction of the microcantilever beam, the fundamental natural frequency of the microcantilever nanocomposite beam rises by up to 10.7 %.

Khilari S. et al, (2018) [44] studied the fundamental frequencies of free vibrations of FG-CNTRC Timoshenko beams. The Eshelby–Mori–Tanaka studies the effect of CNTs orientation on properties of the material. various distributions of the CNTs along the thickness direction are assumed by the following distribution types: U.D., FG-X, FG-A, FG-O. Hamilton's principle is used to obtain differential equations that are solved by the finite element method (FEM). effects of several parameters such as boundary conditions, carbon nanotube (CNT) volume fraction, slenderness ratio, and the distribution of nano-material on the natural frequency of the composite beam were studied. The paper revealed that CNT volume fraction and distribution randomly have a significant effect on the properties of the nano-composite beam.

Vo-Duy T. et al,(2019)[45] used the finite element method with FSDT to analyze the free vibration of laminated functionally graded carbon nanotube-reinforced composite beams. Along the thickness

direction in each layer, single-walled carbon nanotubes were classified as uniformly distributed (UD) or functionally graded (FG). The extended rule of the mixture was used to calculate the effective characteristics of carbon nanotubes (CNTs) and anisotropic polymers. The effect of CNT volume fractions, CNT distributions, CNT orientation angles, boundary conditions, length-to-thickness ratios, and layer count on the frequencies of laminated FG-CNTRC beams was studied, The Result was reached to That the stacking sequence of CNT distributions has little influence on the frequency of the FG-CNTRC beams. Also, the stacking sequence of FG-Λ-X-V gives the largest frequencies.

Talebitooti M. et al.(2019) [46] investigated the vibration stability of a sandwich composite beam supported by two layers of the magnetic actuator. Closed-loop velocity control using proportional control to reduce vibration amplitude. The kinematic equations were obtained using TBT and Hamilton's principle. In this case, the differential square approach was used. The effect of distribution pattern, CNT volume fraction, and angular velocity on vibration extinction were studied for different sandwich beam patterns. The volume fraction and type of carbon nanotube distribution considerably affect the rotating sandwich beam's overshoot response.

Fadaee M., (2019)[47] investigated the dynamic stability of adaptive sandwich beams composed of two FG-CNT layers and a magnetorheological elastomer MRE core based on TBT. CNTs are placed in six distinct patterns over the thickness of the beam's three uppers and three lower layers. Hamilton's theory used to generate the equations of motion and appropriate boundary conditions of the dynamic sandwich beam. To solve the governing equations, the differential

quadrature method DQM was applied. The shear modulus of the magnetorheological elastomer core was monitored using a magnetic field. As a result, the angular velocity increases while the loss factors decrease. Because the structure stiffness improves as the centrifugal tensile force increases. As the hub radius increases, the natural frequencies and corresponding loss factors become more responsive to the angular velocity. Natural frequencies were highest in the FG-X types.

2.5 Summary

Tabel 2. 1: shows the papers the effect of gradient index (f) *, slenderness ratios* (L/h) *, and boundary conditions on free vibration and deflection on classical FG*

Authors	Condition	Observation
Mesut Simsek and Mohammed Al-shujairi,(2015) [23]	Three FG sandwich beam models one of as FG-classical beam is interesting in the study boundary conditions (i.e., CC, SS, CF), changed gradient index (f), from ceramic to metal. And the effect of the aspect ratio (L/h) such as (L/h) = 5, 20. and the Lagrange multiplier and FSDT are used.	The frequency of FG and sandwich of classical beams decrease when the gradient index (f) increases. Timoshenko beam theory (TBT) is smaller than the natural frequency values of Euler (EBBT) since TBT has a sheer effect, the shear deformation effect when slenderness of $(L/h=20)$ =20. But less important with thin sandwiches beams, $(L/h=5)$. And vice versa results with deflection.

Tabel 2. 2: shows that the papers are investigating the modified couple stress theory as well as the effect of the power-law index, length scale parameter, aspect ratio, and Poisson effect on the free vibration and deflection of functionally graded microbeams.

Authors	Condition	Observation
M.Simsek and T. Kocatürk (2013)[28]	The aspect ratio, dimensionless material length parameter, and gradient index are explored for the FG microbeam exposed to uniform and point loads to investigate the center deflection of the FG microbeam.	The FG microbeam's central deflection is significant when the aspect ratio is less than 10, dimensionless material length parameter ratio is $(h/lm = 8)$. The gradient index is closed to the total volume fraction of metal.
M. Simsek and J.N Reddy (2013)[27]	By several beam theories investigate the frequency and deflection of the FG micro beam for the gradient index $(f = 0,0.3,1,10)$ from (i.e., smoothly transition from ceramic to metal), dimensionless material length scale parameter $(h/l = 1,2,4,8)$, and aspect ratio $(L/h = 10,100)$	The higher frequency and the lower deflection of the FG micro occurred when the gradient index $(f = 0)$ means has (i.e., FG-full ceramic

		surface), the dimensionless material length scale parameter is equal $(L/h=10)$ and the aspect ratio $(L/h=100)$

Tabel 2. 3: shows papers that is studying the porosity with the performance of FG classical beam and FG microbeam and the effect of the boundary condition, material, and porosity volume fraction on it.

Authors	Condition	Observation
Wattanasakulpong N. and haikittiratana A. (2015)[11]	FGM beams with porosity were subjected to vibration analysis. Many significant factors must be considered, such as the boundary condition, material, porosity volume fraction (i.e. smooth transition from ceramic to metal), beam thickness ratio.	Increasing the power-law index and the beam length to thickness ratio reduces frequency results for both perfect and imperfect FGM beams. The C–C beam has the highest natural frequencies, followed by the C–H, H–H, and C–F beams.
Yousef S. Al Rjoub and Azhar G. Hamad (2016)[33]	The impacts of boundary conditions, power-law index, slenderness ratio, beam theory, and porosity on natural frequency are investigated in this work.	The nondimensional natural frequencies decrease as the value of power-law index increases.

Tabel 2. 4: shows the papers is studying the natural frequencies and bending deflection and the effect of nanotube volume fraction, slenderness ratio, CNT distributions, and boundary conditions on FG-CNTRC beams of FG microbeam.

Authors	Condition	Observation
M.H. Yas and N. Samadi ,(2012) [40]	The influence of foundation stiffness parameters and several parameters, such as nanotube volume fraction, slenderness ratios, CNTs distribution, and boundary conditions on free vibrations and buckling analysis of nanocomposite is numerically verified by using (GDQM)and (TBT)	The results showed that the high frequency and buckling FG-CNT reinforced polymer composite with FG-X distribution increased with nanotube volume fraction in 0.28 with decreasing aspect ratio, and boundary conditions type clamped-clamped.
Feng Lin, Yang Xiang, (2013) [42]	It is used the first order and third order beam theories to determine the effect of Vibration frequency parameters represented as CNT volume fraction, distribution, beam span to depth ratio, and boundary conditions on the free vibration of FG-beam.	Results discovered that the difference between frequency parameters based on first-order theory and third-order theory increases first when the L/h value ranges from 10 to 20 and then reduces as the L/h value increases further. At the CNT volume fraction from 0.12 to 0.17, there is a large difference in frequency while the CNT volume fraction from 0.17 to 0.28 has little frequency difference.

Puneet Kumar and J. Srinivas,(2017)[49]	This paper studied the static and dynamic behaviors of beams FG-CNT reinforced polymer and hybrid laminated composite containing layers of carbon-reinforced polymer with CNT by FEM and Ritz) methods. Under the influence of different CNT volume fractions, several CNT distribution types, boundary conditions, and aspect ratios.	Demonstrate the FG-X has the highest frequency all the following boundary conditions: C-F, S-S, C-S, and C-C. and an increase in the number of walls in MWCNT lead to decrease frequency and buckling load and increase the dimensionless bending deflection
Nuttawit Wattanasakulpong , Variddhi Ungbhakorn(2012). [50]	The beams resting on the Pasternak elastic foundation, including a shear layer and Winkler spring, are considered. With different patterns of reinforcement. New results of bending،buckling and vibration analyses of CNTRC beams based on several higher-order shear deformation theories are presented.	found FG X-Beam has the highest natural frequency, followed by the UD-, V-, and O-Beams. also found increased constant factors of the elastic foundation's spring leading to a reduction in transverse displacement and frequency increases.
T. Vo-Duy, V. Ho-Huu[47]	It is Studied the free vibration of laminated functionally graded CNT reinforced composite beams and, the influence of the CNTs	By dependent, a finite element technique found FG X-Beam has the highest natural frequency, followed by the UD-, V-, and O-

	volume fractions, CNTs distributions, CNTs orientation angles, B.C, length-to-thickness ratios, and the numbers of layers is analyzed	Beams. also found increased constant factors of the elastic foundation's spring leading to a reduction in transverse displacement and frequency increases. and is found The FG-X distribution yields the largest frequency, while the FG-O distribution yields the smallest frequency of laminated FG-CNTRC beams.

2.6 Scope of The Present Work

This thesis aims to apply the concept of FGMs to Three different states of the FG microbeams as follows.

State I: study for a model of FG microbeam made of ceramic and metal.

State II: study porous FG microbeam. as a model, I, add porosity graded thickness and find the effect of porous distribution through the modified rule of mixture .**State III:** study the FG-SWCNT microbeam.By adding the CNT as reinforcement composite to polymethyl acrylate (PMME) based on a functionally graded manner. The mechanical properties study by the extended rule of mixture**.** and obtain their fundamental natural frequencies and transverse deflection numerically. Different functionally graded volume fraction profiles, which are a function of the micro-beam length. The micro-beam model is based on modified couple stress theory which introduces a material length scale parameter following the study by Yang et al.

CHAPTER THREE: THEORETICAL AND NUMERICAL WORK

3.1 Functionally Graded Micro-Model

The functionally graded (FG) microbeam shown in Figure (3.1) has a length L, a width b, and a thickness h. A uniform distribution load (q) is applied to the FG microbeam. The coordinates L, b, and h are chosen to correspond to the length, width, and thickness of the FG microbeam, respectively. For case studies of B.Cs are presented in this work : (C-C), (C-S), (S-S), and (C-F). It assumed that the FG microbeam is constructed of ceramic and metal and that the FG beam's effective material properties (i.e., Young's modulus E, Poisson's ratio ν, and shear modulus G) vary continuously in the thickness direction (in the z-direction). The microbeam's bottom and top surfaces are made of ceramic and metal, respectively.

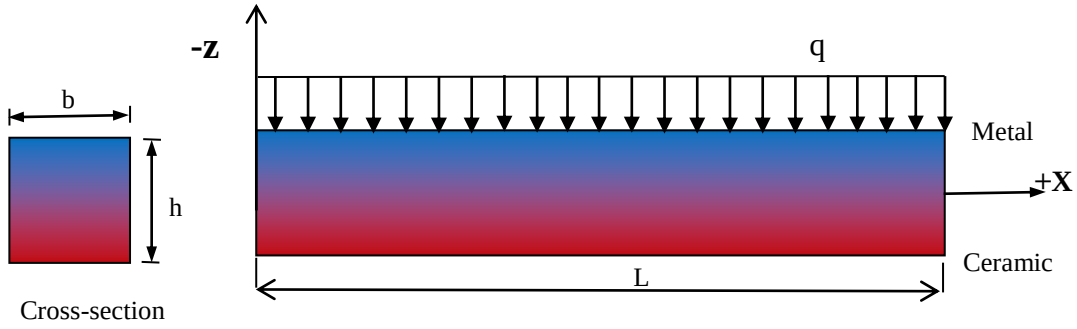

Figure 3. 1: Geometrical dimensions of FCM microbeam. [27]

3.2 Functionally graded material properties

According to the rule of mixture method, where $V(z)$ is the volume fraction of the phase materials, and the subscripts (m) and (c) denote metal and ceramic phases, respectively. The volume fractions of the

metal and the ceramic constituents in the FG material is as follows **[27-29]:**

$$V_m(z)+V_c(z)=1 \qquad \text{……(3.1a)}$$

$$V_c=\left(\frac{z}{h}+\frac{1}{2}\right)^f \qquad \text{……(3.1b)}$$

where (f) is the non-negative variable parameter (power-law exponent) which dictates the material variation profile through the thickness of the beam. The mechanical properties $P(z)$ of the classical FG-material beams are varied continuously through the thickness; the changed properties for both metal properties (P_m) and ceramic properties (P_c) can be called the effective properties using the power-law (the rule of the mixture) as follows:

$$P=P_mV_m+P_cV_c \qquad \text{…..(3.2a)}$$

$$P(z)=(P_c-P_m)\left(\frac{z}{h}+\frac{1}{2}\right)^f+P_m \qquad \text{…..(3.2b)}$$

Mechanical properties are represented by Young's modulus $E(z)$, while $\rho(z)$ is denoted by density mass and $\nu(z)$ is the passions' ratio.

$$E(z)=(E_c-E_m)\left(\frac{z}{h}+\frac{1}{2}\right)^f+E_m \qquad \text{..... (3.3)}$$

$$\rho(z)=(\rho_c-\rho_m)\left(\frac{z}{h}+\frac{1}{2}\right)^f+\rho_m \qquad \text{..... (3.4)}$$

$$\nu(z)=(\nu_c-\nu_m)\left(\frac{z}{h}+\frac{1}{2}\right)^f+\nu_m \qquad \text{..... (3.5)}$$

It is easily seen that $E=E_c$, $\nu=\nu_c$ when $z=-h/2$, and $E=E_m$, $\nu_m=\nu$ when $z=+h/2$.

When the beam is small in micro size, the power-law cannot provide an accurate value for the effective material properties, one of the most applicable schemes of homogenization is the Mori–Tanaka scheme for estimating the effective properties of FG microbeam. According to Mori–Tanaka homogenization scheme is given by as follows **[27]**:

$$K_f = \frac{V_c\left(K_c - K_m\right)}{1+V_m\left[\left(K_c - K_m\right)/\left(K_m + 4G_m/3\right)\right]} + K_m \qquad \ldots\ldots(3.6)$$

$$G_f = \frac{V_c\left(G_c - G_m\right)}{1+V_m\left(G_c - G_m\right)/\left[G_m + G_m\left(9K_m + 8G_m\right)/\left(6\left(K_m + 2G_m\right)\right)\right]} + G_m \qquad \ldots. (3.7)$$

$$K_{(m,c)} = \frac{E_{(m,c)}}{3\left(1-2\nu_{(m,c)}\right)} \qquad \ldots.(3.8)$$

$$G_{(m,c)} = \frac{E_{(m,c)}}{2\left(1+\nu_{(m,c)}\right)} \qquad \ldots. (3.9)$$

where K_f Bulk modulus and G_f Shear modulus is expressed as total efficient physical properties for metal (m) and ceramics (c), respectively. $K_{(m,c)}$ is the local bulk modulus of FG micro-beam and $G_{(m,c)}$ is the local shear modulus the volume fraction $V\left(z\right)$ is calculated for the varied phase materials.

When the Mori-Tanaka homogenization is used, Young's modulus of the FG microbeam is expressed from (3.8) and (3.9) as follows:

$$E\left(z\right) = \frac{9K_fG_f}{3K_f + G_f} \qquad \ldots.. (3.10)$$

Mori Tanaka homogenization allows for the calculation of the Poisson's ratio of the FG microbeam as follows:

$$\nu(z)=\frac{3K_f-2G_f}{6K_f+2G_f} \quad \text{…. (3.11)}$$

While the variation in the mass density of the FG microbeam is the same Eq.(3.4):

Figures (3.2a) and (3.2b) depict the effective properties of ceramic and metal as they change smoothly from ceramic to metal. The colour lines in the figures depict the changing effective properties of the FG beam as the thickness of the beam increases; the relationship is regulated by the power index (f). Materials' characteristics are represented by (modulus of elasticity, Poisson, and density).

For example, studying the property of the elastic modulus of the FG beam composed of ceramic and metal: it is noticed that at $(f=0)$ and (z/h) (bottom surface), the properties are all ceramic; when (f) and (z/h) increases, the properties of ceramics begin to decrease and the properties of metal appear. At the highest (f) value and (z/h) reaching (the top surface), only the metallic beam properties are FG. Thus, can be concluded that the FG beam (ceramic - metal) is from the bottom surface of the solid because the modulus of elasticity of the ceramic is high, and it is less rigid in the upper surface because of the modulus of elasticity of the metal is low. In Figure (3.2c), the effects of gradient index (f) and different estimation methods to study the properties of materials. It is noted that the results obtained using the Mori-Tanaka scheme are lower than those obtained with the classical base of the mixture due to different estimates of the properties of the active substance.

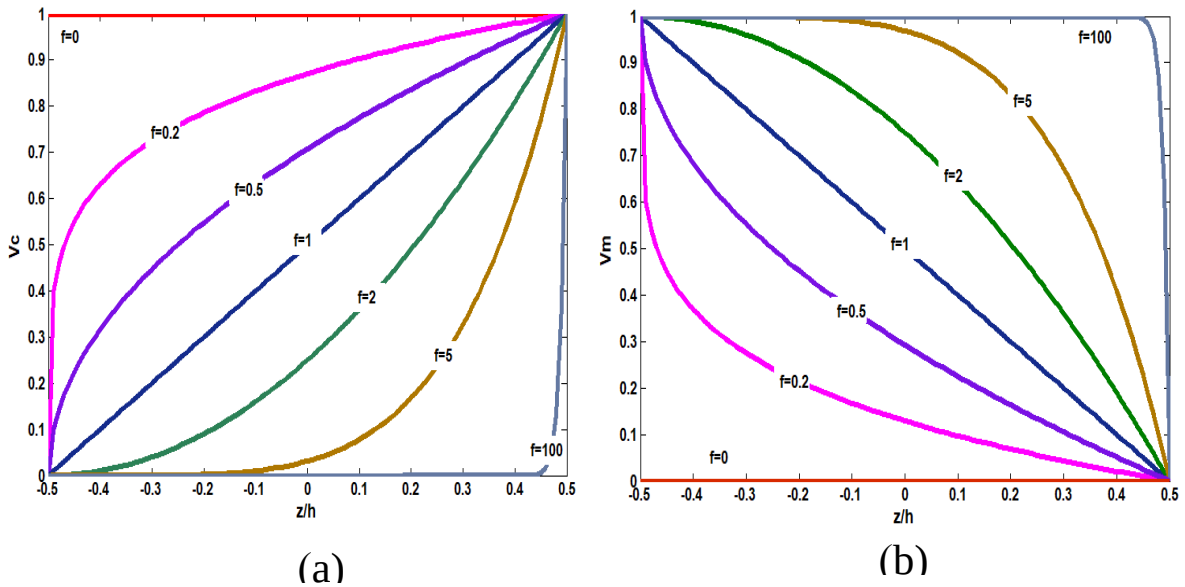

(a) (b)

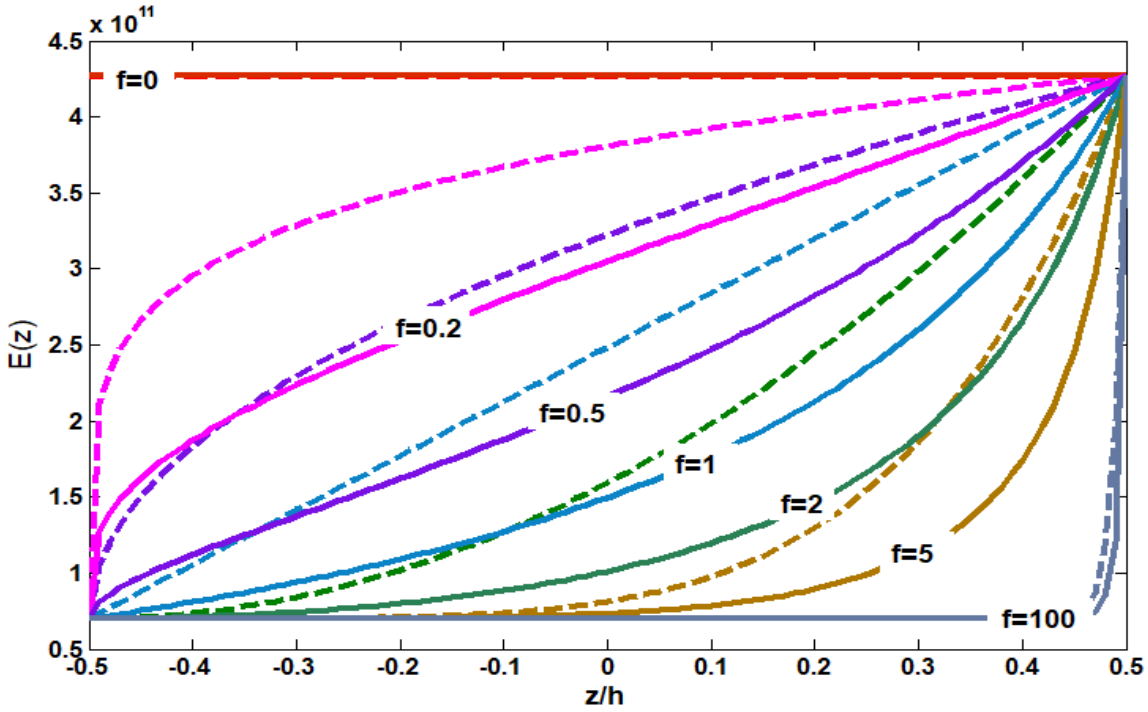

(c)

(a). Variation of the volume fraction of the ceramic constituent through the thickness of the FG microbeam.

(b). Variation of the volume fraction of the metal constituent through the thickness of the FG microbeam.

(c). Variation of Young's modulus along with a thickness of the FG microbeam;(—): Solid lines: Mori–Tanaka homogenization, (- - -): Dashed lines: Classical rule of mixture.

Figure 3. 2: Mechanical Properties of FG micro-beam

3.3 Functionally graded porous properties

In this investigation, the imperfect microbeam is assumed to have porosities spreading within the beam cross-section due to defects during production. Consider an imperfect FGM with a porosity volume fraction $\alpha,(\alpha<1)$ distributed evenly and unevenly among the metal and ceramic, the Modified Rule of Mixture has estimated FG material effective properties with porous.

In this thesis, the effect of the functional grading of porosity on the microbeam is studied by assuming three FG-porosity models. The first, perfect (FGM) is FG-microbeam without porosity. The second, imperfect (FGM-I) is the porosity evenly distributed in FG- microbeam and The third model, imperfect (FGM-II) is unevenly porosity distribution where porosity concentration is at in the cross-section center. Figure (3.3) is shown, second and third models. The formulas of the three models [11] [34] are:

$$P(z)=(P_c-P_m)V_C+P_m \qquad \text{(FGM)} \quad \ldots.(3.12)$$

$$P(z)=(P_c-P_m)V_C+P_m-(\alpha/2)(P_c-P_m) \qquad \text{(FGM I)} \quad \ldots.(3.13)$$

$$P(z)=(P_c-P_m)V_C+P_m-(\alpha/2)(P_c-P_m)(1-2\left|\frac{z}{h}\right|) \qquad \text{(FGM II)} \quad \ldots.(3.14)$$

When analyzing the FG-microbeam cross-section using the FGM-II model, porosity is concentrated in the middle zone of the cross-section, where the quantity of porosity appears to be on a linear drop to zero at both the top and bottom of the cross-section.

As observed, the main difference between FGM-I and -II is the function so that it can be concluded that FGM-II has half of the porosity volume

fraction over the cross-section compared to that of FGM-I. From the comparisons, also Figure (3.3) illustrates the profiles of the material property of perfect and imperfect FGM beams using Eqs. (3.12) to (3.14).

If we have a cross-section of one square meter, the volume fraction of materials can obtain as $V_c = \int_{-0.5}^{0.5} (\frac{z}{h} + \frac{1}{2})^f dz$ and $V_m = 1 - V_c$. The porosity phases function reduces (Vc) and, (Vm) equally for imperfect FGM beams. As can be seen, the fundamental difference between FGMP-I and -II is the function of $\int_{-0.5}^{0.5} (1 - 2\left|\frac{z}{h}\right|) dz = 0.5$, implying FGM-II has half the porosity volume fraction over the cross-section as FGM-I, for any value of (α) [11] .

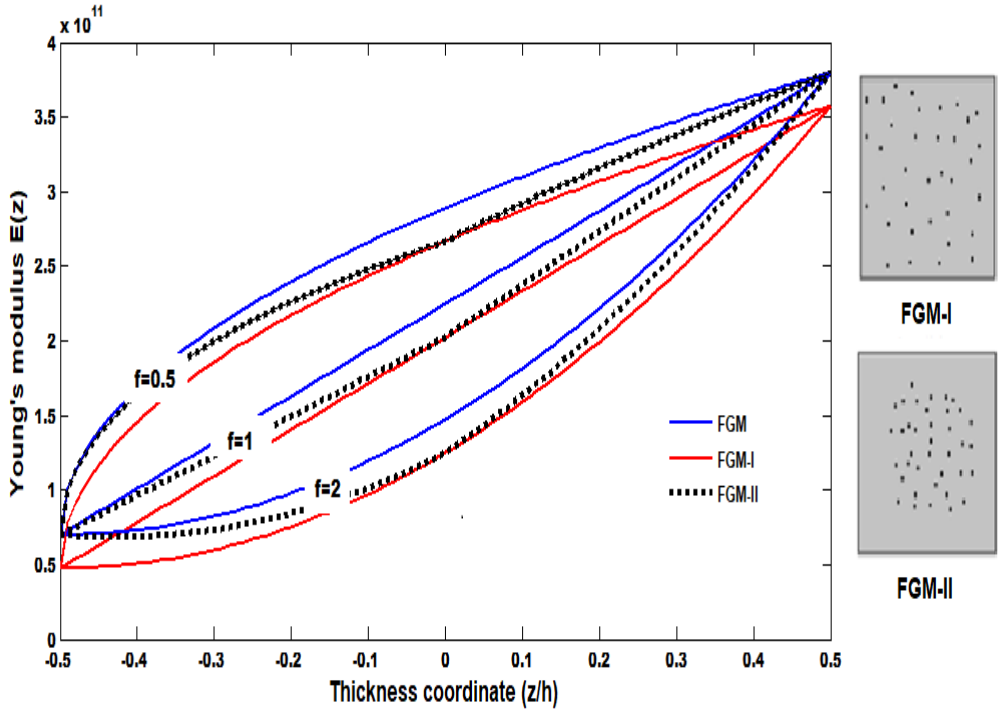

Figure 3. 3: young's modulus through the thickness for three porosity models FGM microbeams with porosity volume fraction. and Cross-section areas for even (FGPM-I) and uneven(FGPM–II).

The value of the porosity volume fraction is less than one $(\alpha < 1)$. The porosity interacts as a sub-function with physical properties (modulus of elasticity (E), mass density(σ), and passion's ratio(ν), which are represented as FGM I and FGM II in the **law of modified rule of mixture**.

3.4 Material Properties of FG-CNTRC Beams

According to Figure. 3.4, the micro-composite beam is considered with length L, width b, and thickness h. The extended rule of the mixture is employed to estimate the effective properties of carbon nanotube reinforced composites (CNTRC) material. For FG micro-composite beam reinforced [40] [49] [45]**.**

$$V_{cnt} + V_m = 1 \qquad \ldots\ldots (3.15)$$

where V_{cnt} and V_m are CNT and matrix volume fractions, respectively. V_{cnt} is defined for a different distribution of CNT. In this thesis, four types of CNT distribution are assumed as follows: FG-X, UD-CNTRC, FG-A, and FG-O.

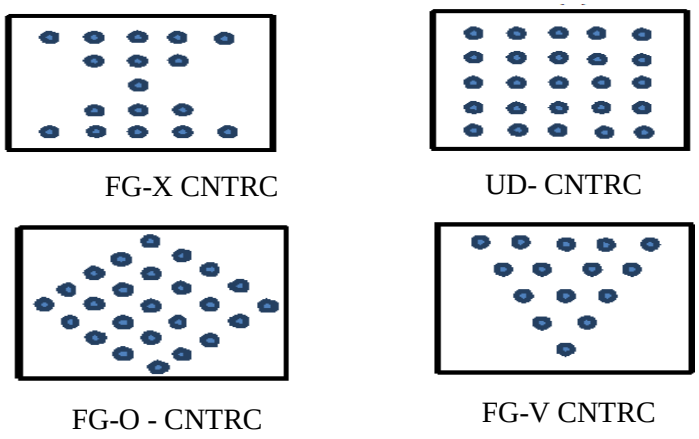

Figure 3. 4: Configurations of the carbon nanotube-reinforced composite beams.

The following is an example of how the extended rule of the mixture is applied to the calculation of FG-CNTRC:

$$FG-X \qquad V_{cnt} = 4V_{cnt}^{*}\left(|z|/h\right) \qquad \left(-h/2 \le z \le h/2\right) \qquad \text{..... (3.16)}$$

$$UN \qquad V_{cnt} = V_{cnt}^{*} \qquad \left(-h/2 \le z \le h/2\right) \qquad \text{.... (3.17)}$$

$$FG-V \qquad V_{cnt} = V_{cnt}^{*}\left(1+2\frac{z}{h}\right) \qquad \left(-h/2 \le z \le h/2\right) \qquad \text{.... (3.18)}$$

$$FG-O \qquad V_{cnt} = 2V_{cnt}^{*}\left(1-2|z|/h\right) \qquad \left(-h/2 \le z \le h/2\right) \qquad \text{.... (3.19)}$$

Where V_{cnt}^{*} is the volume fraction of the carbon nanotubes, three different values (0.12, 0.17, and 0.28) were imposed, where the values V_{cnt}^{*} were taken from the below formula.

$$V_{cnt}^{*} = \frac{m_{cnt}}{m_{cnt} + \left(\frac{\rho_{cnt}}{\rho_m}\right) - \left(\frac{\rho_{cnt}}{\rho_m}\right) m_{cnt}} \qquad \text{..... (3.20)}$$

m_{cnt}, ρ_{cnt} *and* ρ_m are a mass fraction of CNT, the density of CNT and matrix, respectively.

According to the extended rule of a mixture model, the effective Young's modulus, shear modulus, Poisson's ratio, and mass density of CNTRC microbeams can be expressed as :

$$E_{11}(z) = \eta_1 Vcnt(z) E_{11}^{cnt} + V_m(z) E_m \qquad \text{.....(3.21)}$$

$$G_{12}(z) = \eta_3 \Big/ \left(\left(\frac{V_{cnt}(z)}{G_{22}^{cnt}}\right) + \frac{V_m}{G_m} \right) \qquad \text{.....(3.22)}$$

$$\nu_{12}(z) = V_{cnt}(z)\nu_{21}^{cnt} + V_m(z)\nu_m \qquad \text{.....(3.23)}$$

$$\rho(z) = V_{cnt}(z)\rho^{cnt} + V_m\rho_m \qquad \text{.... (3.24)}$$

Where Young's modulus $\left(E_{11}^{cnt}\right)$, shear modulus $\left(G_{22}^{cnt}\right)$, Poisson's ratio $\left(\nu_{cnt}\right)$, and density $\left(\rho_{cnt}\right)$are the properties of SWCNTs. The properties isotropic matrix are also represented by Young's modulus $\left(E_m\right)$, shear modulus $\left(G_m\right)$, Poisson's ratio $\left(\rho_{cnt}\right)$, and density mass $\left(\rho_m\right)$.

Whereas η_1,η_2 And η_3 are represented as the efficiency parameters of the carbon nanotubes on the matrix of microbeam were calculated by identical of elastic Young's modulus resulting from the molecular dynamics simulation with the extended rule of mixture. The following values are adopted in Table (3.1) as the FG-CNT beam efficiency parameters[42].

Table 3. 1:Efficiency parameters FG-CNTRC

Efficiency parameters	$V_{CNT}^{*}=0.12$	$V_{CNT}^{*}=0.17$	$V_{CNT}^{*}=0.28$
η_1	**0.137**	**0.142**	**0.141**
η_2	**1.022**	**1.626**	**1.585**
η_3	**0.715**	**1.138**	**1.109**

3.5 The modified couple stress theory (MCST):

Classical continuity theory cannot predict a precise mechanical response to a microstructure. Experiments have proven that the mechanical response of small-sized structures is affected by the microscopic scale represented by the length of the materials. As a result, many continuity theories have been generated that depend on the material length scale parameter.

In classical couple stress theories (Toupin, 1962; Mindlin and Tiersten, 1962; Koiter, 1964; Mindlin,1964), the equilibrium of forces and moments are the same as those in conventional mechanics.

The deformation measures conjugate The couple stress theory is applied to the strain energy (E_s) of an elastic microbeam, where the strain energy (stored energy) through the virtual displacement (δu) and the virtual rotation $(\delta\theta)$. the strain energy formal

$$E_s = \frac{1}{2}\int_0^L\int_0^w\int_{-h/2}^{h/2}\left(\sigma_{ij}\,(\varepsilon_{ij}+\theta_{ij})+m_{ij}\,(\chi_{ij}+\gamma_{ij}\right)dz\,dy\,dx \qquad i,j,k=x,y,z \quad \ldots(3.25)$$

is consist of two parts, where the first part is represented the transitional components of the classical stress tensor $\left(\sigma_{ij}\right)$ and strain tensor $\left(\varepsilon_{ij}\right)$ the antisymmetric rotation part of displacement gradient $\left(\theta_{ij}\right)$, the second part is the rotation components of the deviatory of the couple stress tensor $\left(m_{ij}\right)$ and the symmetric part strain curvature tensor $\left(\chi_{ij}\right)$. the antisymmetric part of rotation gradient $\left(\gamma_{ij}\right)$: For linear elastic materials, there are two independent length scale parameters associated with the symmetric and antisymmetric parts of the curvature tensor, respectively.

Let us denote the symmetric parts of the displacement gradient and the rotation gradient, respectively, a

$$\varepsilon_{ij} = \frac{1}{2}\left(u_{i,j}+u_{j,i}\right) \qquad \ldots..\ (3.26)$$

$$\chi_{ij} = \frac{1}{2}\left(\theta_{i,j}+\theta_{j,i}\right) \qquad \ldots\ldots(3.27)$$

the components of the rotation vector, the rotation vector is defined by

$$\theta_i = \frac{1}{2}\left(e_{ijk}u_{k,j}\right) \qquad \ldots\ldots(3.28)$$

the antisymmetric curvature tensor, define as

$$\theta_{ij} = \frac{1}{2}\left(u_{i,j} - u_{j,i}\right) \qquad \ldots\ldots(3.29)$$

$$\gamma_{ij} = \frac{1}{2}\left(\theta_{i,j} - \theta_{j,i}\right) \qquad \ldots\ldots(3.30)$$

"In the Modified couple stress theory, an equilibrium relation for moments of couples is introduced to remedy the free-floating nature of the couple vector. The additional equilibrium relation restricts the couple stress tensor to be symmetric. As a result, the deformation energy becomes independent of the antisymmetric part of the curvature tensor. Consequently, for linear isotropic elastic materials, there is only one independent length scale parameter in the couple stress theory, and it is associated with the symmetric curvature tensor. The single length scale parameter can be determined by twisting slim cylinders of different diameters." [53]

$$E_s = \frac{1}{2}\int_0^L \int_0^w \int_{-h/2}^{h/2} \left(\sigma_{ij}\,\varepsilon_{ij} + m_{ij}\,\chi_{ij}\right) dz\,dy\,dx \qquad i,j,k = x,y,z \qquad .....(3.31)$$

Where the components of the stress tensor can be written as

$$\sigma_{ij} = \lambda(z)\varepsilon_{kk}\delta_{ij} + 2G(z)\varepsilon_{ij} \qquad .....(3.32)$$

The couple stress tensor (m_{ij}) can be expressed as follows

$$m_{ij} = 2\,l_m^2\,G(z)\,\chi_{ij} \qquad \ldots\ldots (3.33)$$

The values $\lambda(z)$ and, $G(z)$ are constants known as lame's constants They are based on the modulus of elasticity (E) and the Poisson ratio (v). For the microbeam used in FGM, which can be expressed as

$$\lambda = \frac{E(1-\upsilon_m)}{(1+\upsilon_m)(1-2\upsilon_m)} \quad ,G = \frac{E}{2(1+\upsilon_m)} \qquad \ldots\ldots(3.34a)$$

$\lambda(z)$ and, $G(z)$ lame's constants, where represent the normal stress and shear stress are given by linear elastic constitutive law For FG-SWCNT microbeam that can be written as

$$\lambda = \frac{E_{11}(1-\upsilon_{12})}{(1+\upsilon_{12})(1-2\upsilon_{12})} \quad G = G_{12} \qquad \text{……(3.34b)}$$

The dilation strain (ε_{kk}) referred to the elongation at each direction of the microbeam while (δ_{ij}) is the Kronecker delta and the permutation tensor (e_{ijk}) are represented the mathematical expression where $(e_{ijk}=1)$ and $(e_{kji}=0)$ utilized in the dot and cross product that can be used to obtain the magnitude of normal tensor and direction of the tensor vector, (l_m) is indicated the scale of a material length parameter and is mathematically calculated from the root of the ratio of the bending modulus to the shear modulus as following From the geometry of the Figure (3.5),

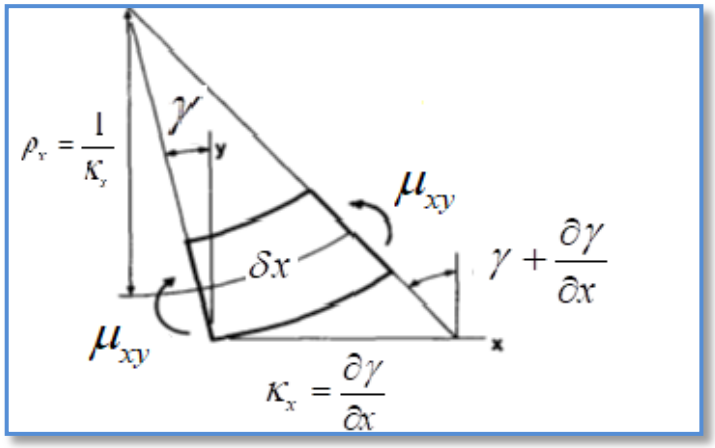

Figure (3.5)--Curvatures produced by couple-stresses

where the couple-stresses is balanced produce curvatures (κ_x) related to a local rigid of the antisymmetric rotation (γ_{ij}) as,

$$\kappa_x = \frac{\partial \gamma}{\partial x} \qquad \text{……(3.35a)}$$

and It is assumed that the curvatures are proportional to the couple-stresses:

$$\kappa_x = \frac{1}{4B}\mu_{xy} \qquad \text{……(3.35b)}$$

"where B is a modulus of curvature or bending and factor 4 is introduced as a convenience. Couple stress has the dimensions of a couple per unit area or force per unit length; curvature is the reciprocal of a length; hence B has the dimensions of force."

Through two equations we get the constant material (l_m), and its formula[53],

$$l_m^2 = \frac{B}{G} \qquad \text{……(3.36)}$$

With $(l_m \neq 0)$, high-stress gradients may lead to large couple-stresses. The setting $(l_m = 1)$ is equivalent to assuming that the material has no resistance to local curvature.

3.6 Used theories in present work

In terms of kinematics, numerous beam theories have been widely used to investigate the behavior of FG beam structures as shown in Figure (3.6). To begin, the Euler-Bernoulli beam theory (EBBT) is based on the assumption that after bending, the plane cross-sections of the beam remain plane and normal to the deformed axis of the beam. This idea is extremely beneficial for narrow beams (slender beams). While the Euler-Bernoulli beam is the most widely used beam theory in engineering due to its simplicity, it tends to lose accuracy when analyzing deep beam structures. This is because the shear deformation is ignored. Hence, Timoshenko (1921) proposed a different beam theory taking account of the shear deformation and rotational bending effects. [8]

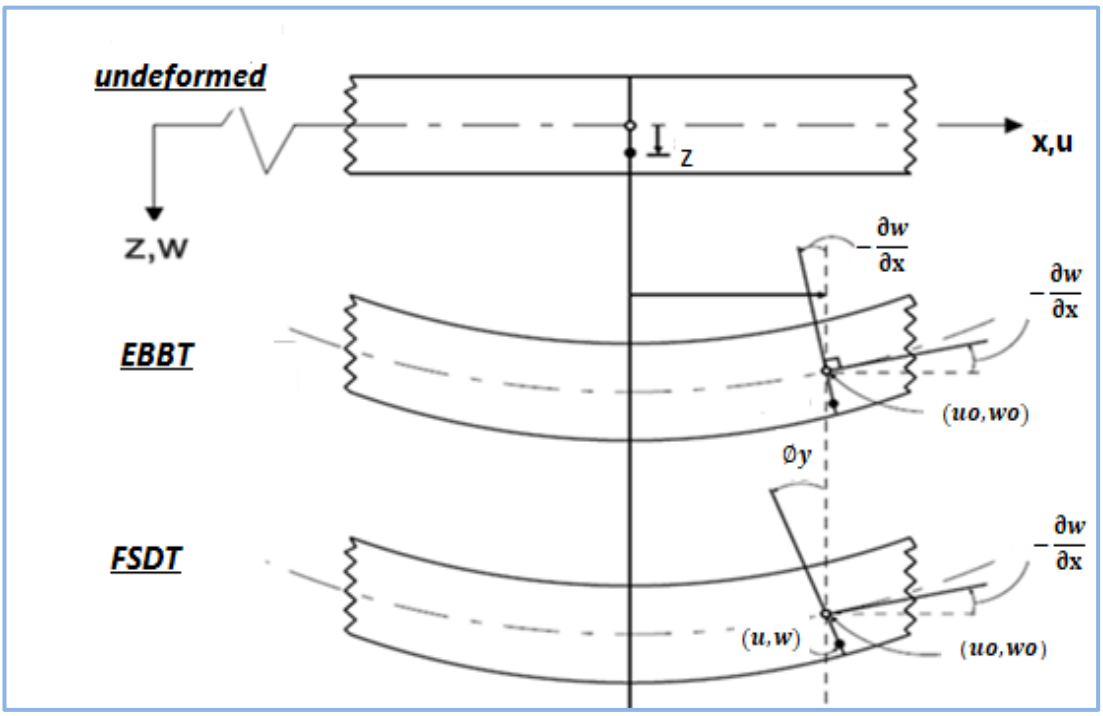

Figure 3.6: Geometries of an unreformed and deformed beam in various beam theories. In-plane displacement is denoted by u_0. (Ref. [52]*modified).*

3.7 The governing equations for FG micro-beams

3.7.1 Euler- Bernoulli beam theory (EBBT)

For EBBT is the assumption for beams with a thickness to length ratio of less than 1/20. The displacement amplitude functions for minor deformations are stated as[17].

$$u_x(x,z,t)=u-z\frac{\partial w}{\partial x},\ u_y(x,z,t)=0,\ u_z(x,z,t)=w \qquad \ldots. (3.37)$$

By substituting Eq. (3.37) into Eq. (3.26), the non-zero classical axial strain component of Euler- Bernoulli beam theory as:

$$\varepsilon_{xx}=\frac{\partial u}{\partial x}-z\frac{\partial^2 w}{\partial x^2} \quad , \gamma_{xz}=0 \qquad \ldots.. (3.38)$$

The rotation of the total banding vector can be calculated by the displacements vector with the permutation symbol which affected the

bending moment, Also, substituting for Eqs. (3.37), (3.28), and (3.29) gives as:

$$\theta_y = \frac{1}{2}\left(e_{yxz}\frac{\partial u_z}{\partial x} + e_{xyz}\frac{\partial u_x}{\partial z}\right) \Rightarrow \theta_y = -\frac{\partial w}{\partial x} \quad , \quad \theta_x = \theta_z = 0 \qquad \text{….. (3.39)}$$

into Eq. (3.27) to obtain the symmetric curvature tensor (χ_{xy})

$$\chi_{xy} = \frac{1}{2}\left(\frac{\partial \theta_x}{\partial y} + \frac{\partial \theta_y}{\partial x}\right) = -\frac{1}{2}\frac{\partial^2 w}{\partial^2 x},$$
$$\chi_{xx} = \chi_{yy} = \chi_{zz} = \chi_{xz} = \chi_{yz} = 0$$

…… (3.40)

the equation of governing motion in terms of the displacements is by using EEBT and modified couple stress theory (MCST). The strain energy $\left(E_s\right)$ for the microbeam can be written to describe a deformed isotropic linear of elastic material.

$$E_s = \frac{1}{2}\int_0^L \int_0^w \int_{-h/2}^{h/2} \left(\sigma_{xx}\varepsilon_{xx} + 2\sigma_{xz}\varepsilon_{xz} + 2m_{xy}\,\chi_{xy}\right) dz\, dy\, dx$$
$$= \frac{1}{2}\int_0^L \left(A_{xx}\left(\frac{\partial u}{\partial x}\right)^2 - 2B_{xx}\left(\frac{\partial u}{\partial x}\right)\left(\frac{\partial^2 w}{\partial x^2}\right) + D_{xx}\left(\frac{\partial^2 w}{\partial x^2}\right)^2 + l_m^2 A_{xz}\left(\frac{\partial^2 w}{\partial x^2}\right)^2 \right) dx \qquad \text{...(3.41)}$$

The following rigidities are defined. Where $\left(A_{xx}, B_{xx}, D_{xx}\right)$, and A_{xz} the extensional, couple, bending, and transverse shear rigidities, respectively.

$$\left(A_{xx}, B_{xx}, D_{xx}\right) = \int_A E(z)\left(1, z, z^2\right) dA \qquad \text{…. (3.42a)}$$

$$A_{xz} = \int_A G(z)\, dA \qquad \text{..…. (3.42b)}$$

The first variation of the strain energy in the microbeam can be obtained in terms of the displacement as follows:

$$\delta\int_0^t E_S\,dt=\int_0^t\int_0^L\left[\begin{array}{l}A_{xx}\left(\frac{\partial u}{\partial x}\frac{\partial\delta u}{\partial x}\right)-B_{xx}\left(\frac{\partial u}{\partial x}\right)\left(\frac{\partial^2\delta w}{\partial x^2}\right)-B_{xx}\left(\frac{\partial^2 w}{\partial x^2}\right)\left(\frac{\partial\delta u}{\partial x}\right)\\+\left(D_{xx}+l_m^2A_{xz}\right)\left(\frac{\partial^2 w}{\partial x^2}\frac{\partial^2\delta w}{\partial x^2}\right)\end{array}\right]dx\,dt \quad \text{.... (3.43)}$$

It is simplified as in Eqs. (A1.b). The general form of work done by the externally applied force is obtained as follows:

$$E_w=\int_0^L\left(f\,u+q\,w\right)dx \qquad \text{..... (3.44)}$$

Virtual work done by the externally applied loads is given as follow

$$\delta\int_0^t E_W\,dt=\int_0^t\int_0^L\left(f\,\delta u+q\delta w\right)dx\,dt \qquad \text{..... (3.45)}$$

Where (f) and (q) are the (x), and (z) components of the body forces per unit length respectively.

The kinetic energy (E_K) of the FG micro beam according to Euler-Bernoulli can be written as

$$E_k=\frac{1}{2}\int_0^L\int_0^A\rho(z)\left(\left(\frac{\partial u_x}{\partial t}\right)^2+\left(\frac{\partial u_z}{\partial t}\right)^2\right)dA\,dx \qquad \text{.....(3.46)}$$

the following formula for kinetic energy is simplified from (A1.c):

$$E_k=\frac{1}{2}\int_0^L\left[I_A\left(\left(\frac{\partial u}{\partial t}\right)^2+\left(\frac{\partial^2 w}{\partial t^2}\right)^2\right)-2I_B\left(\frac{\partial u}{\partial t}\right)\left(\frac{\partial^2 w}{\partial x\,\partial t}\right)+I_D\left(\frac{\partial^2 w}{\partial x\,\partial t}\right)^2\right]dx \qquad \text{.....}$$

(3.47)

Where the inertia coefficients appearing in Eq. (3.47) are defined as

$$\left(I_A,I_B,I_D\right)=\int_A\rho(z)\left(1,z,z^2\right)dA \qquad \text{..... (3.48)}$$

$\rho(z)$ is the mass density of the functionally graded microbeam. The variation of kinetic energy δE_K is simplified by integrating by part as Eq.(A1.d):

$$\delta E_k = \int_0^t \int_0^L \begin{pmatrix} I_A \frac{\partial u}{\partial t}\frac{\partial \delta u}{\partial t} + I_A\left(\frac{\partial w}{\partial t}\frac{\partial \delta w}{\partial t}\right) - I_B\left(\frac{\partial u}{\partial t}\frac{\partial^2 \delta w}{\partial x\,\partial t}\right) \\ -I_B\left(\frac{\partial^2 w}{\partial x\,\partial t}\frac{\partial \delta u}{\partial t}\right) + I_D\left(\frac{\partial^2 w}{\partial x\,\partial t}\frac{\partial \delta^2 w}{\partial x\,\partial t}\right) \end{pmatrix} dx dt \quad \ldots\ldots (3.49)$$

Hamilton's principle is used to analyze a physical system to obtain the governing equations of motion that are consist of (E_k) is the kinetic energy, (E_s) is the strain energy, and (E_w) is the work done exposed to externally applied loads, as follows

$$\delta \int_0^t \left[E_K - (E_S + E_w)\right] dt = 0 \quad \ldots\ldots (3.50)$$

After is used integrating by parts method as in Eqs. (3.43)(3.45)(3.49), and (3.50) setting the coefficient $\delta u, \delta w$, $\frac{\partial \delta w}{\partial x}$ to zero lead. The following are the equations of motion of FG-microbeam according to (MCST) are written as:

$$\delta u = 0, \quad -A_{xx}\frac{\partial^2 u}{\partial x^2} + B_{xx}\frac{\partial^3 w}{\partial x^3} - I_A\frac{\partial^2 u}{\partial t^2} + I_B\frac{\partial^3 w}{\partial x\,\partial^2 t} - I_D\frac{\partial^3 w}{\partial x\,\partial^2 t} + f = 0 \ldots. (3.51a)$$

$$\delta w = 0, \quad -B_{xx}\frac{\partial^3 u}{\partial x^3} + (D_{xx} + A_{xz} l_m)\frac{\partial^4 w}{\partial x^4} + I_B\frac{\partial^3 u}{\partial t^3} - I_A\frac{\partial^2 w}{\partial t^2} + q = 0 \quad \ldots. (3.51b)$$

$$\frac{\partial \delta w}{\partial x} = 0, \quad -B_{xx}\frac{\partial^2 u}{\partial x^2} + (D_{xx} + A_{xz} l_m)\frac{\partial^3 w}{\partial x^3} - I_B\frac{\partial^2 u}{\partial t^2} = 0 \quad \ldots. (3.51c)$$

The corresponding boundary conditions (consist part of Integration part) at the FG microbeam end are derived at 0< x < L as followed:

$$\delta u = 0 \quad or \quad A_{xx}\frac{\partial u}{\partial x} - B_{xx}\frac{\partial^2 w}{\partial x^2} \quad \ldots. (3.52a)$$

$$\frac{\partial \delta w}{\partial x} = 0 \quad or \quad -B_{xx}\frac{\partial u}{\partial x} + \left(D_{xx} + l_m^2 A_{xz}\right)\frac{\partial^2 w}{\partial x^2} \quad \ldots. (3.52b)$$

$$\delta w = 0 \quad or \quad -B_{xx}\frac{\partial^2 u}{\partial x^2}+\left(D_{xx}+l_m^2 A_{xz}\right)\frac{\partial^3 w}{\partial x^3} \qquad \text{..... (3.52c)}$$

The following are the equations of motion and boundary condition of FG-microbeam according to Classical beam theory (CBT) when the setting $(l_m = 0)$ is written as:

$$\delta u = 0, \quad -A_{xx}\frac{\partial^2 u}{\partial x^2}+B_{xx}\frac{\partial^3 w}{\partial x^3}-I_A\frac{\partial^2 u}{\partial t^2}+I_B\frac{\partial^3 w}{\partial x\,\partial^2 t}-I_D\frac{\partial^3 w}{\partial x\,\partial^2 t}=0 \qquad \text{.... (3.53a)}$$

$$\delta w = 0, \quad -B_{xx}\frac{\partial^3 u}{\partial x^3}+D_{xx}\frac{\partial^4 w}{\partial x^4}+I_B\frac{\partial^3 u}{\partial t^3}-I_A\frac{\partial^2 w}{\partial t^2}-q=0 \qquad \text{..... (3.53b)}$$

$$\frac{\partial \delta w}{\partial x} = 0, \quad -B_{xx}\frac{\partial^2 u}{\partial x^2}+D_{xx}\frac{\partial^3 w}{\partial x^3}-I_B\frac{\partial^2 u}{\partial t^2}=0 \qquad \text{..... (3.53c)}$$

The corresponding boundary conditions at the FG microbeam $(l_m = 0)$ are derived according to Euler-Bernoulli Classical beam theory (CBT) at $0 < x < L$ as followed:

$$\delta u = 0 \quad or \quad A_{xx}\frac{\partial u}{\partial x}-B_{xx}\frac{\partial^2 w}{\partial x^2} \qquad \text{..... (3.54a)}$$

$$\frac{\partial \delta w}{\partial x} = 0 \quad or \quad -B_{xx}\frac{\partial u}{\partial x}+D_{xx}\frac{\partial^2 w}{\partial x^2} \qquad \text{..... (3.54b)}$$

$$\delta w = 0 \quad or \quad -B_{xx}\frac{\partial^2 u}{\partial x^2}+D_{xx}\frac{\partial^3 w}{\partial x^3} \qquad \text{..... (3.54c)}$$

Another expression used the internal stress instead of the expression displacement in the internal strain energy through the EBBT and MCST to obtain the equations of governing motion.

$$\begin{aligned} E_s &= \int_0^L\int_0^w\int_{-h/2}^{h/2}\left(\sigma_{xx}\varepsilon_{xx}+2\sigma_{xz}\varepsilon_{xz}+2m_{xy}\,\chi_{xy}\right)dz\,dy\,dx \\ &= \int_0^L\int_0^w\int_{-h/2}^{h/2}\left(\sigma_{xx}\frac{\partial u}{\partial x}-\sigma_{xx}\,z\,\frac{\partial^2 w}{\partial x^2}-m_{xy}\,\frac{\partial^2 w}{\partial^2 x}\right)dz\,dy\,dx \end{aligned} \qquad \text{.....(3.55)}$$

The first variation of the internal strain energy of Euler- Bernoulli beam theory in terms of the internal stresses are defined as:

$$\delta\int_0^t E_S\,dt=\int_0^t\int_0^L\left[N\left(\frac{\partial u}{\partial x}\frac{\partial\delta u}{\partial x}\right)-\left(M+Y_{xy}\right)\left(\frac{\partial^2 w}{\partial x^2}\frac{\partial^2\delta w}{\partial x^2}\right)\right]dx\,dt \qquad \ldots.(3.56)$$

The equation for the internal stresses (3.56) is simplified by integrating by part as Eq.(A1.e), where the classical and non-classical stress resultants in above can be defined as:

$$N=\int_A\sigma_{xx}dA \qquad \ldots\ldots (3.57a)$$

$$M=\int_A z\sigma_{xx}dA \qquad \ldots\ldots (3.57b)$$

$$Y_{xy}=\int_A m_{xy}dA \qquad \ldots\ldots (3.57c)$$

Where N and M is devoted to classical of the normal stress and bending momentY_{xy} is non-classical coupling moment. Integrating by parts and setting the coefficient δu, δw to zero lead to the following boundary conditions are written below:

$$\delta u=0 \quad or \quad N\frac{\partial u}{\partial x}=0 \qquad 0<\text{x}<\text{L} \qquad \ldots.(3.58a)$$

$$\delta w=0 \quad or \quad \left(M+Y_{xy}\right)\frac{\partial^3 w}{\partial x^3}=0 \qquad 0<\text{x}<\text{L} \qquad \ldots.(3.58b)$$

$$\frac{\partial\delta w}{\partial x}=0 \quad or \quad \left(M+Y_{xy}\right)\frac{\partial^2 w}{\partial x^2}=0 \qquad 0<\text{x}<\text{L} \qquad \ldots.(3.58c)$$

Integrating by parts and setting the coefficient δu, δw to zero lead to the following equations of motion are written below:

$$\delta u=0, \quad or \quad +N\frac{\partial^2 u}{\partial x^2}+I_A\frac{\partial^2 u}{\partial t^2}+I_B\frac{\partial^3 w}{\partial x\,\partial^2 t}-I_D\frac{\partial^3 w}{\partial x\,\partial^2 t}=0 \qquad \ldots.(3.59a)$$

$$\delta w=0, \quad or \quad \left(M+Y_{xy}\right)\frac{\partial^4 w}{\partial x^4}+I_B\frac{\partial^3 u}{\partial t^3}-I_A\frac{\partial^2 w}{\partial t^2}-q=0 \qquad \ldots.(3.59b)$$

$$\frac{\partial\delta w}{\partial x}=0, \quad or \quad -\left(M+Y_{xy}\right)\frac{\partial^3 w}{\partial x^3}-I_B\frac{\partial^2 u}{\partial t^2}=0 \qquad \ldots.(3.59c)$$

3.7.2 First shear deformation beam theory (FSBT)

The first shear deformation theory is defined from the deformation of the beam in the following displacement field (u_x, u_z, ϕ) in cartesian coordinates (x, y, z) as follows:

$$\begin{aligned} u_x(x,z,t) &= u(x,t) - z\,\phi(x,t) \\ u_y &= 0 \\ u_z &= w(x,t) \end{aligned} \qquad \ldots. (3.60)$$

The FSDT is taken into concern shear deformation and, rotational bending for the micro-beam. The strain field of Timoshenko beam theory can be obtained from the used displacement equation Eqs. (3.60) in Equ. (3.26)

$$\varepsilon_{xx} = \frac{\partial u_o}{\partial x} - z\,\frac{\partial \phi}{\partial x}, \qquad \ldots\ldots (3.61a)$$

$$\varepsilon_{xz} = \left(-\phi + \frac{\partial w}{\partial x}\right), \qquad \ldots\ldots (3.61b)$$

$$\varepsilon_{yy} = \varepsilon_{zz} = \varepsilon_{xy} = \varepsilon_{yz} = 0 \qquad \ldots\ldots (3.61c)$$

By using Equ. (3.28) and (3.29) the rotation of the total banding vector can be calculated by displacements vector with the permutation symbol which affected the moment bending as :

$$\theta_y = \frac{1}{2}\left(\underset{=-1}{e_{yxz}}\,\frac{\partial u_z}{\partial x} + \underset{=+1}{e_{yzx}}\,\frac{\partial u_x}{\partial z}\right), \qquad \ldots\ldots (3.62)$$

$$= -\frac{1}{2}\left(\frac{\partial w}{\partial x} + \phi\right), \quad \theta_x = \theta_z = 0. \qquad \ldots\ldots (3.62)$$

The symmetric curvature tensor is obtained from Substitution of Eq. (3.62) into Eq. (3.27)

$$\chi_{xy} = -\frac{1}{4}\left(\frac{\partial^2 w}{\partial x^2} + \frac{\partial \phi}{\partial x}\right) ,$$

$$\chi_{xx} = \chi_{yy} = \chi_{zz} = \chi_{xz} = \chi_{yz} = 0 \quad \ldots.(3.63)$$

The strain energy formula for the micro-beams can be obtained from the Timoshenko Modified couple stress theory as follows:

$$\begin{aligned} E_S &= \frac{1}{2}\int_0^V \left[\sigma_{xx}\,\varepsilon_{xx} + 2\sigma_{xz}\,\varepsilon_{xz} + 2m_{xy}\,\chi_{xy} \right] dV \\ &= \frac{1}{2}\int_0^L \int_0^w \int_{-h/2}^{h/2} \left(E\,\varepsilon_{xx}{}^2 + 2\sigma_{xz}\,\varepsilon_{xz} + 2l_m^2 A_{xz}\,\chi^2{}_{xy} \right) dz\,dy\,dx \end{aligned} \quad \ldots. (3.64)$$

Another expression of the governing equation in terms the displacement. Where The strain energy formula of the micro-beams can be found classical normal force, classical moment, and classical shear force with the displacements and rotations field as follows:

$$E_s = \frac{1}{2}\int_0^L \int_0^w \int_{-h/2}^{h/2} \left(E\,\varepsilon_{xx}{}^2 + 4ks\,A_{xz}\,\varepsilon_{xz}{}^2 + 2l_m^2 A_{xz}\,\chi^2{}_{xy} \right) dz\,dy\,dx \quad \ldots(3.65)$$

where (ks) is the shear correction factor and can be simplified as Eq.(A2.a). The first variation of the strain energy in the microbeam in terms of the displacement is as follows:

$$\delta E_S = \int_0^L \begin{bmatrix} A_{xx}\left(\frac{\partial u}{\partial x}\frac{\partial \delta u}{\partial x}\right) - B_{xx}\left(\frac{\partial u}{\partial x}\frac{\partial \delta\phi}{\partial x}\right) - B_{xx}\left(\frac{\partial \phi}{\partial x}\frac{\partial \delta u}{\partial x}\right) + D_{xx}\left(\frac{\partial \phi}{\partial x}\frac{\partial \delta\phi}{\partial x}\right) \\ + k_s A_{xz}\,\phi\,\delta\phi - k_s A_{xz}\left(\phi\frac{\partial \delta w}{\partial x}\right) - k_s A_{xz}\left(\frac{\partial w}{\partial x}\delta\phi\right) + k_s A_{xz}\left(\frac{\partial w}{\partial x}\frac{\partial \delta w}{\partial x}\right) \\ + \frac{1}{4}l_m^2 A_{xz}\left(\frac{\partial \phi}{\partial x}\frac{\partial \delta\phi}{\partial x}\right) + \frac{1}{2}l_m^2 A_{xz}\left(\frac{\partial \phi}{\partial x}\frac{\partial \delta^2 w}{\partial x^2}\right) + \frac{1}{2}l_m^2 A_{xz}\left(\frac{\partial^2 w}{\partial x^2}\frac{\partial \delta\phi}{\partial x}\right) \\ + \frac{1}{4}l_m^2 A_{xz}\left(\frac{\partial^2 w}{\partial x^2}\frac{\partial \delta^2 w}{\partial x^2}\right) \end{bmatrix} dx \quad \ldots(3.66)$$

is simplified by integrating by part as Eq.(A2.b). Virtual work done by the externally applied loads is given as Eq.(3.45). The kinetic energy (E_K) of the FG micro beam according to Timoshenko beam theory (TDT) can be shown as (A2.c):

$$E_k = \frac{1}{2}\int_0^t \int_0^L \left[I_A\left(\frac{\partial u}{\partial t}\right)^2 + I_A\left(\frac{\partial w}{\partial t}\right)^2 - 2I_B\left(\frac{\partial u}{\partial t}\right)\left(\frac{\partial \phi}{\partial t}\right) + I_D\left(\frac{\partial \phi}{\partial t}\right)^2 \right] dx\,dt \quad \ldots.(3.67)$$

, Where the inertia coefficients (I_A, I_B, I_D) are calculated in Eq. (3.49).

The following formula gives the first variation of the kinetic energy based on the theory of the first-order shear deformation beam:

$$\delta\int_0^t E_k\,dt = \int_0^t\int_0^L \begin{bmatrix} I_A\left(\frac{\partial u}{\partial t}\frac{\partial \delta u}{\partial t}\right)+I_A\left(\frac{\partial w}{\partial t}\frac{\partial \delta w}{\partial t}\right)-I_B\left(\frac{\partial u}{\partial t}\frac{\partial \delta \phi}{\partial t}\right) \\ -I_B\left(\frac{\partial \phi}{\partial t}\frac{\partial \delta u}{\partial t}\right)+I_D\left(\frac{\partial \phi}{\partial t}\frac{\partial \delta \phi}{\partial t}\right) \end{bmatrix} dx\,dt \qquad .....(3.68)$$

is simplified by integrating by part as Eq.(A2.d). Hamilton's principle Eq.(3.51) is used to obtain the governing equations of motion for FSDBT in conjunction with modified couple stress theory (MCST) in terms of the displacements. At the beam ends ($x = 0$ and, $x = L$), the corresponding boundary conditions were determined.

$$\delta u \Rightarrow \quad A_{xx}\left(\frac{\partial u}{\partial x}\right)-B_{xx}\left(\frac{\partial \phi}{\partial x}\right)=0 \Leftrightarrow (u=0) \qquad ....(3.69a)$$

$$\delta w_x \Rightarrow -k_s A_{xz}(\phi+\frac{\partial w}{\partial x})+\frac{1}{4}A_{xz}l_m^2\left(\frac{\partial \phi}{\partial x}+\frac{\partial^2 w}{\partial x^2}\right)=0 \Leftrightarrow (w_x=0) \qquad ....(3.69c)$$

$$\delta\phi \Rightarrow -B_{xx}\left(\frac{\partial u}{\partial x}\right)+(D_{xx}+\frac{1}{4}A_{xz}l_m^2)\left(\frac{\partial \phi}{\partial x}\right)+ks\,A_{xz}\phi+\frac{1}{4}l_m^2A_{xz}\left(\frac{\partial^2 w}{\partial x^2}\right)=0 \Leftrightarrow (\phi=0) \quad ....(3.69d)$$

The following differential equations of motion for FSDBT are obtained by integrating by parts and setting the coefficients $\delta u, \delta w, and\ \delta\phi$ to zero, respectively are given below:

$$\delta u = 0,\ -A_{xx}\left(\frac{\partial^2 u}{\partial x^2}\right)+B_{xx}\left(\frac{\partial^2 \theta}{\partial x^2}\right)+I_A\left(\frac{\partial^2 u}{\partial t^2}\right)-I_B\left(\frac{\partial^2 \theta}{\partial t^2}\right) \qquad (3.70a)$$

$$\delta w = 0, \qquad -k_s A_{xz}\left(\left(\frac{\partial^2 w}{\partial x^2}\right)+\left(\frac{\partial \theta}{\partial x}\right)\right)-\frac{1}{4}l_m^2A_{xz}\left(\frac{\partial^4 w}{\partial x^4}+\frac{\partial^3 \theta}{\partial x^3}\right)+I_A\left(\frac{\partial^2 w}{\partial t^2}\right) \qquad (3.70b)$$

$$\begin{aligned}\delta\phi = 0,\ & B_{xx}\left(\frac{\partial^2 u}{\partial x^2}\right)-(D_{xx}+\frac{1}{4}A_{xz}l_m^2)\left(\frac{\partial^2 \phi}{\partial x^2}\right)-k_sA_{xz}(\frac{\partial w}{\partial x}) \\ & +\frac{1}{4}l_m^2A_{xz}\left(\frac{\partial^3 w}{\partial x^3}\right)-I_B\left(\frac{\partial^2 u}{\partial t^2}\right)+I_D\left(\frac{\partial^2 \phi}{\partial t^2}\right)=0\end{aligned} \qquad (3.70c)$$

Whereas for the classical continuum theory, the governing equations for FSDBT are given by putting and $l_m = 0$ in Eq. (3.70), as follow

$$\delta u \Rightarrow \quad A_{xx}\left(\frac{\partial u}{\partial x}\right) - B_{xx}\left(\frac{\partial \theta}{\partial x}\right) = 0 \Leftrightarrow (u = 0)$$

....(3.71a)

$$\delta w_x \Rightarrow -k_s A_{xz}(\phi + \frac{\partial w}{\partial x}) = 0 \Leftrightarrow (w_x = 0) \qquad \ldots.(3.71b)$$

$$\delta\phi \Rightarrow -B_{xx}\left(\frac{\partial u}{\partial x}\right) + D_{xx}\left(\frac{\partial \phi}{\partial x}\right) + ks\, A_{xz}\phi = 0 \Leftrightarrow (\phi = 0) \qquad \ldots.(3.71c)$$

Through the internal stresses, of the strain energy in the microbeam can be obtained as follows:

$$\delta\int_0^t E_S\, dt = \int_0^t\int_0^L \left[N\,\frac{\partial \delta u}{\partial x} + M\,\frac{\partial \delta\phi}{\partial x} + Q\left(\frac{\partial \delta w}{\partial x} - \delta\phi\right) - \frac{1}{2}Y_{xy}\left(\frac{\partial^2 \delta w}{\partial x^2} + \frac{\partial \delta\phi}{\partial x}\right)\right] dx\, dt \quad \ldots.(3.72)$$

As shown below, the classical stress results were represented by (N, M, Q) and the non-classical stress results (Y) which depended on the parameter of the material length (lm) according to MCST.

$$N = \int_A \sigma_{xx} dA = A_{xx}\frac{\partial u}{\partial x} - B_{xx}\frac{\partial \phi}{\partial x} \qquad \ldots\ldots (3.73a)$$

$$Q = \int_A K_s \sigma_{xz} dA = K_S A_{xz}\left(\frac{\partial w}{\partial x} - \phi\right) \qquad \ldots.. (3.73b)$$

$$M = \int_A z\sigma_{xx} dA = B_{xx}\frac{\partial u}{\partial x} - D_{xx}\frac{\partial \phi}{\partial x} \qquad \ldots.. (3.73c)$$

$$Y_{xy} = \int_A m_{xz} dA = 2\mu(z) l^2{}_m \chi_{xy} dA = -\frac{1}{2}A_{xz} l^2\left(\frac{\partial^2 w}{\partial x^2} + \frac{\partial \phi}{\partial x}\right) \qquad \ldots\ldots (3.73d)$$

Where (k_s) is the shear correction factor. Relying on Hamilton's principle of physical system analysis to obtain the equations of motion for FSDT are as follow:

$$\frac{\partial N}{\partial x} + f = -I_A\frac{\partial^2 u}{\partial t^2} + I_B\frac{\partial^2 \phi}{\partial t^2} \qquad \ldots. (3.74)$$

$$\frac{\partial Q}{\partial x} + \frac{1}{2}\frac{\partial^2 Y_{XY}}{\partial x^2} + q = I_A\frac{\partial^2 w}{\partial t^2} \qquad \ldots..(3.74)$$

$$\frac{\partial M}{\partial x}+\frac{1}{2}\frac{\partial Y_{XY}}{\partial x}-Q=+I_B\frac{\partial^2 u}{\partial t^2}-I_D\frac{\partial^2 \phi}{\partial t^2} \quad \ldots.(3.74)$$

3.8 Numerical solution

The Lagrange multiplier technique [23] where is the displacement functions are dependent to solve the governing equations with the B.C at $x=0,L$. As the product of the undetermined terms of the time-dependent generalized coordinates coefficients and known auxiliary functions. Below are meant to be displacement fields.

When functions of infinite dimensions can be described in terms of generalized coordinates, Hamilton's principle can be expressed as Lagrange equations. As a result, to apply the Lagrange equations, the displacement function $w(x,t),u(x,t),\varphi(x,t)$ is approximated by a series of acceptable functions that must fulfill the following necessary (geometric) boundary conditions[23]:

$$\begin{aligned} w(x,t)&=\sum_{m=1}^{N}A_m(t)\phi_m(x) & \phi_m(t)&=g_w(x)x^{m-1}\\ u(x,t)&=\sum_{m=1}^{N}B_m(t)\alpha_m(x) & \alpha_m(x)&=g_u(x)x^{m-1}\\ \varphi(x,t)&=\sum_{m=1}^{N}C_m(t)\beta_m(x) & \beta_m(x)&=g_f(x)x^{m-1} \end{aligned} \quad \ldots.(3.75)$$

Where $A_m(t), B_m(t)$ and $C_m(t)$ are indeterminate generalized coordinates to be calculated, and $g_w(x)$, $g_u(x)$ and $g_f(x)$ are auxiliary functions that are used to satisfy the essential boundary conditions. The auxiliary functions can be written in the following form[23]:

$$g_w(x)=\left(x+\frac{L}{2}\right)^{p_w}\left(x-\frac{L}{2}\right)^{q_w}$$
$$g_u(x)=\left(x+\frac{L}{2}\right)^{p_u}\left(x-\frac{L}{2}\right)^{q_u} \qquad \ldots\ldots(3.76)$$
$$g_f(x)=\left(x+\frac{L}{2}\right)^{p_f}\left(x-\frac{L}{2}\right)^{q_f}$$

Where p_i and q_i, $i=(u,w,f)$ are the boundary exponents that are related to the boundary conditions. The related values p_i and q_i are provided in Table (3.2) for the considered boundary conditions.

For Example $w(x,t)$ for studying the Bending of the FG micro-beam in this thesis, the derivatives of the time must be equal to zero and the external load represented by f and c vanish. where f is the x component of the body forces per unit length, c is the y component of the body couple per unit length.

On the other hand, the transverse force as distribution load represented by q is presented and the transverse displacements of the microbeam are determined for displacement $x=(L/2)$ as follow :

$$w(x,t)=\sum A_m(t)\phi_m(x) \quad ;$$
$$w(x,t)=\sum A_m(t)g_w(x)x^{m-1} \qquad \ldots(3.77)$$
$$w(x,t)=\sum A_m(t)\left(x+\frac{L}{2}\right)^{p_w}\left(x-\frac{L}{2}\right)^{q_w}x^{m-1}$$

the principle Lagrangian (L) shows the behavior of the beam's motion at a point in time. that represents the lowest value deformation of the object that results from the differential in kinetic energy (E_k) and subtracts from it the potential energy (Es). at various direction points as follows: pi and qi (i=w, u, f) are the boundary exponents that are related to the boundary conditions. The related values of pi and qi are provided in Table 3.2.

Table 3. 2: Boundary exponents for several microbeam types [23]

B.Cs	Left end			Right end		
	p_w	p_u	p_f	q_w	q_u	q_f
C-C	1	1	1	1	1	1
C-S	1	1	1	1	0	0
S-S	1	1	0	1	0	0
C-F	1	1	1	0	0	0

3.8.1 Numerical solution based on (EBBT)

The kinetic energy and strain energy according to (EBBT) in terms of the product of the undetermined terms of the time-dependent generalized coordinates coefficients can be written as:

$$E_k = \frac{1}{2}\int_0^t\int_0^L \left[I_A \left(B_m \alpha_m\right)^2 + I_A \left(A_m \phi_m\right)^2 - 2I_B \left(B_m \alpha_m\right)\left(A_m \phi'_m\right) + I_D \left(A_m \phi'_m\right)^2 \right] dx\, dt \quad \text{.....(3.78a)}$$

$$\delta E_k = \int_0^L \left[I_A \left(B_m \alpha_m \alpha_k + A_m \phi_m \phi_k\right) - I_B (B_m \alpha_m)(A_m \phi'_k) - I_B (A_m \phi'_m)(B_m \alpha_k) + I_D \left(A_m \phi'_m \phi'_k\right) \right] dx \quad \text{...(3.78b)}$$

$$E_s = \frac{1}{2}\int_0^L \left[A_{xx} \left(B_m \alpha'_m\right)^2 - 2B_{xx} \left(B_m \alpha'_m\right)\left(A_m \phi''_m\right) + D_{xx} \left(A_m \phi''\right)^2 + l_m^2 A_{xz} \left(A_m \phi''\right)^2 \right] dx \quad \text{.....(3.79a)}$$

$$\delta E_S = \int_0^L \begin{bmatrix} A_{xx} \left(B_m \alpha'_m \alpha'_k\right) - B_{xx} \left(B_m \alpha'_m\right)\left(A_m \phi''_k\right) - B_{xx} \left(A_m \phi''_m\right)\left(B_m \alpha'_k\right) \\ + D_{xx} \left(A_m \phi''_m \phi''_k\right) + A_{xz} l_m{}^2 \left(A_m \phi''_m \phi''_k\right) \end{bmatrix} dx \quad \text{.....(3.80b)}$$

$$E_w = -\int_0^L \left(f\,(\alpha_m B_m) + q(\phi_m A_m)\right) dx \quad \text{....(3.81a)}$$

$$\delta E_w = -\int_0^L \left(f\,(\alpha_k B_m) + q(\phi_k A_m)\right) dx \quad \text{....(3.81b)}$$

The equations of motion solution are depended on the EBBT and are utilized the Lagrange equations as follows:

$$\frac{d}{dt}\left(\frac{\delta E_k}{\delta \dot{\mathrm{X}}_k}\right) + \frac{\delta E_s}{\delta \mathrm{X}_k} + \frac{\delta E_w}{\delta \mathrm{X}_k} = 0 \qquad k = 1, 2, 3, ..., 3N \quad \text{....(3.82)}$$

the following abbreviations that refer in Eq.(3.82) are:

$$\begin{aligned} X_k &= A_k \qquad k = 1,2,.....,N \\ X_k &= B_{k-N} \qquad k = N+1,.....,2N \end{aligned} \qquad \ldots.(3.83)$$

Applying the Lagrange equations to find the solution equations of motion in the transverse displacements as shown below :

$$(1).\ \frac{d}{dt}\left(\frac{\delta E_k}{\delta A_k}\right)+\frac{\delta E_s}{\delta A_k}+\frac{\delta E_w}{\delta A_k}=0 \qquad k=1,2,3,.....,3N \qquad \ldots..(3.83)$$

$$\int_0^L \left[\begin{aligned} &I_A \ddot{A}_m \phi_m \phi_k - I_B \ddot{B}_n \alpha_m \phi_k' + I_D\left(\ddot{A}_m \phi_m' \phi_k'\right) - B_{xx}\left(B_m \alpha_m' \phi_k''\right) \\ &+(D_{xx}+A_{xz}\ell^2)\left(A_m \phi_m'' \phi_k''\right) - q\ \phi_k A_m \end{aligned}\right] = 0 \qquad .....(3.84)$$

Applying the Lagrange equations to find the solution equations of motion in the axial displacement as shown below:

$$(2).\ \frac{d}{dt}\left(\frac{\delta E_k}{\delta B_k}\right)+\frac{\delta E_s}{\delta B_k}+\frac{\delta E_w}{\delta B_k}=0 \qquad k=1,2,3,.....,3N \qquad \ldots.(3.85)$$

$$\int_0^L \left[I_A \ddot{B}_m \alpha_m \alpha_k - I_B \ddot{A}_m \phi_m' \alpha_k + A_{xx} B_m \alpha_m' \alpha_k' - B_{xx} A_m \phi_m'' \alpha_k' - f\ \alpha_k B_m\right] = 0 \qquad \ldots.(3.86)$$

The Eigenvalue problem represented the solution equilibrium governing of the micro-beam which determined stiffness matrix ,the coefficients parameter are calculated as follows:

$$\begin{aligned} K_{11} &= +\int_0^L (D_{xx} + \frac{1}{4} l_m^2 A_{xz})\, \phi_m'' \phi_K''\, dx, \\ K_{12} &= -\int_0^L B_{xx} \alpha_m' \phi_K''\, dx, \\ K_{21} &= -\int_0^L B_{xx} \alpha_k' \phi_m''\, dx, \\ K_{22} &= \int_0^L A_{xx} \alpha_m' \alpha_k' dx. \end{aligned} \qquad \ldots..(3.87)$$

And inertia matrix, the coefficients parameter are calculated as follows:

$$M_{11} = +\int_0^L (I_A \phi_m \phi_k dx + I_D \phi'_m \phi'_k) dx,$$
$$M_{12} = -\int_0^L I_B \alpha_m \phi'_k dx,$$
$$M_{21} = -\int_0^L I_B \phi'_m \alpha_k dx, \quad \ldots.(3.88)$$
$$M_{22} = \int_0^L I_A \alpha_m \alpha_k dx,$$

And the external forces matrix, the coefficients parameter are calculated as follows:

$$F_1 = \int_0^L q\ A_m \phi_k dx,$$
$$F_2 = \int_0^L f\ B_m \alpha_k dx = 0. \quad \ldots.(3.89)$$

For the free vibration, the coefficients of the eigenvalue problem are obtained by substituting Eq.(87) and Eq.(88) into Eq.(89) as follows.

$$\left(\begin{bmatrix} K_{11} & K_{12} \\ K_{12} & K_{22} \end{bmatrix} - \omega_n^2 \begin{bmatrix} M_{11} & M_{12} \\ M_{21} & M_{22} \end{bmatrix} \right) \begin{Bmatrix} A_n \\ B_n \end{Bmatrix} = \begin{Bmatrix} F_1 \\ F_2 \end{Bmatrix} \quad \ldots (3.90)$$

The free vibration response can be represented by the fundamental frequency(ω_n), which can obtain by a coefficient of matrix stiffness and matrix inertia from equation (3.90) when all the external forces are equal to zero.

For the static bending problem, the external force (f) is set to zero, and only the applied transverse load (q) represents the eigenvector. It is obtained by Eq.(3.91)when a coefficient of matrix inertia equals zero.

$$\begin{bmatrix} K_{11} & K_{12} \\ K_{12} & K_{22} \end{bmatrix} \begin{Bmatrix} A_n \\ B_n \end{Bmatrix} = \begin{Bmatrix} F_1 \\ F_2 \end{Bmatrix} \quad \ldots (3.91)$$

3.8.2 : Numerical solution based on FSBT

The Lagrange equations are employed on the solution of the motion equation that is dependent on the FSBT that referring in Eq. (3.97) and the following abbreviations that represent as follows:

$$\begin{aligned} X_k &= A_k \qquad k = 1,2,.....,N \\ X_k &= B_{k-N} \qquad k = N+1,.....,2N \\ X_k &= C_{k-2N} \qquad k = 2N+1,.....,3N \end{aligned} \qquad \ldots.(3.92)$$

The kinetic energy and strain energy according to (FSDT) in terms of the product of the undetermined terms of the time-dependent generalized coordinates coefficients can be written as:

$$E_s = \frac{1}{2}\int_0^L \begin{bmatrix} A_{xx}\left(B_m\alpha'_m\right)^2 - 2B_{xx}\left(B_m\alpha'_m\right)\left(C_m\beta'_m\right) + (D_{xx} + \frac{1}{4}l_m^2 A_{xz})\left(C_m\beta'_m\right)^2 + k_s A_{xz}\left(C_m\beta_m\right)^2 + \\ -2k_s A_{xz}\left(A_m\phi'_m\right)\left(C_m\beta_m\right) + k_s A_{xz}\left(A_m\phi'_m\right)^2 + \frac{1}{2}l_m^2 A_{xz}\left(A_m\phi''_m\right)\left(C_m\beta'_m\right) + \frac{1}{4}l_m^2 A_{xz}\left(A_m\phi''_m\right)^2 \end{bmatrix} dx \qquad \ldots(3.93)$$

$$E_k = \frac{1}{2}\int_0^L \left[I_A\left(\left(B_m\alpha_m\right)^2 + \left(A_m\phi_m\right)^2\right) - 2I_B\left(B_m\alpha_m\right)\left(C_m\beta_m\right) + I_D\left(C_m\beta_m\right)^2 \right] dx \qquad ....(3.94)$$

Applying the Lagrange equations to find the solution equations of motion as :

$$\frac{\partial L}{\partial A_k} = \int_0^L \begin{bmatrix} +k_s A_{xz}\left(A_m\phi'_m\phi'_k\right) + \frac{1}{4}A_{xz}l_m^2\left(A_m\phi''_m\phi''_k\right) + \frac{1}{4}l_m^2 A_{xz}\left(C_m\beta'_m\phi''_k\right) \\ -k_s A_{xz}\left(C_m\beta_m\phi'_k\right) + I_A\left(\ddot{A}_m\theta_m\theta_k\right) \end{bmatrix} dx \qquad .....(3.95)$$

$$\frac{\partial L}{\partial B_k} = \int_0^L \left[A_{xx}\left(B_m\alpha'_m\alpha'_k\right) - B_{xx}\left(C_m\beta'_m\alpha'_k\right) + I_A\left(\ddot{B}_m\alpha_m\alpha_k\right) - I_B\left(\ddot{C}_m\beta_m\alpha_k\right) \right] dx \qquad .....(3.96)$$

$$\frac{\partial L}{\partial C_k} = \int_0^L \begin{bmatrix} -k_s A_{xz}A_m\phi'_m\beta_k + \frac{1}{4}l_m^2 A_{xz}A_m\beta'_k\phi''_m - B_{xx}B_m\alpha'_m\beta'_k \\ +(D_{xx} + \frac{1}{4}l_m^2 A_{xz})C_m\beta'_m\beta'_k + k_s A_{xz}C_m\beta_m\beta_k - I_B\ddot{B}_m\alpha_m\beta_k + I_D\ddot{C}_m\beta_m\alpha_k \end{bmatrix} dx \qquad .....(3.97)$$

The Eigenvalue problem represented the solution equilibrium governing of the micro-beam which determined stiffness matrix; the coefficients parameter are calculated as follows:

$$K_{11} = +A_{xz}\int_0^L (k_s\phi'_m\phi'_k + \frac{1}{4}l_m^2\phi''_m\phi''_K)dx\,,$$
$$K_{12} = 0,$$
$$K_{13} = A_{xz}\int_0^L (-k_s\phi'_k\beta_m + \frac{1}{4}l_m^2\beta'_k\phi''_m)dx\,,$$
$$K_{21} = 0,$$
$$K_{22} = A_{xx}\int_0^L \alpha'_m\alpha'_k dx\,,$$
$$K_{23} = -B_{xx}\int_0^L \alpha'_k\beta'_m dx\,,$$
$$K_{31} = A_{xz}\int_0^L (-k_s\phi'_m\beta_k + \frac{1}{4}l_m^2A_{xz}\beta'_k\phi''_m)dx\,,$$
$$K_{32} = -B_{xx}\int_0^L \alpha'_m\beta'_k dx\,,$$
$$K_{33} = \int_0^L ((D_{xx} + \frac{1}{4}l_m^2)A_{xz}\beta'_m\beta'_k + k_sA_{xz}\beta_m\beta_k)dx$$

……(3.98)

And inertia matrix, the coefficients parameter are calculated as follows:

$$M_{11} = I_A\int_0^L \phi_m\phi_k dx\,,$$
$$M_{12} = M_{21} = M_{13} = M_{31} = 0,$$
$$M_{22} = I_A\int_0^L \alpha_m\alpha_k dx\,,$$
$$M_{23} = -I_B\int_0^L \beta_m\alpha_k dx\,,$$
$$M_{32} = -I_B\int_0^L \alpha_m\beta_k dx\,,$$
$$M_{33} = I_D\int_0^L \beta_m\beta_k dx\,.$$

……(3.99)

The external forces, the coefficients parameter are calculated as follows:

$$F_1 = q\int_0^L \phi_k dx$$

$$F_2 = f\int_0^L \alpha_k dx \qquad \text{….(3.100)}$$

$$F_3 = c\int_0^L \beta_k dx$$

The coefficients of the eigenvalue problem as represented equilibrium equation are obtained by substituting Eq.(3.98-3.100) into Eq.(3.101) as follows:

$$\left(\begin{bmatrix} k_{11} & 0 & k_{13} \\ 0 & k_{22} & k_{23} \\ k_{31} & k_{32} & k_{33} \end{bmatrix} - \omega_n^2 \begin{bmatrix} M_{11} & 0 & 0 \\ 0 & M_{22} & M_{32} \\ 0 & M_{23} & M_{33} \end{bmatrix}\right) * \begin{Bmatrix} A_n \\ B_n \\ C_n \end{Bmatrix} = \begin{Bmatrix} 0 \\ 0 \\ 0 \end{Bmatrix} \qquad \text{…(3.101)}$$

The fundamental frequency denoted to the free vibration response can be obtained by the coefficient of matrix stiffness and coefficient of matrix inertia from equation (3.101) in case the external forces are equal to zero.

For the static bending problem, where f is the x component of the body forces per unit length, and c is the y component of the body couple per unit length. are set to zero, and only the applied transverse load (q) is z components of the body forces per unit length, representing the eigenvector. It is obtained by Eq.(3.102) when a coefficient of matrix inertia equals zero.

$$\begin{bmatrix} k_{11} & 0 & k_{13} \\ 0 & k_{22} & k_{23} \\ k_{31} & k_{32} & k_{33} \end{bmatrix} \begin{Bmatrix} A_n \\ B_n \\ C_n \end{Bmatrix} = \begin{Bmatrix} F_1 \\ F_2 \\ F_3 \end{Bmatrix} \qquad \text{… (3.102)}$$

CHAPTER FOUR: RESULTS AND DISCUSSIONS

4.1: Verification of the Present Results

Ahead of doing detailed parametric analysis, the current formulation's results are validated by comparing them to existing literature.

4.1.1: Accuracy of the results of free vibration of FG-microbeam

The convergence of the results of the modified couple stress theory of the free vibration response of the FG-microbeam was made and compared with Ref. [27]. Ensure the precision of the thesis's results, which are based on the numerical method known as Langrage multiples, and implemented in the Matlab programming language. Table (4.1) shows a good convergence of the results, the results seemed to prove after the sixth grid ($N = 6$). six grids were adopted in a study.

Table 4. 1: Accuracy of the fundamental dimensionless frequency $\bar{\omega}=\omega L^2 \Big/ h\sqrt{\rho_m/E_m}$ *of FG micro-beam with various aspect ratios, gradient index,* $f=0.3$.

L/h	Theory	Number of grids					Ref. [27]
		5	6	7	8	9	
10	EBBT	12.893	12.889	12.889	12.889	12.889	12.9004
	FSDT	12.598	12.596	12.596	12.596	12.596	12.6058
100	EBBT	12.956	12.956	12.956	12.956	12.956	12.9565
	FSDT	12.957	12.953	12.953	12.953	12.953	12.9533

4. 4.1.2: Comparison of the numerical result

4.1.2.1.1: Comparison of static of FG-microbeam

Comparison of the transverse deflection shows in Table (4.2). The static obtained by using Euler -Bernoulli beam theories (EBBT) and Timoshenko beam theories (TBT) according to modified couple stress

theory when the material length scale parameter (l_m) equal to zero, with different aspect ratios and power-law indexes.

The following data of the material properties of FG micro-beam is taken from Ref. [27] as follow:

Steel : $E_m = 70$ GPa,, $\rho_m = 2702\,\mathrm{kg/m^3}, \nu_m = 0.3$

Alumina (Al_2O_3) : $E_c = 427$ GPa, $\rho_c = 3100\,\mathrm{kg/m^3}, \nu c = 0.17$

Table 4. 2: Dimensionless transverse deflection, $\left(\bar{w} = 100w\,(E_m I/qL^4)\right)$ *of the functionally graded simply microbeam of FG microbeams (EBBT) and (FSDT).*

(h/lm)	Method	L/h=10			L/h=100		
		f=1	f=3	f=10	f=1	f=3	f=10
1	Ref. [27]	0.0859	0.1262	0.1698	0.0859	0.1262	0.1698
	EBBT	0.086	0.1263	0.1699	0.086	0.1264	0.17
	Ref. [27]	0.0902	0.133	0.1797	0.086	0.1263	0.1699
	FSDT	0.0902	0.1331	0.1798	0.0861	0.1264	0.1701
2	Ref. [27]	0.2227	0.3068	0.3939	0.2227	0.3068	0.3939
	EBBT	0.2228	0.3069	0.394	0.2231	0.3073	0.3945
	Ref. [27]	0.2292	0.3175	0.4095	0.2228	0.3069	0.394
	FSDT	0.2293	0.3176	0.4096	0.2232	0.3074	0.3946
4	Ref. [27]	0.3698	0.4776	0.5876	0.3698	0.4778	0.5878
	EBBT	0.37	0.4778	0.5878	0.371	0.4791	0.5894
	Ref. [27]	0.3794	0.4928	0.6093	0.3699	0.4778	0.5878
	FSDT	0.3795	0.493	0.6096	0.2232	0.4792	0.5896
8	Ref. [27]	0.4429	0.5548	0.67	0.4429	0.5548	0.67
	EBBT	0.4432	0.5552	0.6704	0.4456	0.5582	0.6499
	Ref. [27]	0.4542	0.5723	0.6946	0.443	0.555	0.6702
	FSDT	0.4545	0.5727	0.6951	0.4457	0.5584	0.6743
0	Ref. [27]	0.4741	0.5864	0.7028	0.4741	0.5864	0.7028
	EBBT	0.4742	0.5865	0.7029	0.4745	0.5869	0.7034
	Ref. [27]	0.4862	0.6049	0.7286	0.4743	0.5866	0.731
	FSDT	0.4863	0.605	0.7288	0.4747	0.5871	0.7037

Table (4.2) reveals a high degree of convergence between this work and Ref.**[27]**

4.1.2.1.2: Comparison of the free vibration of FG-microbeam

The following comparison, for the natural frequency of the FG microbeam according to the MCST. $(l_m = 0)$ and $(l_m \neq 0)$ are shown in Tables (4.3) and Table (4.4) respectively as follows.

Table (4.3) shows the frequency of FG-microbeam is obtained by using Timoshenko beam theory and Modified couple stress theory when the material length scale parameter (l_m) is equal to zero. This means that the Modified Couple Stress Theory (MCST) performs similarly to the classical beam theory. The dimensionless fundamental frequency $(\bar{\omega})$ results from Ref. **[11]** are gotten from the Chebyshev collection method (CCM) with Timoshenko beam theory (TBT). The material properties for the beam consisted of Aluminum and alumina.

$E_m = 70$ GPa, $\rho_m = 2702$ kg/m^3, $\nu_m = 0.3$
$E_c = 380$ GPa, $\rho_c = 3960$ kg/m^3, $\nu_c = 0.3$

Table 4. 3: Convergence of first three dimensionless frequencies for FGM microbeams at aspect ratio (L/h=20), and various power-law index, TBT, $\bar{\omega} = \omega L^2 / h\sqrt{\rho_m / E_m}$.

B.Cs	f	Mode	ω_1	ω_2	ω_3
Clamped-Clamped	0	Present	12.2201	32.9705	62.8988
		Ref. [11]	12.2201	32.9705	62.8986
		Ref. [53]	12.2235	-	-
	1	Present	9.4292	25.5042	48.7963
		Ref. [11]	9.4292	25.5042	48.7961
		Ref. [53]	9.4314	-	-
	2	Present	8.602	23.2551	44.4638
		Ref. [11]	8.602	23.2551	44.4636
		Ref. [53]	8.604	-	-

The second comparison with Ref [33]. The fundamental frequency of the free vibration of the FG-micro beam obtained vai using MCST with different values of the material length scale parameter ratio $(h/l_m = 1,4,0)$. The models of FG micro-beam are the bottom surface contains ceramic-rich (silicon carbide) and the top surface is metal-rich (aluminum). The mechanical properties are studied by the More Tanaka technique .

$$E_m = 70 \text{ GPa}, \quad \rho_m = 2702 \text{ kg/m}^3, \quad \nu_m = 0.3$$
$$E_c = 427 \text{ GPa}, \quad \rho_c = 3100 \text{ kg/m}^3, \quad \nu_c = 0.17$$

Table 4. 4: Comparison of the dimensionless natural frequency $\bar{\omega} = \omega L^2/h\sqrt{\rho_m/E_m}$ *of FG microbeams (EBBT) and (FSDT) based on MCST for various gradient index (f) and material length scale parameters (h/lm)at slenderness ratio* $L/h = (10,100)$ $(l_m = 17.6\mu m)$ [17]. $(b = 2h)$. *B.C(SS)*

h/l_m	Method	L/h=10			L/h=100		
		f=1	f=3	f=10	f=1	f=3	f=10
1	EBBT	10.648	8.942	7.8011	10.699	8.9845	7.8348
	Ref.[33]	10.627	8.9257	7.7965	10.699	8.9844	7.8349
	FSDT	10.398	8.711	7.5835	10.696	8.982	7.8325
	Ref.[33]	10.381	8.6979	7.5799	10.696	8.919	7.8325
4	EBBT	5.1348	4.5978	4.1945	5.159	4.6195	4.2126
	Ref.[33]	5.1263	4.5907	4.1924	5.1589	4.6195	4.2127
	FSDT	5.0692	4.5256	4.1184	5.1583	4.6187	4.2118
	Ref.[33]	5.0613	4.5192	4.1165	5.1582	4.6187	4.2119
0	EBBT	4.5348	4.1494	3.8353	4.5561	4.1619	3.8519
	Ref.[33]	4.5274	4.1431	3.8334	4.5561	4.169	3.8519
	FSDT	4.4775	4.0848	3.7661	4.5555	4.1684	3.8512
	Ref.[33]	4.4775	4.079	3.7644	4.5555	4.1684	3.8512

Table (4.4), is shown the convergence of the results of the dimensionless fundamental frequency of size-dependent microbeam with the **Ref.**[33] when adopting MCST with (EBBT) (FDSBT) .

The results of the dimensionless natural frequency based on beam theories are given in Table (4.3), and Table (4.4). Fairly well agreement between the present results and the results in **Refs. [11],[53]** and **Ref.[33],** respectively are observed. This clearly shows the reliability of the present solution method for studying the size effect analysis of FG microbeam.

4.1.2.2: Compared the static and free vibration analysis for FG porous microbeam.

The effect of porosity on the dimensionless deflection of FG porous is shown in Table (4.5), using the imperfect beam model (FGM-I), using (MCST) with the material length scale parameter equal to zero, so is done that to get classical beam theory (CBT) for comparison. The material features of the beams include a high concentration of steel on the bottom surfaces of the FG beams. Additionally, alumina (Al_2O_3), a ceramic material, is abundant on the top surfaces of the FG beams. The material properties with porosity can be represented by a function that depends on the thickness of the FG beam and changes smoothly according to a modified rule of mixture law. The following material qualities are incorporated into the design:

Steel: $E_m = 210\ \text{GPa},\ \rho_m = 7800\,\text{kg/m}^3,\ \nu_m = 0.3$

Alumina (Al_2O_3): $E_c = 380\ \text{GPa},\ \rho_c = 3960\,\text{kg/m}^3,\ \nu_c = 0.3$

Table (4.5) compares dimensionless natural frequencies obtained using various power-law indexes and porosity indexes. the Ref.[37].It

depended on the Finite Element Method (FEM) for the solution. The result of the comparison is satisfactory with Ref.[37].

Table 4 .5: Comparison of non-dimensional transverse deflection and fundamental frequency of the functionally graded porous beam Model (FGM-I) with the distributed load, EBT, B.Cs (SS)

	f	$\bar{w} = 100w\,(L/2)(E_c I/qL^4)$				$\bar{\omega} = \omega L^2 * \sqrt{\rho_c A/E_c I}$			
		$\alpha = 0$	$\alpha = 0.05$	$\alpha = 0.1$	$\alpha = 0.2$	$\alpha = 0$	$\alpha = 0.05$	$\alpha = 0.1$	$\alpha = 0.2$
Ref. [37]	**0**	**1.3056**	**1.3707**	**1.3872**	**1.5500**	**9.9679**	**9.9268**	**10.5842**	**10.6858**
Present		**1.3021**	**1.3547**	**1.4117**	**1.5414**	**9.8692**	**10.056**	**10.2716**	**10.8182**
Ref. [37]	**1**	**1.6965**	**1.8020**	**1.8920**	**2.1362**	**7.0451**	**7.0434**	**7.0067**	**7.0274**
Present		**1.7250**	**1.8214**	**1.9295**	**2.1913**	**7.0366**	**7.0258**	**7.0137**	**6.9800**
Ref. [37]	**4**	**1.8917**	**2.0139**	**2.0352**	**2.4619**	**6.1449**	**6.1429**	**6.0844**	**6.0133**
Present		**1.9244**	**2.0450**	**2.1822**	**2.5232**	**6.0920**	**6.0372**	**5.9762**	**5.8300**
Ref. [37]	**8**	**2.0139**	**2.1520**	**2.1987**	**2.6736**	**5.8237**	**5.7839**	**5.6840**	**5.5431**
Present		**2.0185**	**2.1497**	**2.2994**	**2.6733**	**5.8092**	**5.7447**	**5.6736**	**5.5059**

4.1.2.3: Compared The Static Analysis of FG-SWCNT microbeam

The work seeks to identify the lowest central deflection for microbeam reinforced by an SWCNT, based on the Modified Couple Stress Theory and First shear deformation theory. Several factors affect the bending behavior, including volume fraction CNT, SWCNT distributions types, aspect ratio (L/h), boundary condition, and material length parameter ratio (h/lm). In this study, the following material properties are dependent on Ref. [42]. It is used the Polymethyl methacrylate (PMMA) properties and CNTs type of armchair (10,10) is chosen as reinforcements :

$(\text{PMMA}): E_m = 2.5\ \text{GPa},\ \rho_m = 1190\,\text{kg.m}^{-3}\ \ \upsilon^m = 0.3$

$(\text{CNTs}): E_{11}^{cnt} = 5646.6\ \text{GPa}, E_{22}^{cnt} = 7080\ \text{GPa},\ \rho^{cnt} = 2100\ \text{kg.m}^{-3}\ ,\ \upsilon^{CNT} = 0.17$

Also, Efficiency parameters FG-CNTRC $\eta_i\ (i = 1,2,3)$ are estimated, for example, as Table (3.1). Table (4.6) Compares the dimensionless transverse deflection of the FG-CNT microbeam for various aspect ratios, volume CNT fractions, and material length parameters $(l_m = 0)$ and $(h = 17.6\mu m)$ As can be seen the good result, the results of this study parallel those of Ref.[50] and, Ref.[49], respectively

Table 4. 6: Dimensionless transverse deflection $\bar{w} = 100E_m h^3/q_o L^4 w$ *of FG-CNT micro-beams with B.Cs(C-C),* $b=2h,\ L/h = 15\ , k_s = 5/6.$

V_{CNT}	0.12			0.17			0.28		
L/h	10	15	20	10	15	20	10	15	20
Ref.[49]	0.7037	0.5217	0.4580	0.4485	0.3421	0.3049	0.3254	0.2337	0.2016
Ref.[50]	0.704	0.524	0.461	0.449	0.344	0.307	0.325	0.235	0.203
Present	0.6829	0.5036	0.4408	0.4422	0.3360	0.2988	0.3298	0.2352	0.2021

The second comparison is the verification of the fundamental frequency of the FG-SWCNT microbeam.

The mechanical behavior of the FG-SWCNTRC micro-beam is obtained by (TBT) and (MCST). The length material parameter is zero. The material properties from polymethyl methacrylate referred to PMMA, and reinforced by the armchair (10,10) of SWCNTs, as the following, Ref.**[42]** : $E_m = 2.5\ \text{GPa},\ \ \rho_m = 1190\,\text{kg/m}^3$

$$E_{11}^{cnt} = 5646.6\ \text{GPa}, E_{22}^{cnt} = 7080\ \text{GPa},\ \ \rho^{cnt} = 2100\,\text{kg/m}^3$$
$$h = 17.6\times10^{-6}\ \text{m},\ \ b = 2h,\ \ L = 15h$$

Table (4.7), shows the first three natural frequencies for boundary conditions (Clamped-Clamped). An excellent agreement, between present discoveries the numerical solutions. The references **[40], [42]**and **[45]** are utilized (GDQ), Ritz methods, and Finite element method(FEM) are revealed.

Table 4. 7: First three natural frequencies of FG-SWCNT beam with various types of FG-SWCNT distribution, $(FSDT)$ $L/h=15$ *with,* $vcnt=0.28$ $l_m=0$ *B.C.(C-F)*

B.C	Model No.	LMM (present)	FEM (Ref.[45])	p-Ritz (Ref.[42])	GDQM (Ref.[40])
FG-X	1	0.6596	0.6566	0.6566	0.6586
	2	2.6533	2.6797	2.6763	2.6987
	3	5.4967	5.5759	5.5589	5.6150
-UD	1	0.5725	0.5601	0.56	0.5612
	2	2.4429	2.4482	2.4449	2.4614
	3	5.1642	5.2175	5.2005	5.2446
FGM-V	1	0.4880	0.4754	0.4753	0.4761
	2	2.2701	2.2578	2.2543	2.2685
	3	4.9624	4.9767	4.9590	5.0007

4.2 Numerical results of static bending analysis

This section examines the behavior of transverse deflection for three models of FG microbeams as follows: material gradation model, porous material model, and Polymer model reinforced by gradation of carbon nanotube. This study, is intended to show the accuracy of the prediction of the deflection of micro-size through the use of Modified Coupled Stress Theory (MCST) and Classical Beam Theory (CBT), Observe the effect of various factors on the FG-micro.

4.2.1: FG-material microbeam

Functionally graded microbeam model as shown in Figure (3.1) is made from silicon carbide (SiC) and aluminum (Al), the data are taken from the Ref.[27] . The studying of static deflection of the beam is presented via exploring the effects of many effective parameters on FG-microbeam as follows:

4.2.1.1: Effect of The aspect ratio (L/h)

From Table (4.2), when the aspect ratio $(L/h=100)$ increases, the static deflection of EBBT remains constant at the same value as the power-law index (f). Meanwhile, the static deflection of the FSDT increases as a result of the reduction in shear deformation. In the end, the result of FSDT close to EBBT deformation is becoming more apparent.

(Aspect ratio) and shear deformation (bending rotation angle) These parameters characterize the first shear deformation theory, which enables it to find the deflection of the thick micro beam where the bending rotation generated by the shear deformation can be calculated. With a decrease in length to thickness, the rotation of the beam decreases until it disappears, thus returning to the Euler-Bernoulli beam theory.

4.2.1.2: Effect of The power law index (f)

Table (4-2) shows the increasing transverse deflection of FG-micro-beam when the power-law index (f) increases. The reason is shown in Figure (4.1) where the power-law index $(f=0)$ means that full ceramic i.e. high young modulus and lowest elastic beam. The power-law index $(f=100)$ means a low young modulus and high elastic beam.

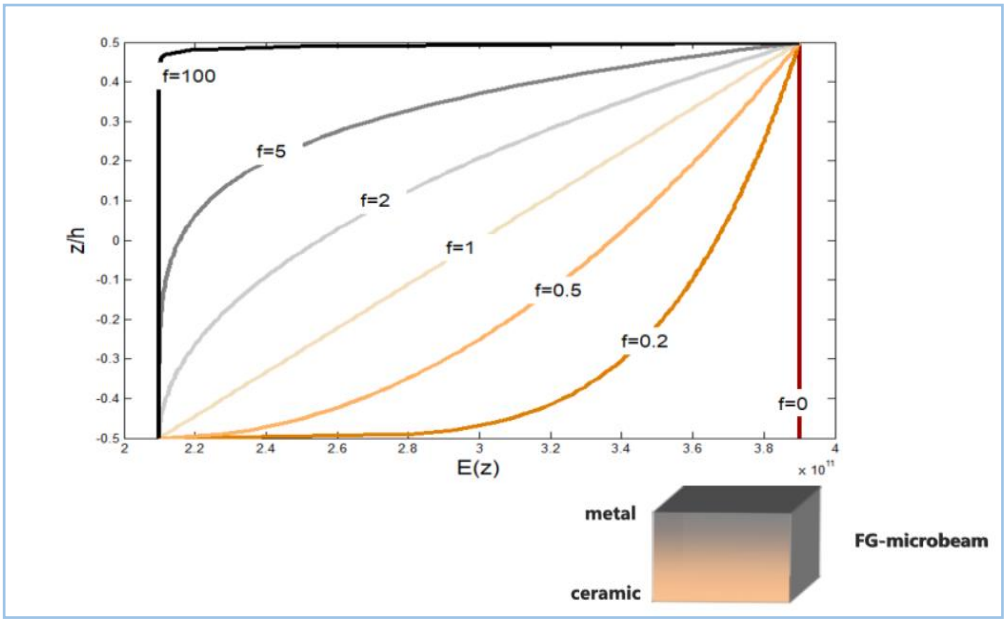

Figure 4. 1: Variation of Young's modulus of ceramic to the metal via thickness for FG micro-beam

4.2.1.3: Effect of Mori-Tanaka and rule of mixture method

Both the Mori Tanaka Technique and the rule of mixture method are used in this study to investigate the mechanical properties of the FG beam. But it is preferable to rely on Mori Tanka in studying the properties of the FG microbeam, the reason is shown in Figure (4.2). This figure shows the ability to estimate the largest static dimensionless deflection. And it turns out that different estimation methods for material properties have different effects on the dimensionless static deflection. Consequently, the Mori Tanaka technique yields greater results than the rule of the mixture. This is due to the good ability of Mori Tanaka's technique in studying and predicting the material properties for beams in micro size.

In general, it is deduced from Figure (4.2): First, a higher gradient index (f) is meaning more deflection. When the gradient index (f) is increased, the transverse deflection of the FG micro beam increases

because the mechanical properties changed from ceramic to metal along the thickness direction. As the small modulus of the FG micro beam changes from ceramic $(E_c = 427\ \mathrm{GPa})$ which is less flexible compared to metal $(E_m = 70\ \mathrm{GPa})$.

Second, it is noticed that the transverse deflection of the microbeam FG at a value $(h/lm = 1)$, is greater than a value $(h/lm = 8)$, this is due to the length material parameter ratio that governs the couple stress theory is decreasing (h/lm), means that increase (l_m), . It means the large ability of modified couple stress theory to predict the small deflection.

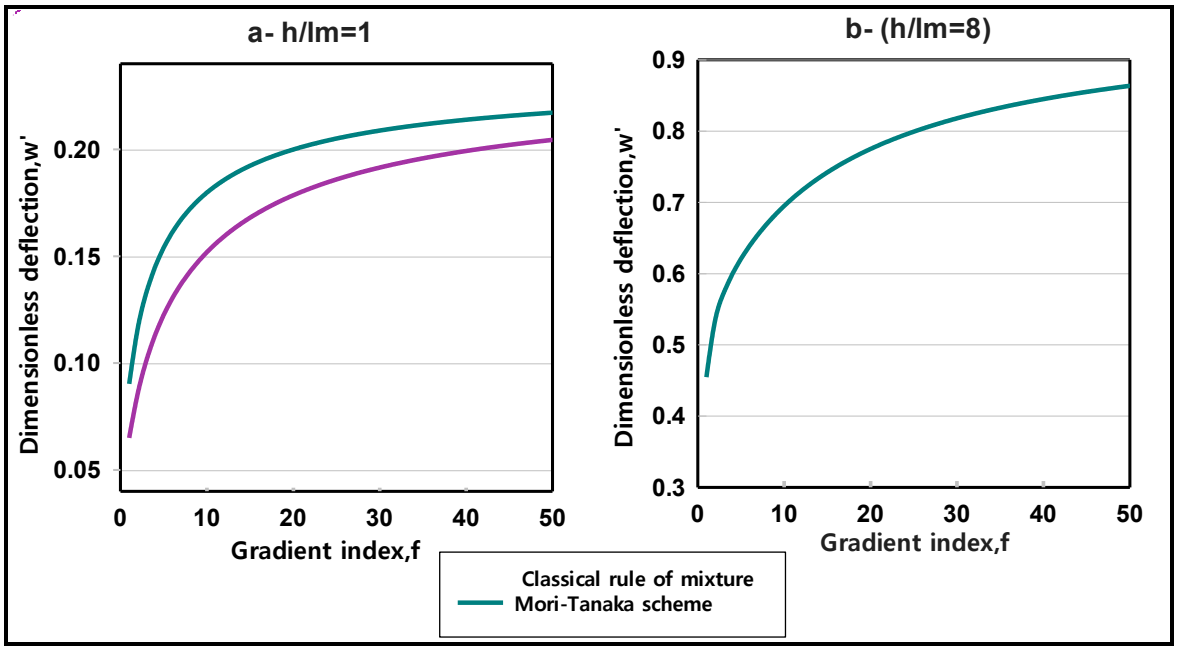

Figure 4. 2: Variation of dimensionless transverse deflection of the FG-micro-beam according to two rules a material model with the gradient index

4.2.1.4: Effect of the Poisson effect

(Ma et al., 2008) is found that adding Poisson's coefficient $[1-\upsilon(z)]/[1+\upsilon(z)][1-2\upsilon(z)]$ to the elasticity equation $E(z)$ reduces the results error. The stiffness values FG of the elasticity modulus $E(z)$ is modified to $(A_{xx}, B_{xx}, D_{xx}) = \int_A [E(z) * [1-\upsilon(z)]/[1+\upsilon(z)][1-2\upsilon(z)]](1, z, z^2) dA.$

this adding to the equation of the elastic modulus, leading to an improvement in the stiffness values of the FG microbeam.Ref.[27]

Figure (4.3) when increasing the gradient index, the static deflection **with** the Poisson effect is small compared **without** Poisson effect whether the classic beam or the microbeam. The reason is, The Poisson ratio parameter $(\upsilon_m = 0.3)$ for the Poisson effect is metal only, and It is known the metal of the Poisson ratio $(\upsilon_m = 0.3)$ is higher than the metal of the Poisson ratio $(\upsilon_c = 0.17)$ therefore static deflection with passion effect is decreased and the FG microbeam is more stiffness according to the mathematical relationship between stiffness and the Poisson effect. It is noticed that the deflection increases with the increase of the gradient index. The reason is the increase in the gradient index indicates a gradual decrease in the modulus of elasticity from ceramic (high hardness) to metal (low hardness) for FG microbeams. An increase in the Poisson effect is needed when the length material parameter ratio increases $(h / lm = 8),$ while $(h / lm = 1),$ the Poisson effect is less needed, as shows in Figure. (4.3).

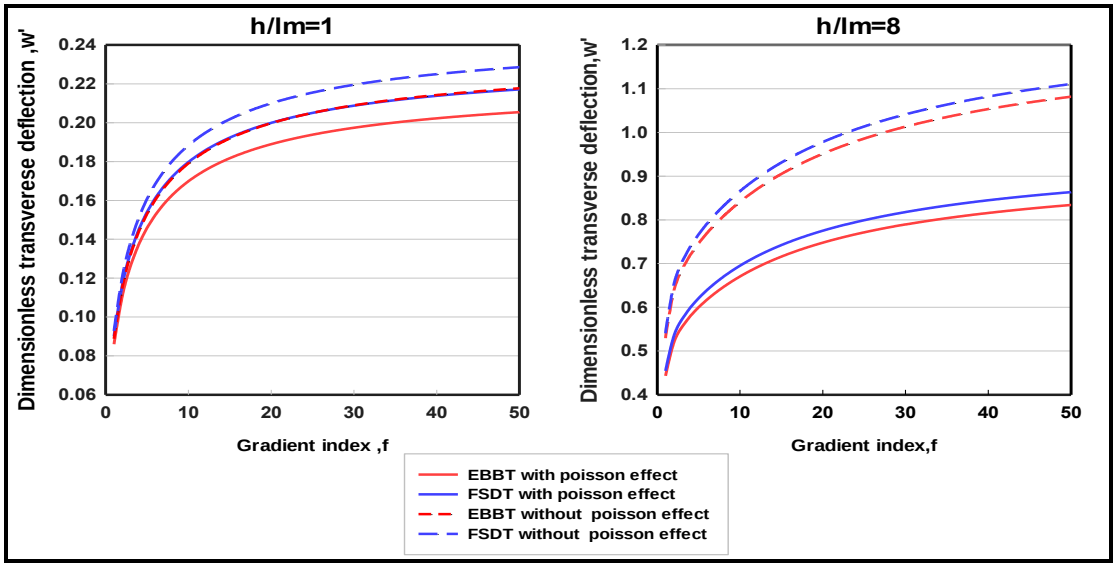

Figure 4. 3: Poisson effect on the variation of dimensionless transverse deflection of the FG micro-beam at (a) h = lm, (b) h = 8lm.,(L/h=10)

4.2.1.5: Effect of a length material scale parameter (lm)

The transverse deflection of FG-microbeam is studied by increasing of length material scale parameter ratio (h/lm). The transverse deflection predicted by (EBBT,FSDT) of modified couple stress theory (MCST) is always less than the transverse deflection predicted by (EBBT,FSDT) classical beam theory (CBT) in studying microbeams. Also, the length material parameter ratio increases due to a loss of reliability in the interpretation of static deflection of FG-micro-beams so which is similar to classical beam theory (CBT).it appears in Figure (4.4)

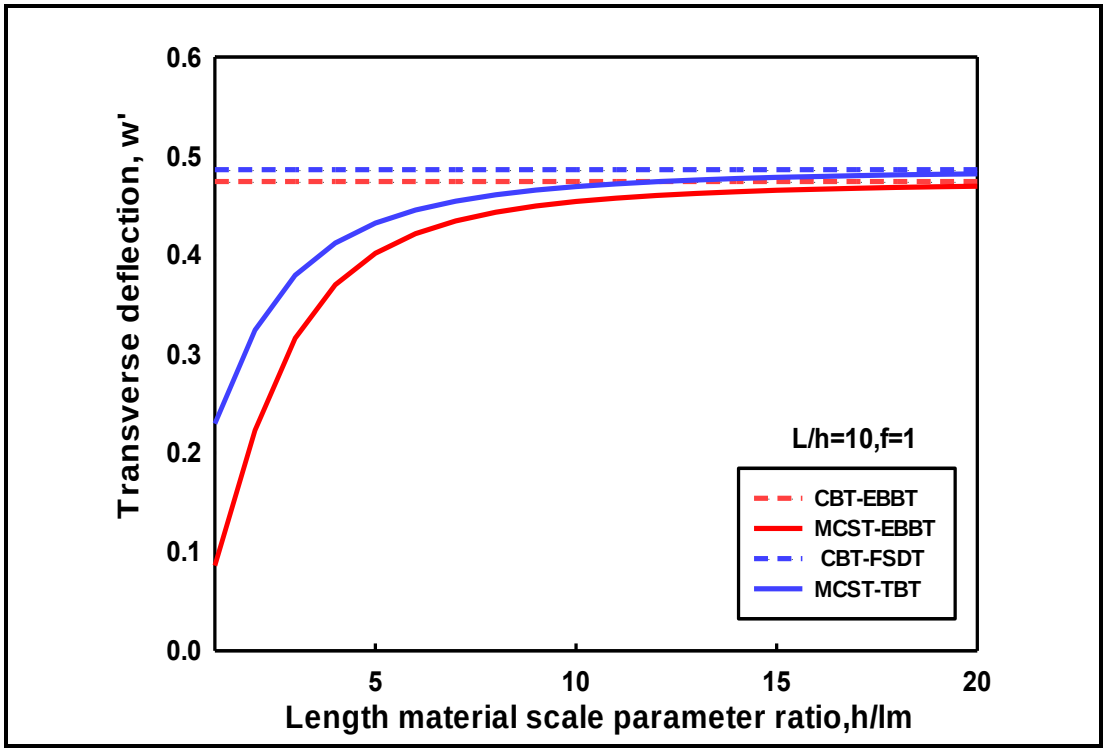

Figure 4. 4: Variation of the dimensionless transverse deflection of the FG micro-beam according to (EBBT, FSDT) of MCST, CBT with increasing the length material parameter ratio.

4.2.1.6: Effect of using MCST and CBT

To explore the size effect, it used a function of the dimensionless length material parameter ratio (h/lm), to study the behavior of the dimensionless static deflections for FG-microbeam. It can be seen that the deflection predicted by the modified couple stress theory (MCST) is always smaller than those of the classical beam theory(CBT). As shown in Figures (4.4), the difference in the static deflection of Euler-Bernoulli and First shear deformation beam theories of (MCST) and (CBT) for microbeams, especially when (h/lm), is small due to the high ability of the modified couple stress theory (MCST) to predict the least amount of deflection. This feature disappears on increment the dimensionless length material parameter ratio (h/lm), and its ability to predict

deflection is somewhat similar to classical beam theory, which offers unreliable solutions for microbeams. In general, the behavior of the modified couple stress theory can be defined by three parameters: The length material scale parameter (lm) and The length material scale parameter ratio $\left(\frac{lm}{h}\right)$, which are directly proportional to the theory, and this means that the increase of each of (lm) and The length material to thickness ratio$\left(\frac{lm}{h}\right)$, indicates that the theory can predict the deformation of micro structures. Whereas The length material scale parameter ratio $\left(\frac{h}{lm}\right)$ increases, the less the MCS theory's ability to predict deformation becomes, and it becomes similar to the classical theory(CBT) that lacks a parameter (lm)**.**

4.2.2: Static bending of FG- porous microbeam

The presence of pores in the FG-micro beam is assumed as a manufacturing defect produced. The modified rule of mixture estimating FG material microbeam effective properties with porous. In this work, three models are used to study the porosity of the FG-micro beam. Denoted by FGM-II, the FG-micron beam has an uneven pore distribution as the pores collect in the center of the cross-section. Figure (4.5) shows two porosity models (FGM-I, FGM-II).

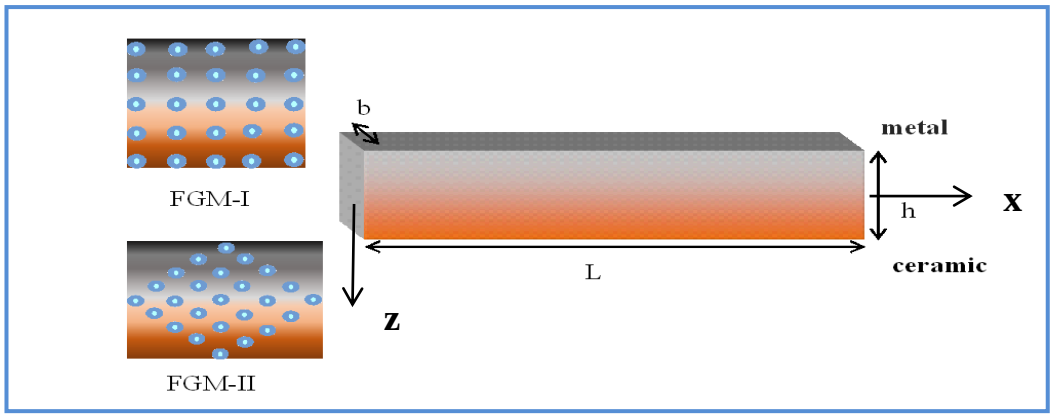

Figure 4. 5: Functionally Graded of micro-beam with two imperfect cross-section models (FGM-I, FGM-II)

Dimensionless transverse deflection $(\bar{w} = 100 w\, E_m I / q_o L^4)$ of the FG-porous microbeam is studied by the Euler Bernoulli and First shear deformation theory vai Modified Couple Stress Theory (MCST). Many variables affecting on three models are studied**.** Their material properties are taken from ref [11].

Aluminum (Al) $(E_m = 70\ \text{GPa},\ \rho_m = 2702\ \text{kg/m}^3\ \nu_m = 0.3)$;

Alumina (Al_2O_3) $(E_c = 380\ \text{GPa},\ \rho_c = 3960\ \text{kg/m}^3,\ \nu_c = 0.3)$.

The transverse deflections of perfect FGM and imperfect model FGM (I, II) that effect from many factors, including the length material scale parameter (l_m), length material scale parameter ratio (h/l_m), boundary condition (CC, CS, SS, and CF), power-law index (f), porosity volume fraction index (α), and aspect ratio (L/h). The value passion effect $\left[\left[1-\upsilon(z)\right]/\left[1+\upsilon(z)\right]\left[1-2\upsilon(z)\right]\right]$ is assumed to equal one. Table (4.8) shows the effect of a group of factors on the porous FG-microbeam, which will be mentioned in detail.

Table 4.8: The transverse deflection of perfect FGM and imperfect model FGM (I, II) porosity fraction index $(\alpha = 0.1)$ *, B.C (SS)*

	Modes	Theory	L/h	Power law index				
				$(f=0)$	$(f=0.5)$	$(f=1)$	$(f=2)$	$(f=5)$
CBT $(h/lm=0)$	FGM	FSDT	10	0.0448	0.0626	0.0776	0.1005	0.1393
			50	0.0428	0.0600	0.0744	0.0964	0.1331
		EBBT	10	0.0427	0.0593	0.0726	0.0926	0.1278
			50	0.0427	0.0593	0.0726	0.0926	0.1279
	FGM-I	FSDT	10	0.0467	0.0670	0.0850	0.1145	0.1694
			50	0.0446	0.0642	0.0816	0.1099	0.1622
		EBBT	10	0.0445	0.0633	0.0792	0.1044	0.1530
			50	0.0446	0.0634	0.0792	0.1045	0.1530
	FGM-II	FSDT	10	0.0456	0.0645	0.0808	0.10647	0.1518
			50	0.0436	0.0617	0.0774	0.10207	0.1450
		EBBT	10	0.0435	0.0610	0.0754	0.0976	0.1383
			50	0.0435	0.0610	0.0754	0.0976	0.1383
MCST $(h/lm=1)$	FGM	FSDT	10	0.2459	0.3782	0.4914	0.6299	0.7480
			50	0.2402	0.3704	0.4818	0.6175	0.7303
		EBBT	10	0.2399	0.34928	0.4204	0.4993	0.6057
			50	0.2399	0.3493	0.4204	0.4993	0.6059
	FGM-I	FSDT	10	0.2612	0.4189	0.5704	0.7846	0.9832
			50	0.2553	0.4106	0.5600	0.77065	0.9620
		EBBT	10	0.2550	0.3829	0.4720	0.57927	0.7282
			50	0.2550	0.3829	0.4721	0.5793	0.7283
	FGM-II	FSDT	10	0.2496	0.3883	0.5116	0.6698	0.8066
			50	0.2438	0.3803	0.5017	0.6567	0.7872
		EBBT	10	0.2435	0.3572	0.4328	0.5183	0.6340
			50	0.2435	0.3573	0.4328	0.5185	0.6342

4.2.2.1: Effect of the aspect ratio (L/h)

Table (4.8) shows that the transverse deflections of (FGM, FGM-I, and FGM-II) according to EBBT remain constant when the aspect ratio (L/h) increases from 10 to 50. According to FSDT, increasing aspect ratio decreases transverse deflection. Transverse deflection of First shear deformation approximated Euler Bernoulli beam theory as aspect ratio increased because of the loss of shear deformation influence as the aspect ratio increased.

4.2.2.2:Effect of the power-law index (f)

shown in Figure (4.6A) the transverse deflection microbeam of (FGM-I) and (FGM-II) increases because the volume fraction material (f) increase refers to the beam characteristics changing from ceramic to metal, which has low young modulus and density; additionally, the increase of porosity index (α) refers to a drop in the density of the

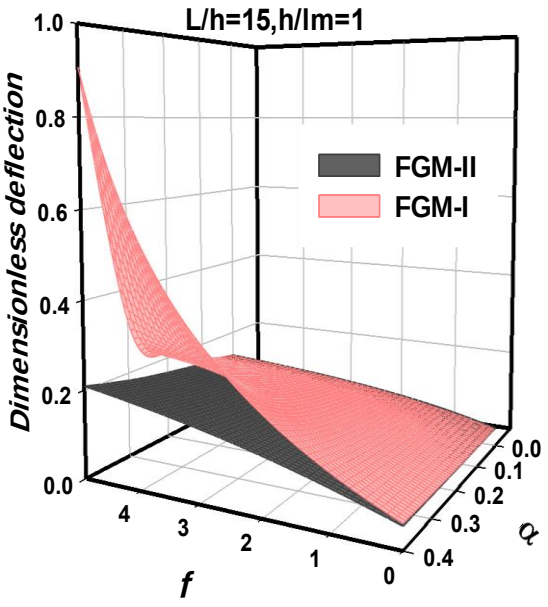

(A)

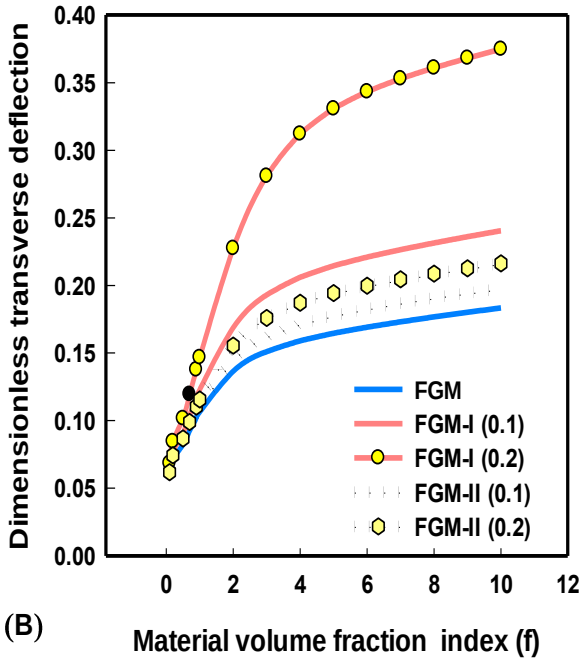

(B)

microbeam, i.e. weak FG-microbeam stiffness, As a result, the perfect FGM has less deflection from FGM-II and FGM-I.

Figure 4. 6: The dimensionless deflection of three models porosity of FGM microbeams, boundary condition (clamped-simply).

4.2.2.3: Effect of the porosity volume fraction (α)

Figure (4.6B) is shown the effect of increasing porosity volume fraction index (α) on an increasing deflection for both imperfect (FGM-I, FGM-II).in the FGM-I model, pore distribution is equal in all cross-sections leads to complete weakness in the structure. While in the FGM-II model, the pore distribution is centered in the middle, the porosity model of FGM-II is a half weakness compared to the FGM-I.

4.2.2.4 Effect of boundary conditions

The boundary conditions effect on perfect and imperfect FG-microbeam as in Figure (4.7), where the highest deflections are clamped-free (C-F), followed by simply-simply (S-S), clamped-simply (C-S), and clamped-clamped (C-C), respectively. Also, Figure (4.7), shows the accuracy of the MCST $(l_m = 1)$ in predicting the least deflection for various B.C$_S$ compared to the classical beam theory CBT $(l_m = 0)$.

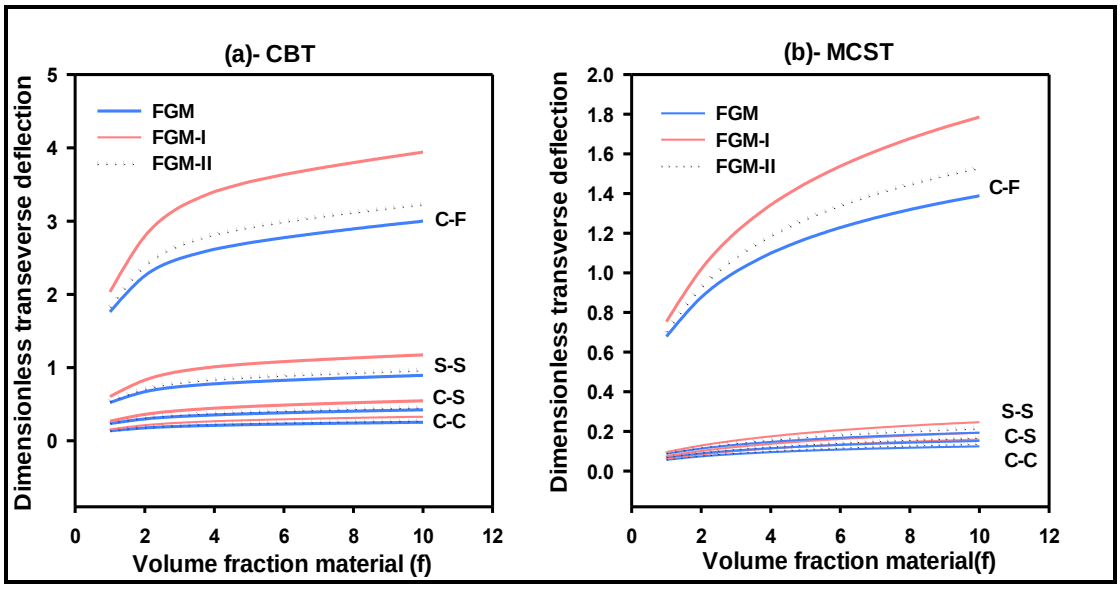

Figure 4. 7: transverse deflection of FGM porous beams according to (CBT, MCST) based on FSDT of various boundary conditions

4.2.2.5: Effect of the length material scale parameter ratio (h / l_m)

As illustrated in Figure (4.8), raising the ratio of (h / lm) results in an increase in deflection. This drops the material length scale parameter, which weakens the MCST ability to anticipate minor deflections.

As the porosity index (α) increases, the dimensionless deflection of both imperfect (FGM-I) and (FGM-II) increases. but, the difference in deflection behavior between (FGM-I) and (FGM-II), belongs to a function $(\int_{-0.5}^{0.5}(1-(2|z|/h))\ dz)$ .this function governs the form of the porosity distribution in FGM-II only. It was observed in Figure (4.9), that increase in volume fraction of FGM-II from (f = 1) to (f = 10), as having functionally gradient characteristics ranging from ceramic to metal, resulting in gradients in flexibility and lightweight for imperfectFG-microbeam.

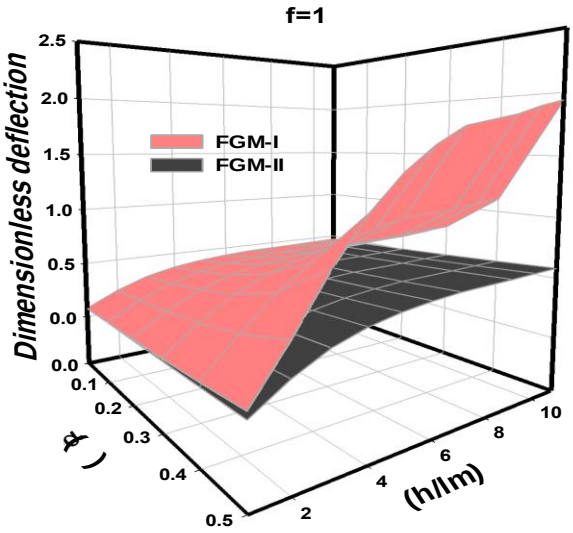

Figure 4. 8: Deflection of imperfect FGM (f=1).

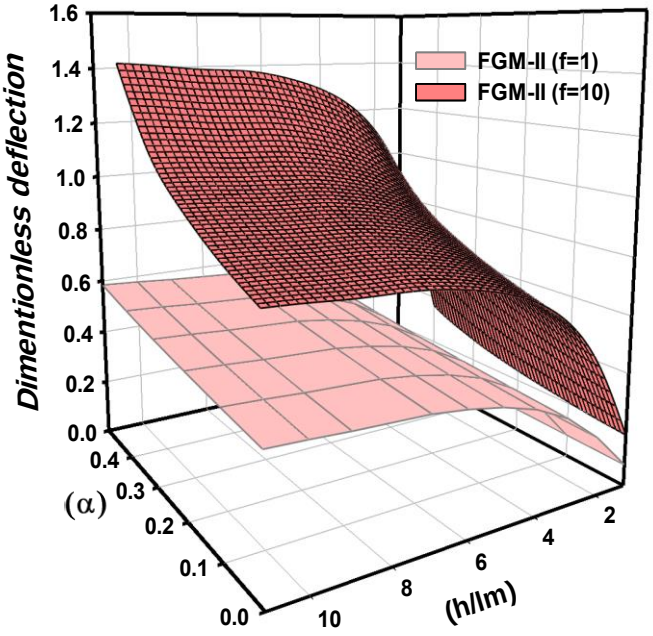

Figure 4. 9: Deflection of FGM-II,(f=1,10).

4.2.2.6: Effect of MCST and CBT

The dimensionless transverse deflection for the Modified Couple Stress Theory (MCST) $(h/l_m = 1)$ and the Classical Beam Theory (CBT) $(h/l_m = 0)$ is shown in Table (4.8). the ability of the MCS theory is shown to predict the least static deflection for microbeams because it has a material length scale parameter. The MCST begins to lose its ability to predict the deformation of the microbeam as this parameter is reduced; its behavior is similar to that of classical beam theory, which could not calculate the deflection of the microbeam.

4.2.3: Static bending of FG-SWCNT microbeam

Based on the Modified Couple Stress Theory and the beam Theories for Euler-Bernoulli and First shear deformation theory, the work seeks to identify the lowest central deflection for microbeam reinforced by an SWCNT. Several factors affect the bending behavior, including the volume fraction of CNT (V_{CNT}), SWCNT distributions types, aspect ratio (L/h), boundary condition, and material length parameter ratio (h/lm) are investigated. In this study, the following material properties are dependent on [42] is used the following: Polymethyl methacrylate (PMMA) properties:

$E_m = 2.5$ GPa, $\rho_m = 1190\,\text{kg.m}^{-3}, \upsilon^m = 0.3$

and (SWCNTs) properties:

$E_{11}^{cnt} = 5646.6$ GPa, $E_{22}^{cnt} = 7080$ GPa, $\rho^{cnt} = 2100$ kg.m^{-3} $\upsilon^{CNT} = 0.17$

,

CNTs type of chair (10,10) are chosen as reinforcements. Also, Efficiency parameters FG-CNTRC are estimated in Table (3.1).

To avoid an error in the MCST results, the Poisson effect is inserted into the stiffness matrix. in the following formula. $\left[E(z)^{*}\ \left[1-\nu_{12}(z)\right]/\left[1+\nu_{12}(z)\right]\left[1-2\nu_{12}(z)\right]\right]$.The formula dimensionless transverse deflection of FG-CNT which used is $(\bar{w}=100w\ E_m h^3/q_o L^4)$.

4.2.3.1: Effect of Used MCST and CBT

Table (4.9) displays the dimensionless transverse deflection for Modified Couple Stress Theory where dimensionless material parameter ratio $(h/l_m=1)$ and Classical beam theory where dimensionless material parameter ratio $(h/l_m=0)$. MCST predicts the least deflection with all boundary conditions and any amount of CNT volume fraction. The deflection of MCST becomes less from CBT, and be similar when the length scale parameter ratio (h/l_m) increases.

Table 4. 9: Dimensionless transverse deflection $\bar{w}=100\,w\ E_m I/q_0 L^4$ *of micro-beams with different B. Cs with CBT* $(l_m=0)$ *andMCST* $(l_m=1)$

$(Vari)$	Model	C-C		S-S		C-F	
		CBT	*MCST*	*CBT*	*MCST*	*CBT*	*MCST*
0.12	FG-X	0.1921	0.1855	0.3902	0.357	1.2695	1.2219
	UD	0.2155	0.2049	0.5036	0.445	1.6549	1.5517
	FG-V	0.2478	0.2293	0.5417	0.473	2.2155	1.9946
	FG-O	0.2814	0.2532	0.8367	0.67	2.7878	2.4108
0.17	FG-X	0.1185	0.1137	0.2571	0.232	0.8405	0.8002
	UD	0.1352	0.1273	0.336	0.292	1.1085	1.0237
	FG-V	0.181	0.1435	0.5699	0.31	1.9041	1.3237
	FG-O	0.1185	0.1592	0.2571	0.44	0.8405	1.5965
0.28	FG-X	0.0939	0.091	0.1828	0.169	0.5929	0.5741

	UD	0.1076	0.1032	0.2352	0.212	0.7695	0.7315
	FG-V	0.119	0.1219	0.2514	0.312	1.0183	1.1167
	FG-O	0.1336	0.1111	0.3812	0.222	1.2672	0.9293

4.2.3.2: Effect of FG-CNTs distribution types

It is clear from Table (4.10). when CNT is concentrated in the medium without beam surfaces, the beam is less rigid and has a higher deflection, as in FG-O. and It is followed by UD, FG-V. As for FG-X, the CNT is concerted in surfaces without the centre, the beam is more rigid and has a smaller deflection.

Table 4. 10: Dimensionless static deflection of the FG-SWCNT micro-beam with different FG-CNTs distribution types and B.Cs

	FG-X	UD	FG-V	FG-O	FG-X	UD	FG-V	FG-O
L/h	CC				CS			
10	0.1763	0.1928	0.1956	0.2061	0.2125	0.2389	0.2528	0.2732
20	0.0605	0.071	0.0808	0.0914	0.087	0.106	0.1269	0.1476
30	0.0385	0.0478	0.0586	0.0692	0.0619	0.0795	0.1017	0.1224
40	0.0307	0.0395	0.0508	0.0613	0.0529	0.07	0.0927	0.1134
50	0.0271	0.0357	0.0471	0.0575	0.0487	0.0656	0.0885	0.1091
60	0.0251	0.0336	0.0451	0.0555	0.0464	0.0632	0.0862	0.1068
L/h	SS				CF			
10	0.2492	0.2946	0.2995	0.3842	0.8486	1.0255	1.2177	1.4146
20	0.1401	0.1823	0.1947	0.2866	0.4769	0.627	0.8257	1.0085
30	0.1195	0.1611	0.1749	0.2683	0.4068	0.5513	0.75	0.9288
40	0.1123	0.1536	0.1679	0.2618	1.0255	0.5245	0.723	0.9001
50	0.1089	0.1502	0.1647	0.2589	0.3706	0.5121	0.7104	0.8867
60	0.1071	0.0336	0.1629	0.2572	0.3644	0.5053	0.7035	0.8793

4.2.3.3: Effect of volume fraction of CNTs

FG-microbeam improves the hardness of all types of CNT distributions. when increasing the amount of CNT as shown in Table (4.11). that it

has a high young modulus Transverse deflection according to MCS theory is less than classical theory, because it can calculate the most accurate deflection for FG-CNT micro polymer beam.

Table 4. 11: Dimensionless transverse deflection of FG-CNT micro-beams with B.C (C-C), $L/h=15$.

Types	$(V_{CNT}=0.12)$		$(V_{CNT}=0.17)$		$(V_{CNT}=0.28)$	
	$(l_m=0)$	$(l_m=1)$	$(l_m=0)$	$(l_m=1)$	$(l_m=0)$	$(l_m=1)$
FG-X	**0.1921**	**0.1855**	**0.1185**	**0.1137**	**0.0939**	**0.0910**
UD	**0.2155**	**0.2049**	**0.1352**	**0.1273**	**0.1076**	**0.1032**
FG-V	**0.2478**	**0.2293**	**0.1810**	**0.1435**	**0.1190**	**0.1219**
FG-O	**0.2814**	**0.2532**	**0.1185**	**0.1592**	**0.1336**	**0.1111**

4.2.3.4: Effect of boundary conditions.

FG-CNT micro-beam deflection is affected by boundary conditions. With all types of FG micro-beam distribution, compared boundary conditions. Figure (4.10) shows that the FG-CNT type (O) has the largest dimensionless transverse deflection. it is shown high deflection belongs to (clamped-free) and is followed by (simply- simply), (clamped- simply), and finally (clamped-clamped).

4.2.3.5: Effect of Aspect Ratio

The effect of EBBT, and FSDT on The dimensionless transverse deflection of the FG-SWCNT microbeam through aspect ratio (L/h) are illustrated in Table (4.12). Based on the MCST, at aspect ratio increases, the first shear deformation theory beam theory is decreasing due to losing the effect of shear deformation and closing value with the deflection of Euler's beam theory EBBT that be no effect on shear deformation and be constant. The high deflection appears when using EBBT in a state of boundary condition (C-F) and distribution (FG-O) type as shown in Figure (4.10).

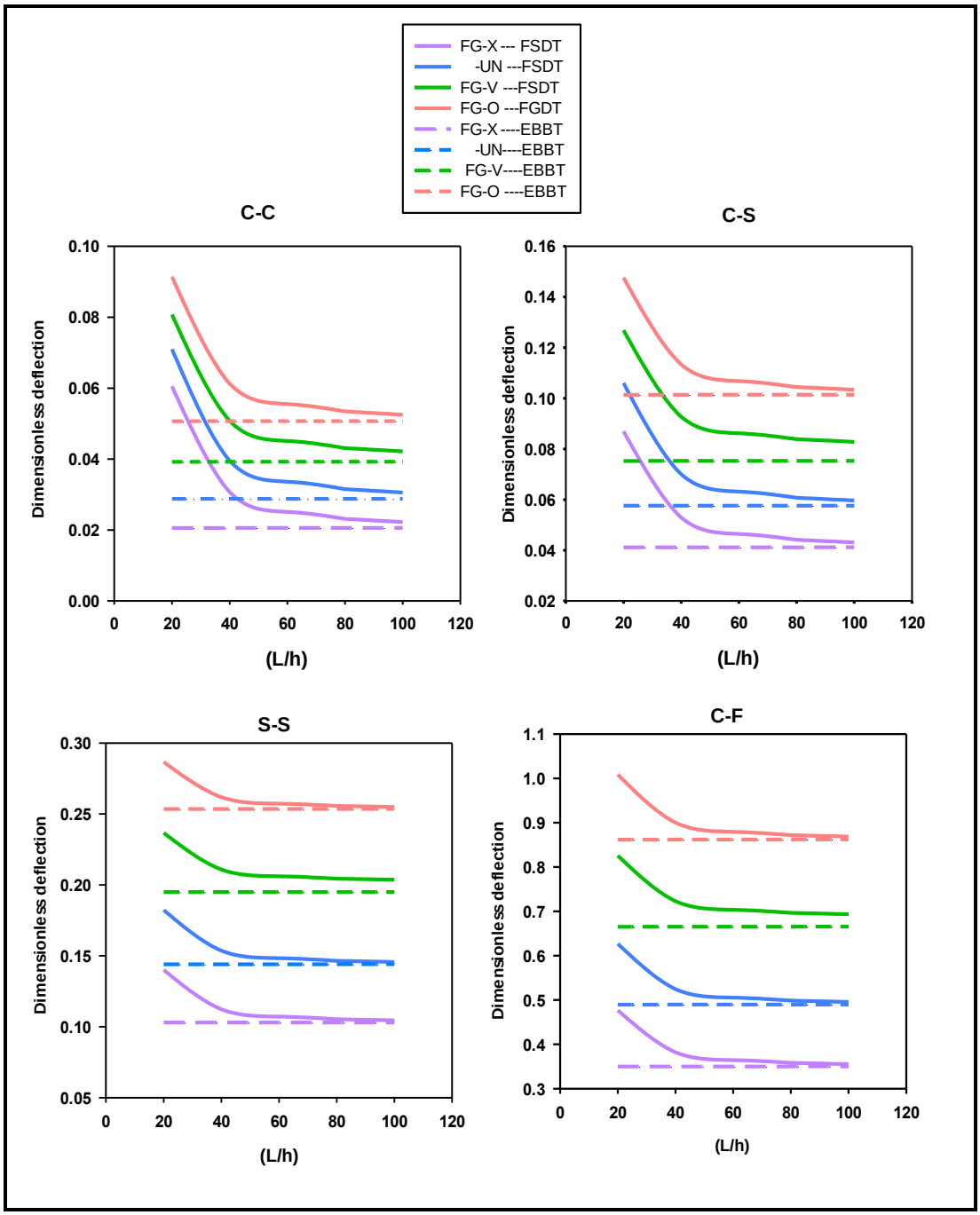

Figure 4. 10: The dimensionless transverse deflection of the FG-SWCNT microbeam with various boundary conditions, $h/l_m = 1$, $V_{CNT} = 0.28$

Table 4. 12:The effect of (EBBT) and (FSDT) on dimensionless deflection for different boundary conditions and different CNT distributions with increasing of aspect ratio, $h/l_m = 1$, $V_{CNT} = 0.28$

	TBT					EBBT				
L/h	20	40	60	80	100	20	40	60	80	100
Model					C-C					
X	0.0605	0.0307	0.0251	0.0231	0.0222	0.0206	0.0206	0.0206	0.0206	0.0206
UN	0.0710	0.0395	0.0336	0.0315	0.0306	0.0288	0.0288	0.0288	0.0288	0.0288
V	0.0808	0.0508	0.0451	0.0431	0.0422	0.0392	0.0393	0.0393	0.0393	0.0393
O	0.0914	0.0613	0.0555	0.0535	0.0525	0.0507	0.0507	0.0507	0.0507	0.0507
					C-S					
X	0.0870	0.0529	0.0464	0.0442	0.0431	0.0412	0.0412	0.0412	0.0412	0.0412
UN	0.1060	0.0700	0.0632	0.0608	0.0596	0.0576	0.0576	0.0576	0.0576	0.0576
V	0.1269	0.0927	0.0862	0.0839	0.0828	0.0753	0.0753	0.0753	0.0753	0.0753
O	0.1476	0.1134	0.1068	0.1045	0.1034	0.1014	0.1014	0.1014	0.1014	0.1014
					S-S					
X	0.1401	0.1123	0.1071	0.1053	0.1045	0.1029	0.1030	0.1030	0.1030	0.1030
UN	0.1823	0.1536	0.1483	0.1465	0.1456	0.1440	0.1440	0.1440	0.1441	0.1441
V	0.2367	0.2108	0.2061	0.2044	0.2036	0.1589	0.1589	0.1589	0.1589	0.1590
O	0.2866	0.2618	0.2572	0.2557	0.2549	0.2535	0.2535	0.2535	0.2536	0.2536
					C-F					
X	0.4769	0.3821	0.3644	0.3582	0.3553	0.3500	0.3500	0.3501	0.3501	0.3502
UN	0.6270	0.5245	0.5053	0.4986	0.4955	0.4896	0.4897	0.4897	0.4898	0.4899
V	0.8257	0.7230	0.7035	0.6966	0.6935	0.6652	0.6653	0.6654	0.6655	0.6656
O	1.0085	0.9001	0.8793	0.8720	0.8686	0.8618	0.8619	0.8620	0.8621	0.8623

4.2.3.6: Effect of material length scale parameter (l_m)

Figure (4.11a), shows that a high value of dimensionless transverse deflection for all CNT distribution models appears when an increase in the material parameter length ratio (h/lm) and, the aspect ratio (L/h) : the highest deflection belongs to (FG-O) then (FG-V) and (-UN), finally (FG-X).

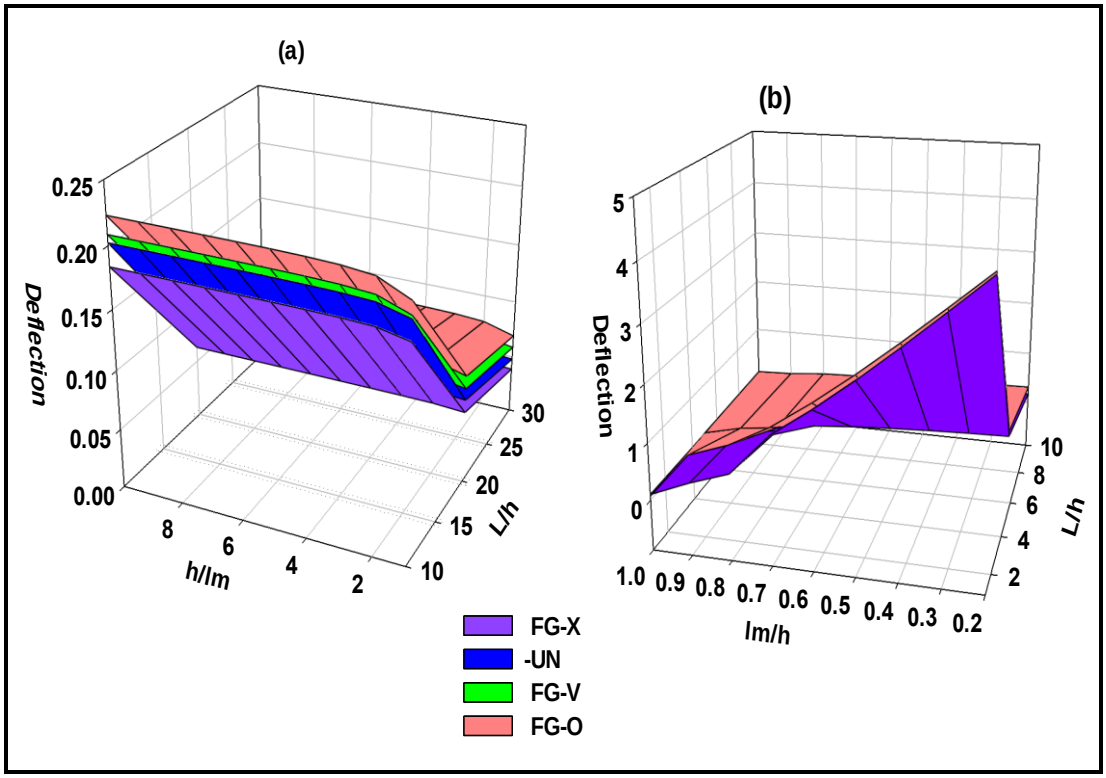

Figure 4. 11: Effect of material length scale parameter and aspect ratio on the dimensionless deflection of FG-CNT, (FSDT)

In Figure (4.11b) the dimensionless transverse deflection decreases as the ratio of length material parameter to thickness (l_m/h) increases from 0 to 1, indicating that the modified couple stress theory is more capable of predicting small sizes of deflection of FG-CNTRC microbeams with small sizes. While an increase in the aspect ratio (L/h) results in a decrease in the amount of shear deformation, according to first shear deformation theory so the slenderness microbeam due to the deflection decreases.

4.3: NUMERICAL RESULTS OF FREE VIBRATION ANALYSIS

4.3.1: Free vibration of FG-material microbeam

Functionally graded microbeam model as shown in Figure (3.1) is made from silicon carbide (SiC) and aluminum (Al), the data beam is taken from the Ref.[27]. The free vibration of the FGM microbeam is studied via exploring the effects of many effective parameters on FG-microbeam as follows:

4.3.1.1: Effect of The aspect ratio (L/h)

As shown in Table (4.4). The frequency of Bernoulli's beam theory is greater more than FSDT theories because it does not take into account the influence of shear deformation on beam stiffness. With the constant of shear deformation shear (5/6), the First Shear Deformation Theory (FSDT) is the most flexible. As the aspect ratio (L/h) increase from 10 to 100, the effect of shear deformation reduces so that dimensionless fundamental frequency for EBBT and FSDT becomes more convergent.

4.3.1.2: Effect of The power law index (f)

Table (4-4) shows the frequency of FG-micro-beam is increasing when the power-law index (f) decreases. the reason is shown in Figure (4.1), The power law index $(f=0)$ means that full ceramic i.e. high young modulus and high stiffness beam while The power law index $(f=100)$ where metal that has a low young modulus and low stiffness.

4.3.1.3: Effect of Mori-Tanaka and rule of mixture

Mori Tanaka's techniques can be giving the best estimates for the effective properties of FG-beam in micro size compared with the rule of

mixture techniques. Table (4.13) can demonstrate the dimensionless frequency of FG micro-beam decrease with increase gradient indexes. Mori-Tanaka scheme is can predict the smallest frequency effect in comparison with the rule of the mixture method since the technique analyzes the effective material properties in micro size.

Table 4. 13: dimensionless fundamental frequency FG micro-beam, b=h, for aspect ratio $L/h=10$, *with* $(h/lm=1),(h/lm=8)$.

Theory	h/lm	The rule of mixture			Mori Tanaka scheme			
		f=1	f=2	f=4	f=10	f=1	f=2	f=10
EBBT	1	12.5182	11.0056	9.6946	8.4661	10.6272	9.4773	7.7965
	8	5.3054	4.7507	4.4568	4.22	4.6843	4.3794	3.9263
FSDT	1	12.2385	10.7573	9.4603	8.2365	10.381	9.2455	7.5799
	8	5.2451	4.6944	4.3946	4.1465	4.6255	4.3173	3.8555

The difference in reading frequency of the micro-beam by Mori Tanaka's and Rule of mixture techniques appear clearly in Figure (4.12) with material length scale parameter ratios, and gradient index is shown.

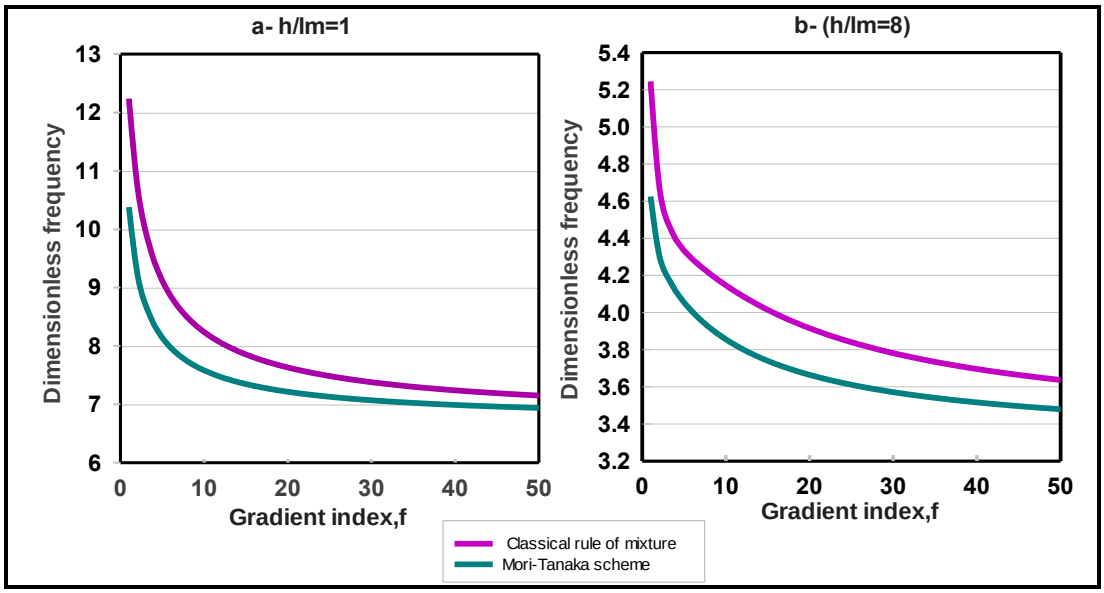

Figure 4. 12: Variation of the dimensionless fundamental frequency of the FG-micro-beam according to two Rules for a material model with the gradient index,(f). for (a) $(h=l_m)$ *, (b)* $(h=8l_m)$

4.3.1.4: Effect of the Poisson effect

The influence of the Poisson effect on the dimensionless fundamental frequency of the FG micro-beam based on MCST. It can be noted in Table (4.14) that ignoring the Poisson effect leads to errors in result, as indicated by (Ma et al., 2008) in studying the effect Poisson of the microstructure of a simply supported beam based on the first shear deformation theory model and modified couple stress theories (MCST). Calculating the frequency without the Poisson effect factor affects the modulus of the elasticity equation.[27] the mathematical relationship between stiffness and the Poisson effect which leads to an improvement in the stiffness values of the FG micro stream.

Table 4. 14: the dimensionless natural frequency $\bar{\omega} = \omega L^2/h\sqrt{\rho_m/E_m}$ *of FG micro-beams with (EBBT) and (FSDT) for various gradient index and material length scales. (with Poisson effect==1) and (without Poisson effect==0) .*

h/lm	Poisson effect	Theory	L/h=10				
			f=1	f=4	f=6	f=8	f=10
1	1	EBBT	10.627	8.5909	8.192	7.9556	7.7965
	0		10.528	8.4431	8.0339	7.7924	7.6303
	1	FSDT	10.381	8.365	7.9694	7.7361	7.5799
	0		10.226	8.1862	7.7903	7.5579	7.4024
2	1	EBBT	6.6046	5.5599	5.3506	5.2166	5.1205
	0		6.3691	5.2773	5.0623	4.9257	4.8281
	1	FSDT	6.5108	5.4612	5.2505	5.1167	5.0214
	0		6.247	5.1651	4.9545	4.8217	4.7272
4	1	EBBT	5.1263	4.4927	4.3596	4.2651	4.1924
	0		4.7955	4.1221	3.9871	3.892	3.8188
	1	FSDT	5.0613	4.4188	4.2835	4.1887	4.1165
	0		4.7119	4.0408	3.9082	3.8156	3.7446
8	1	EBBT	4.6843	4.1836	4.0743	3.9919	3.9263

	0		**4.3133**	**3.7785**	**3.6695**	**3.5874**	**3.5215**
	1	**FSDT**	**4.6255**	**4.1151**	**4.0036**	**3.9208**	**3.8555**
	0		**4.2389**	**3.7045**	**3.5973**	**3.5174**	**3.4536**

Table (4.14) is remarked effect of Poisson on the fundamental frequency for different values of each gradient index, aspect ratio, and the material length parameter ratio. The essential outcome is that the Poisson effect causes an increase in the fundamental frequency. There are also large inaccuracies as a result of ignoring the Poisson effect.

As shown in Table(4-14) and Figure (4.13), the Poisson effect increase with increasing gradient index. Because the volume fraction of the metal constituent grows with the power-law index. The metal component's Poisson's ratio(V_m=0.3) effect that higher than the ceramic component's (V_c=0.17).

The highest frequency is shown by Figure (4.13a) determine the Poisson effect, shear deformation is found since (L/h=1) and the ratio of the material length factor $(h = lm)$, the MCST can predict the size effect of FG-micro-beam, while Figure (4.13d) the lowest frequency is not taking into account the Poisson effect and the loss of the shear distortion effect due to the thinness of the beam and the inability to predict the frequency with the size effect due to the increase in the material length factor ratio

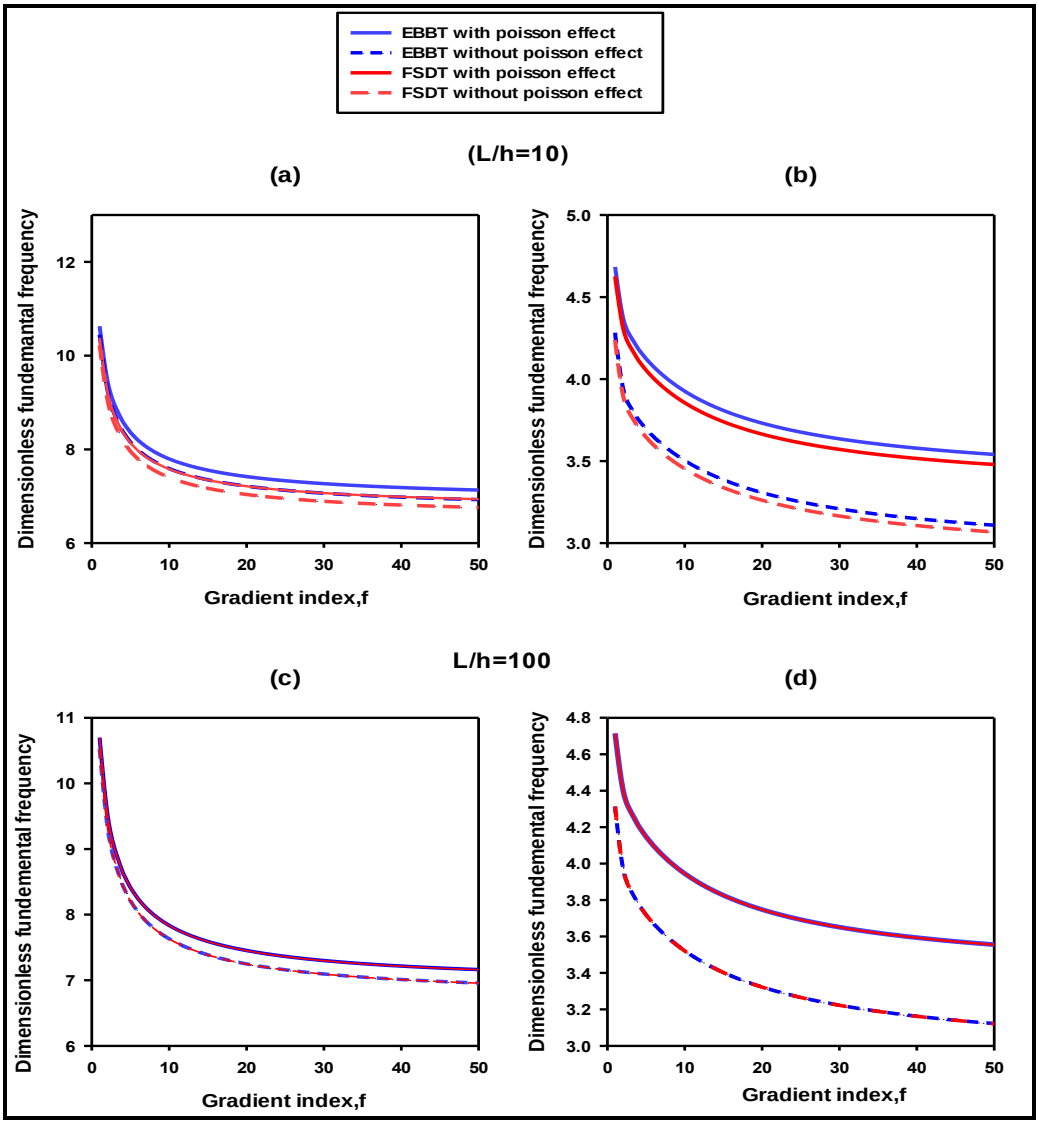

Figure 4. 13: show Poisson effect on dimensionless fundamental natural frequency $\bar{\omega} = \omega L^2 / h\sqrt{\rho_m / E_m}$ *of FG-micro beams at f=1, for (a)(c) h/lm =1, (b)(d) h/lm=8*

4.3.1.5: Effect of a length material scale parameter

It is clear from Figure (4.14), MCST always has the best predicted for characteristic properties compared to CBT because of the ability to study couple stress in micro size. The frequency of MCST is related to the material length scale parameter ratio (h/lm). Decreasing in (h/lm) means increasing the material length scale parameter (lm), thus leading to frequency increase. In Classical beam theory (CBT), the

frequency does not change since not have the material length scale parameter. It can be noted The variances between the frequencies of the Euler–Bernoulli beam theory (EBBT) and the shear deformable beam theory (FSDBT) are more pronounced for the third mode at the model number rises, the shear deformation effect becomes more significant.

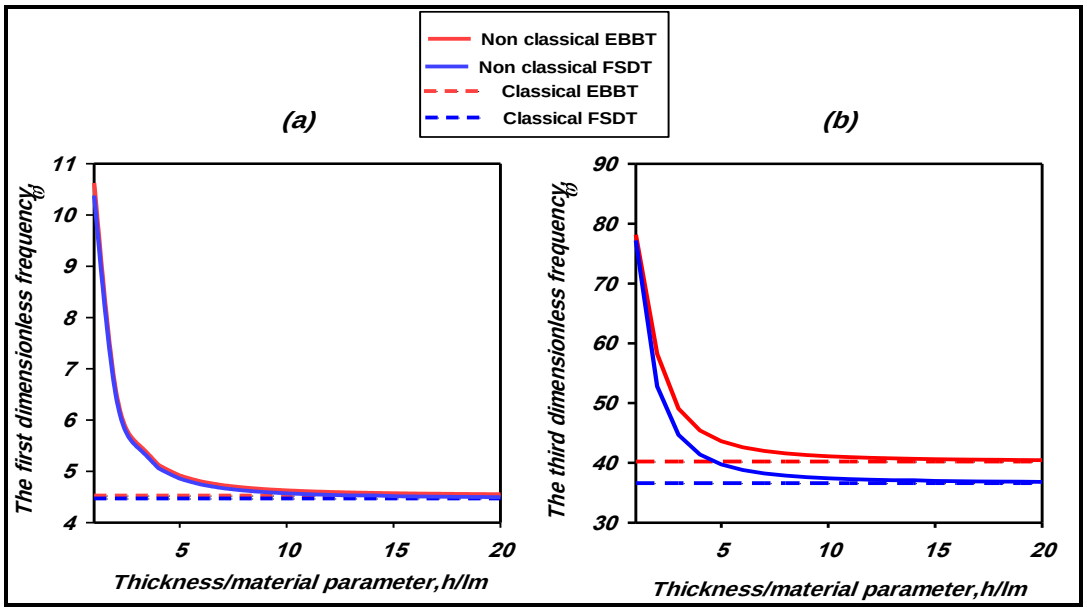

Figure 4. 14*: The first fundamental dimensionless natural frequency* $\bar{\omega} = \omega L^2 / h\sqrt{\rho_m / E_m}$ *of micro-beam L/h =10 and f=1 subjected to uniform load.*

4.3.1.6: Effect of Used MCST and CBT

As shown in Figures (4.14), and Figure (4.15). There is a wide difference in the frequency of the FG-micro-beam according to (CBT) and (MCST) when increasing the aspect ratio parameter, where the coefficient MCST is (lm) can catch the effect of the farthest frequency.

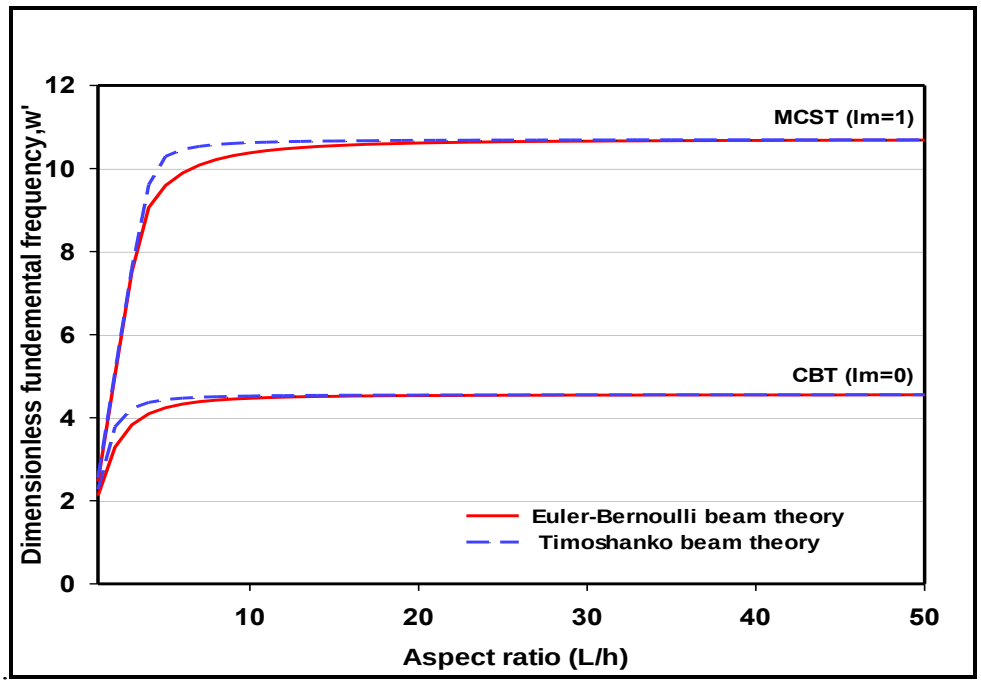

Figure 4. 15: Variation of dimensionless fundamentals frequency of the FG micro-beam subjected to uniform load, h = l, f = 1, according to classical theory, (CBT) and modified couple stress theory, (MCST).

4.3.2 Free vibration of FG- porous microbeam.

The dimensionless fundamentals frequency of three models of the porosity of FGM microbeam is obtained by TBT and MCST. the influence of many factors such as the material length scale parameter, aspect ratio, and power-law index. In general, the frequency of the three porous models decreases as the length scale parameter ratios and aspect ratio are increased.

4.3.2.1 Effected of aspect ratio (L/h)

Table 4.15 shows that increasing aspect ratio, no significant effect on the frequency according to the Euler-Bernoulli beam theory. The frequency of the first shear deformation theory beam decreases with the increase in aspect ratio due to the decrease in shear deformation as shows in Figure (4.16).

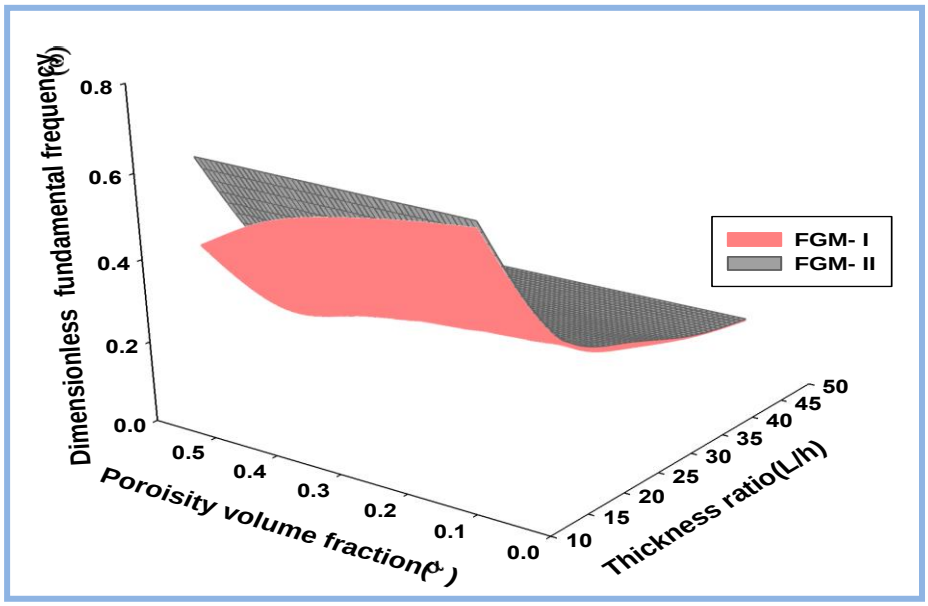

Figure 4. 17: Dimensionless frequencies $\left(\bar{\omega} = \omega L\sqrt{\rho_m / E_m}\right)$ *of imperfect FGM beam with increasing porosity volume fraction index* (α) *and aspect ratio(L/h).*

The decrease in shear deformation made the frequency of TBT close to that of EBBT. The fundamental natural frequency of the three porosity models decreases can be noted from Table (4.15) when the power-law index increases due to the properties of the materials gradually changing from ceramic to metal.

Table 4.15: the dimensionless fundamental frequency of perfect FGM and imperfect models FGM (I, II) beams depending on (EBBT)and (TBT) with various boundary, porosity fraction index $(\alpha = 0.1)$, *and the length material parameter* $(l_m = 0)$.

model	theory	$\frac{L}{h}$	Power law index				
			$f = 0.5$	$f = 0$	$f = 1$	$f = 2$	$f = 5$
B.Cs(C-C)							
FGM	TBT	10	11.652	9.9836	9.0477	8.2478	7.774
		50	12.396	10.559	9.5459	8.7107	8.29
	EBBT	50	12.428	10.618	9.6405	8.8355	8.4002
FGM-I	TBT	10	11.825	9.9827	8.8737	7.8475	7.2314
		50	12.564	10.537	9.3345	8.2509	7.6763
	EBBT	50	12.595	10.602	9.4442	8.4022	7.8173
FGM-II	TBT	10	11.813	10.09	9.0961	8.22	7.703
		50	12.571	10.675	9.5981	8.6812	8.2225
	EBBT	50	12.603	10.736	9.6995	8.8176	8.3462
B.Cs(C-S)							
FGM	TBT	10	8.2426	7.0783	6.4527	5.9281	5.5958
		50	8.5523	7.321	6.6672	6.1315	5.8207
	EBBT	50	8.5644	7.3535	6.7239	6.2077	5.887
FGM-I	TBT	10	8.3603	7.0785	6.3413	5.6733	5.2444
		50	8.6681	7.315	6.5417	5.8546	5.4434
	EBBT	50	8.6801	7.3497	6.6086	5.9475	5.5293
FGM-II	TBT	10	8.3753	7.1568	6.4943	5.9224	5.5629
		50	8.6713	7.4039	6.7113	6.1612	5.7914
	EBBT	50	8.6854	7.4383	6.7725	6.2101	5.8661
B.Cs(S-S)							
FGM	TBT	10	5.3933	4.7323	4.44	4.214	3.9509
		50	5.4797	4.8045	4.5177	4.2846	4.0262
	EBBT	50	5.4825	4.8068	4.52	4.287	4.0288
FGM-I	TBT	10	5.4677	4.7508	4.4281	4.1436	3.8321
		50	5.5537	4.8217	4.4953	4.2114	3.9052
	EBBT	50	5.5565	4.824	4.4974	4.2137	3.9077
FGM-II	TBT	10	5.4688	4.7926	4.4981	4.25	3.9749
		50	5.557	4.8667	4.5692	4.3228	4.0538
	EBBT	50	5.5599	4.869	4.5715	4.3251	4.0565
B.Cs(C-F)							
FGM	TBT	10	1.9381	1.6514	1.4931	1.3622	1.2955
		50	1.9528	1.663	1.5033	1.3718	1.3061
	EBBT	50	1.9533	1.6682	1.5138	1.3865	1.3185
FGM-I	TBT	10	1.9645	1.6482	1.4602	1.2905	1.1997
		50	1.9792	1.6594	1.4698	1.2991	1.2092

	EBBT	50	1.9797	1.6594	1.4826	1.3176	1.226
FGM-II	TBT	10	1.9653	1.6694	1.5012	1.3574	1.2847
		50	1.9804	1.6812	1.5115	1.3671	1.2955
	EBBT	50	1.9809	1.6868	1.523	1.3834	1.3097

4.3.2.2: Effected of boundary conditions

The boundary conditions of three models of the FG-micro-beam are shown in Figure (4.17); the highest frequency at clamped-clamped, clamped- simply, simply-simply, and Clamped free, respectively.

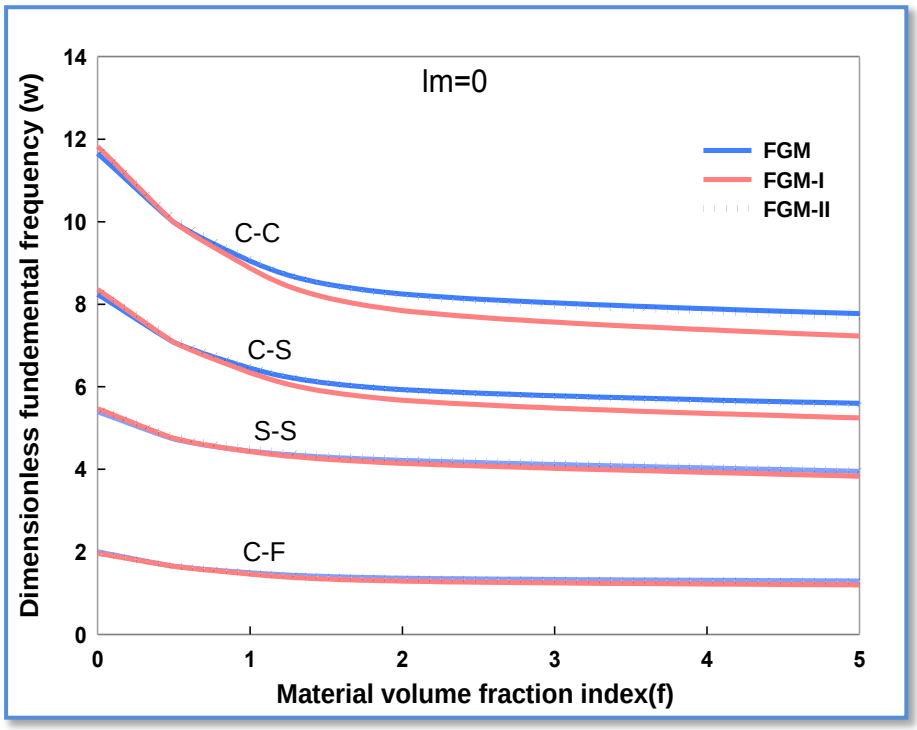

Figure 4. 18: dimensionless fundamental frequency of perfect FGM and imperfect FGM-I, FGM-II beams depended on (TBT) with various boundary conditions, aspect ratio (L/h=10), and porosity volume fraction index $(\alpha = 0.1)$.

4.3.2.3 Effect of the power-law index (f)

The vibration of the three models (FGM, FGM-I, FGM-II) decreases with the increase of the power-law index due to the spatial gradient of the properties is metal-oriented materials with a low modulus of elasticity compared to ceramics.

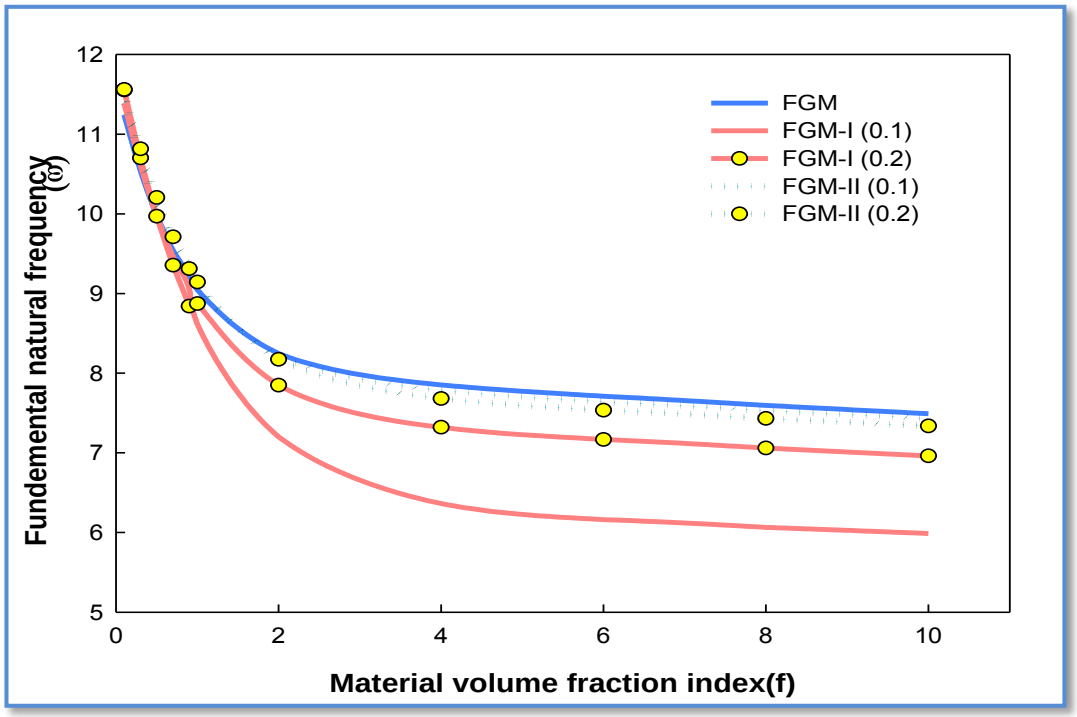

Figure 4. 19: Dimensionless frequencies of three models of FGM beam with increasing porosity volume fraction index (α) and power-law index.

4.3.2.3 Effect of porosity volume fraction

Figure (4.17) also Table (4.15) displays Dimensionless frequencies imperfect FGM-I and FGM-II when the power-law index and the porosity volume fraction index(α) increase. FGM-II and FGM-I frequency models have been reduced. It appears the FGM has the largest frequency due to not having porosity.

4.3.2.3 Effect of the different types of FGM porosity distribution

Dimensionless frequencies depend on the power-law index and the distribution of pores along with the thickness of imperfect FGM-I and FGM-II. For example, as shows in Figure (4.18) also Table (4.15) the value of the power-law index $(f<1)$ the Dimensionless frequencies of

FGM-I is greater than that of FGM-II. while $(f = 1)$ the Dimensionless frequencies of FGM-II and FGM-I are interference, the frequency values are overlapping because that power-law index equal to one where $(Vc = Vm)$. $(f > 1)$ the Dimensionless frequencies FGM-II is greater than that of FGM-I. The FGM-II model is designed by the number of pores along with the thickness via part the function $(\int_{-0.5}^{0.5}(1-(2|z/h|))dz)$, the volume fraction function of FGM-II is half the value of the volume fraction FGM-I.

It appears the (FGM) has the largest frequency due to not having porosity and followed by (FGM-II), and lastly, the imperfect (FGM-I) beam. The different behavior of (FGM, FGM-I, FGM-II).

Figure (4-5) is shown that. The different behavior of porosity models belongs to the function $(\int_{-0.5}^{0.5}(1-(2|z|/h))\ dz)$ that is found in Eqs. (3.16-3.17).

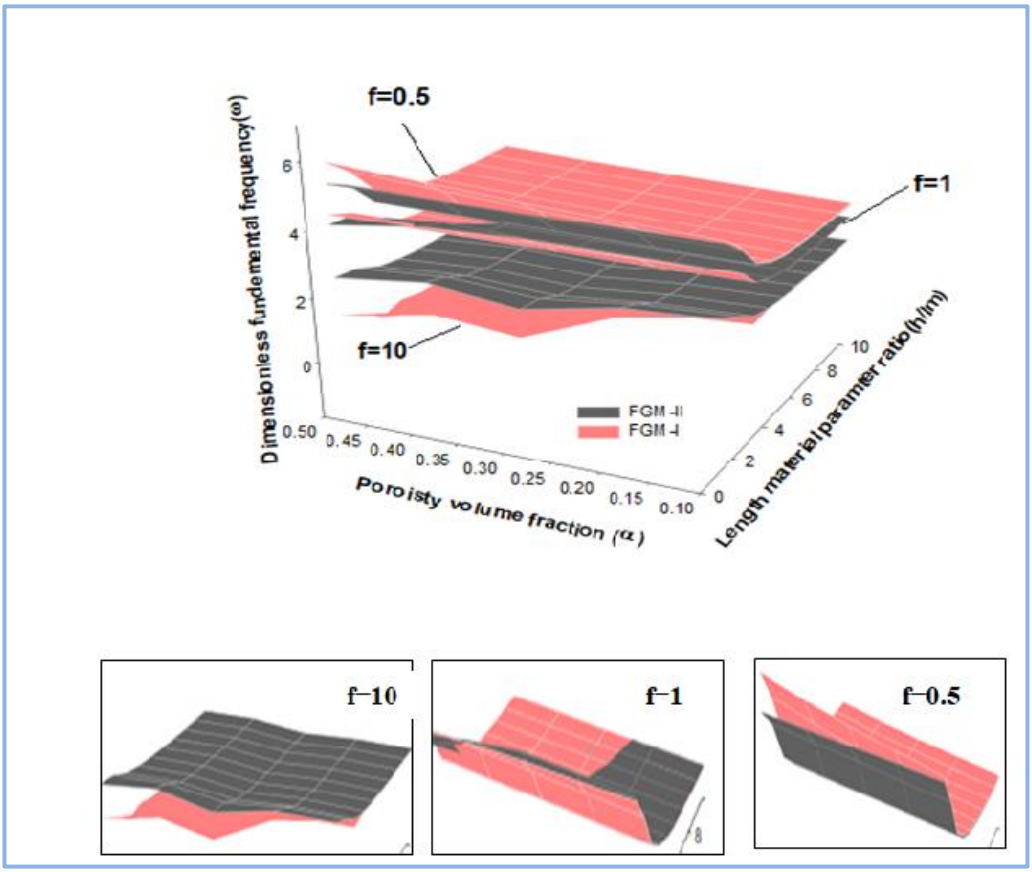

Figure 4. 20: Effect of length of material perimetric the porosity volume fraction (α) *and the power-law index, the frequency*

4.3.2.5: Effect of the length material scale parameter ratio.

Table (4.16) shows the effect of the material scale parameter ratio on the frequencies of three micro-beam models of FGM porosity. The material length scale parameter is the only parameter of the MCST that depends on predicting size effect. The material length scale parameter is determined by the length material parameter ratio, which has the opposite effect; the frequency is decreased as Figure (4.18). In general, the non-dimensional natural frequencies of the three porous models decreased when the porosity volume fraction and length material parameter ratios were increased.

Table 4.16: the effect of the material length scale factor (l_m) on the frequencies of three micro-beam models of FGM porosity at B.Cs(CC).

models	α	$h/l_m=1$	$h/l_m=2$	$h/l_m=5$	$h/l_m=7$	$h/l_m=10$	$h/l_m=0$
FGM	**0**	**4.2392**	**3.7495**	**2.6987**	**2.5698**	**2.4978**	**2.4257**
FGM-I	**0.1**	**4.2703**	**3.7921**	**2.7207**	**2.5887**	**2.5147**	**2.4406**
	0.2	**4.2977**	**3.8361**	**2.741**	**2.6051**	**2.5288**	**2.452**
	0.3	**4.3044**	**3.8815**	**2.7569**	**2.6158**	**2.5363**	**2.4557**
	0.4	**4.1901**	**3.928**	**2.7603**	**2.611**	**2.526**	**2.4385**
	0.5	**3.8203**	**3.7743**	**2.7137**	**2.5447**	**2.4453**	**2.3373**
FGM-II	**0.1**	**4.2257**	**3.7687**	**2.7121**	**2.5828**	**2.5106**	**2.4382**
	0.2	**4.2086**	**3.7871**	**2.7252**	**2.5956**	**2.5231**	**2.4507**
	0.3	**4.1872**	**3.8041**	**2.7378**	**2.6079**	**2.5354**	**2.4628**
	0.4	**4.1609**	**3.8191**	**2.7498**	**2.6197**	**2.5471**	**2.4745**
	0.5	**4.1286**	**3.831**	**2.7609**	**2.6307**	**2.5581**	**2.4855**

4.3.3: Free vibration of FG-SWCNT microbeam

The material properties from polymethyl methacrylate referred to PMMA, and reinforced by SWCNTs, as the following :

$$E_m = 2.5 \text{ GPa}, \quad \rho_m = 1190 \text{kg/m}^3$$

$$E_{11}^{cnt} = 5646.6 \text{ GPa}, E_{22}^{cnt} = 7080 \text{ GPa}, \quad \rho^{cnt} = 2100 \text{kg/m}^3$$

$$L = 15h, h = 17.6\times10^{-6} \text{ m}, \quad b = 2h, \quad [15]$$

The formula dimensionless frequency of FG-CNT is used in the following Eq. $\bar{\omega} = \omega L * \sqrt{\rho_m (1-\nu_m)/E_m}$ [42]

4.3.3.1: Effect of MCST and CBT

Table (4.17) contains the dimensionless fundamental frequency of the FG microbeam based on the beam theories (FSDT) for various values of the volume fraction CNT index ($\mathrm{Vcnt} = 0.12,0.17,0.28$) and all boundary conditions the aspect ratio (Llh), two different values of dimensionless material length scale parameter (h/lm = 0 and 1). Notably, the dimensionless fundamental frequency increases as the dimensionless material length scale parameter (h/lm) decreases, and the frequencies predicted by the non-classical beam models with modified couple stress (MCST) are larger than those predicted by the classical beam (CBT) models.

The effect boundary conditions on FG-SWCNT microbeam represent as the higher frequency gets when FG-SWCNT microbeams restrict motion. By (clamped-clamped) gives a maximum in a dimensionless frequency, followed by (Clamped-simply), (Simply-Simply), and finally (Clamped-Free) has a minimum frequency.

Table 4. 5: First of three dimensionless frequencies of FG-SWCNT beam with various types of FG-SWCNT distribution at the different boundary conditions,

Boundary condition (Clamped-Clamped)							
V_{CNT}	Model	$h/lm=1$			$h/lm=0$		
		ω_1	ω_2	ω_3	ω_1	ω_2	ω_3
0.12	FG-X	1.6917	3.5443	5.8064	1.6596	3.3806	5.3472
	UD	1.614	3.4412	5.7	1.5707	3.2559	5.1987
	FG-V	1.5298	3.3388	5.6047	1.4686	3.1206	5.0404
	FG-O	1.4592	3.2488	5.514	1.3806	2.9991	4.8931
0.17	FG-X	2.1267	4.4898	7.3925	2.0795	4.2676	6.7793
	UD	2.0149	4.3361	7.221	1.9511	4.0839	6.5508
	FG-V	1.9037	4.2067	7.1104	1.8116	3.9022	6.3421
	FG-O	1.8112	4.0863	6.9886	1.6938	3.7352	6.1385
0.28	FG-X	2.2882	4.7732	7.7949	2.2489	4.5616	7.1958
	UD	2.1541	4.5519	7.499	2.1053	4.3248	6.8736
	FG-V	2.0821	4.5108	7.5407	2.0082	4.2333	6.813
	FG-O	1.9928	4.3982	7.4277	1.8986	4.084	6.6327

Boundary condition (Clamped-Simply)							
V_{CNT}	Model	$h/lm=1$			$h/lm=0$		
		ω_1	ω_2	ω_3	ω_1	ω_2	ω_3
0.12	FG-X	1.4541	3.4759	5.7834	1.411	3.299	5.3153
	UD	1.3559	3.3424	5.6646	1.3003	3.1377	5.1493
	FG-V	1.2546	3.2041	5.5503	1.1805	2.9578	4.9641
	FG-O	1.1773	3.0885	5.4421	1.0867	2.8041	4.792
0.17	FG-X	1.8085	4.3843	7.3562	1.7463	4.1419	6.7289
	UD	1.6755	4.1912	7.1666	1.5955	3.9099	6.4748
	FG-V	1.5447	4.0127	7.0267	1.4366	3.6669	6.2246
	FG-O	1.4474	3.8613	6.8803	1.3161	3.4603	5.986
0.28	FG-X	1.9804	4.6929	7.7682	1.9273	4.4666	7.1587
	UD	1.8295	4.4426	7.4614	1.7656	4.1946	6.8212
	FG-V	1.7195	4.3449	7.4764	1.6284	4.0335	6.7227
	FG-O	1.6192	4.1986	7.3423	1.5082	3.8419	6.5127

Boundary condition (simply-Simply)							
V_{CNT}	Model	$h/lm=1$			$h/lm=0$		
		ω_1	ω_2	ω_3	ω_1	ω_2	ω_3
0.12	FG-X	1.216	3.3951	5.7542	1.1631	3.202	5.2747
	UD	1.0898	3.2283	5.6192	1.0247	3.0005	5.085
	FG-V	0.97012	3.0473	5.4762	0.88933	2.7687	4.8587
	FG-O	0.88962	2.9064	5.352	0.79602	2.5838	4.6596
0.17	FG-X	1.484	4.2612	7.3098	1.409	3.9944	6.6639
	UN	1.3246	4.0248	7.0971	1.2335	3.7091	6.3755
	FG-V	1.1759	3.7876	6.9126	1.062	3.3953	6.0615
	FG-O	1.0795	3.6066	6.746	0.94834	3.1526	5.7869
0.28	FG-X	1.6769	4.597	7.7344	1.6107	4.3524	7.112
	UD	1.4982	4.3154	7.4131	1.4212	4.0421	6.7535
	FG-V	1.3439	4.1515	7.3887	1.2423	3.8004	6.5987
	FG-O	1.2357	3.9714	7.2346	1.1182	3.567	6.3555

Boundary condition (Clamped-Free)							
V_{CNT}	Model	$h/lm=1$			$h/lm=0$		
		ω_1	ω_2	ω_3	ω_1	ω_2	ω_3
0.12	FG-X	0.47439	1.9913	4.2913	0.4616	1.922	4.0295
	UD	0.41377	1.86	4.1162	0.39657	1.776	3.822
	FG-V	0.35975	1.7272	3.9373	0.33709	1.6201	3.5945
	FG-O	0.32471	1.6279	3.7956	0.29771	1.4993	3.4076
0.17	FG-X	0.57129	2.4776	5.4057	0.55231	2.3809	5.0516
	UN	0.49751	2.3019	5.157	0.47277	2.1836	4.7581
	FG-V	0.43179	2.1317	4.929	0.39924	1.9774	4.4542
	FG-O	0.39065	2.0065	4.7461	0.35229	1.8213	4.2056
0.28	FG-X	0.66022	2.7123	5.7987	0.64479	2.6249	5.4598
	UD	0.57591	2.507	5.4773	0.55634	2.4077	5.1156
	FG-V	0.50168	2.3643	5.3418	0.47363	2.2312	4.9045
	FG-O	0.4539	2.2353	5.1607	0.42038	2.0766	4.6698

4.3.3.2 Effect of the different types of FG-CNTs distribution

From Table (4.17) the non-dimensional fundamental frequency varies according to the functional gradation of (SWCNT) along the polymer beam. The highest frequency was observed with CNT distribution of type (FG-X) and follows the uniform CNT distribution type (-UD), and FG-A) and finally (FG-O). The FG-X model has more (CNT) distributions in the top and bottom of micro composite beams and the (CNT_) distribution is zero in the neutral axis, and the FG-O model has the opposite distribution, where more (CNT) distributions in the center micro composite beams. The FG-X model has the highest frequency vibration of FG micro composite beams and is followed by the (-UN) model, (FG-V) model and, the FG-O model which has the lowest frequency vibration. It is noticed that the x distribution has the highest frequency because the carbon is concentrated in the surfaces and gradually decreases at the center (similar to the I structure), which imparts rigidity to the beam structure.

4.3.3.3: Effect of volume fraction of CNTs

Table (4-17) is shown the effect of increasing the amount of CNTs which has a high young modulus lead to improving the hardness of all types of CNT distributions in FG-micro beam. It is clear from Figure (4.19) that a higher volume fraction of CNTs leads to an increase in stiffness which may result in higher natural frequencies of the FG-CNTRC beam. The influence of increasing aspect ratio (L/h) on the dimensionless fundamental frequency of the FG- CNTRC microbeams with all types of FG-SWCNT distribution (FG-X,-UN, FG-A, FG-O). also can be shown The frequency of the different distributions CNT decreases with increasing (L/h) ratio.

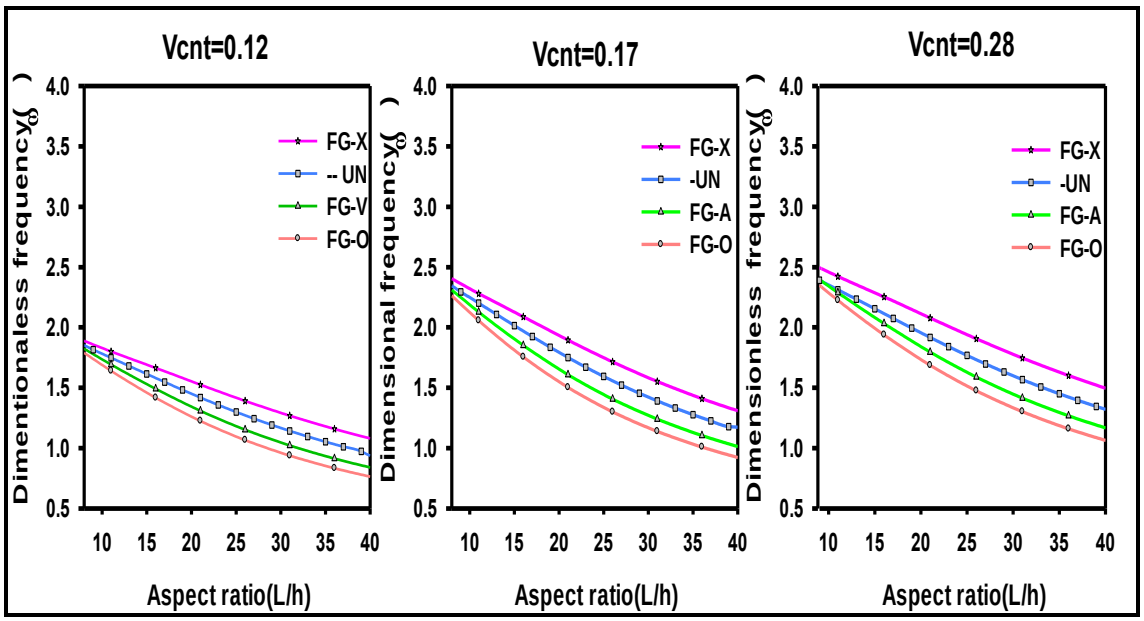

Figure 4. 19: Effect of aspect ratio. the fundamental frequencies according to for different types of FG-CNTs distribution, (h/lm=1)

4.3.3.4: Effect of boundary condition

Figure (4.20) shows the effect of frequencies for different boundary conditions when increasing the aspect ratio. It found that the frequencies of the beams decreased with all types of distributions with the increase of the length material parameter ratio. The fixation by the boundary condition (Clamped-Clamped) gives the highest frequency since the beam is fixed from both ends. followed by (clamped-simply)- (simply, simply) and finally (Clamped-free). It is also clear from the results that a higher volume fraction of CNTs leads to an increase in stiffness which may result in higher natural frequencies of the FG-CNTRC beam.

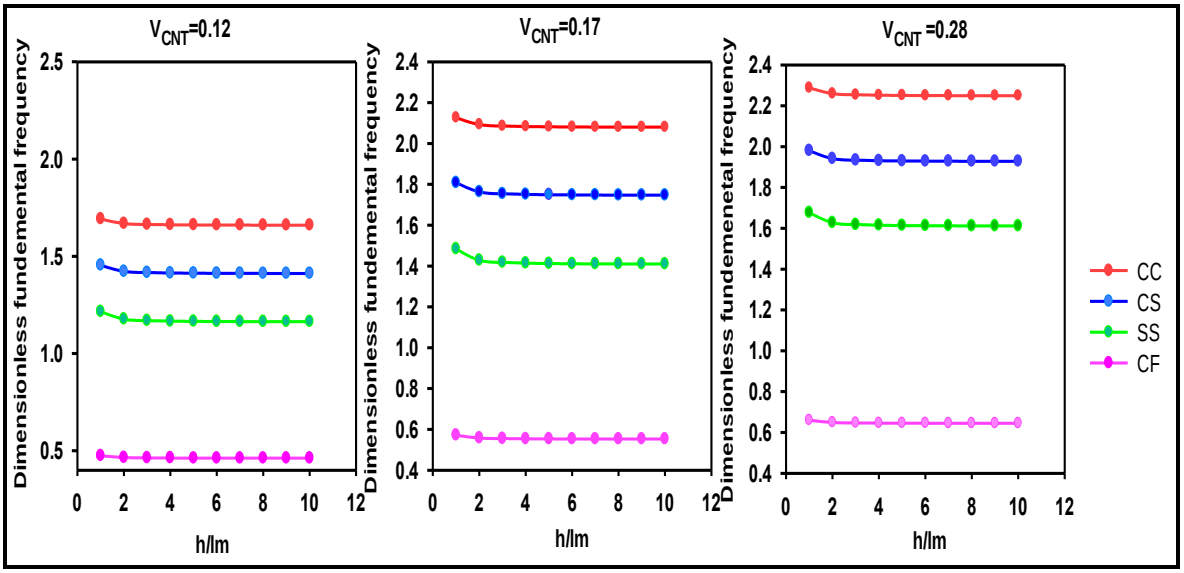

Figure 4.21:fundamental frequencies with length material parameter ratio according to boundary conditions with increasing of CNT volume fraction FG-X..

4.3.3.5: Effect of aspect ratio

As the aspect ratio increases, the decreasing frequency of Euler's beam theory is smaller than Timoshenko's beam theory. A decreased frequency of TBT is due to the reduction of shear deformation as well as its rotational inertia of microbeams, while a decreasing frequency of EBBT is because of rotational inertia only. The largest frequency is concluded from Figure (4.21) by using TBT in the boundary case is (C-C) and the type of distribution is (FG-X).

This fact is illustrated by Table (4.18), the dimensionless fundamental frequency behavior of FG-SWCNT microbeam based on EBBT and FSDT based on MCST is observed for all types of FG-CNT distribution $(\mathrm{FG}-\mathrm{X}, -\mathrm{UN}, \mathrm{FG}-\mathrm{A}, \mathrm{FG}-\mathrm{O})$ with boundary conditions at $(\mathrm{Vcnt} = 0.28)$, $(h/l = 1)$

Also, Figure (4.23) depicts the effect of the aspect ratio (L/h) on frequency for all FG beams at different boundary conditions B.Cs, for all types of FG-microbeam distribution

.

Table 4. 18:shows The effect of (EBBT) and (FSDT) on the first three nondimensional frequencies for different boundary conditions and different CNT distributions with increasing aspect ratio $h/l_m = 1, V_{CNT} = 0.28$

	TBT					EBBT				
L/h	20	40	60	80	100	20	40	60	80	100
Model					C-C					
X	3.6671	1.8355	1.2239	0.9180	0.7344	2.1130	1.4970	1.1065	0.8652	0.7065
UN	3.1008	1.5519	1.0348	0.7761	0.6209	1.9554	1.3212	0.9571	0.7417	0.6028
V	2.6528	1.3279	1.3279	0.8854	0.6641	1.8402	1.1678	0.8270	0.6347	0.5135
O	2.3375	1.1697	0.7800	0.5850	0.4680	1.7330	1.0642	0.7459	0.5701	0.4602
					C-S					
X	2.5274	1.2649	0.8434	0.6326	0.5061	1.7528	1.1214	0.7966	0.6121	0.4954
UN	2.1370	1.0695	0.7131	0.5349	0.4279	1.5883	0.9745	0.6828	0.5217	0.4211
V	1.8694	0.9357	0.6239	0.4680	0.3744	1.4519	0.8463	0.5842	0.4438	0.3572
O	1.6109	0.8061	0.5375	0.4032	0.3225	1.3461	0.7652	0.5248	0.3977	0.3197
					S-S					
X	1.6181	0.8097	0.5399	0.4050	0.3240	1.3825	0.7745	0.5291	0.4003	0.3216
UN	1.3682	0.6846	0.4565	0.3424	0.2739	1.2130	0.6623	0.4497	0.3395	0.2724
V	1.3048	0.6529	0.4353	0.3265	0.2612	1.0648	0.5654	0.3815	0.2874	0.2304
O	1.0314	0.5161	0.3441	0.2581	0.2065	0.9685	0.5076	0.3415	0.2570	0.2059
					C-F					
X	0.6376	0.2885	0.1924	0.1443	0.1154	0.5265	0.2816	0.1903	0.1434	0.1150
UN	0.4877	0.2439	0.1626	0.1220	0.0976	0.4539	0.2393	0.1612	0.1214	0.0973
V	0.4165	0.2083	0.1389	0.1042	0.0833	0.3904	0.2030	0.1364	0.1026	0.0822
O	0.3676	0.1839	0.1226	0.0919	0.0736	0.3513	0.1816	0.1219	0.0916	0.0734

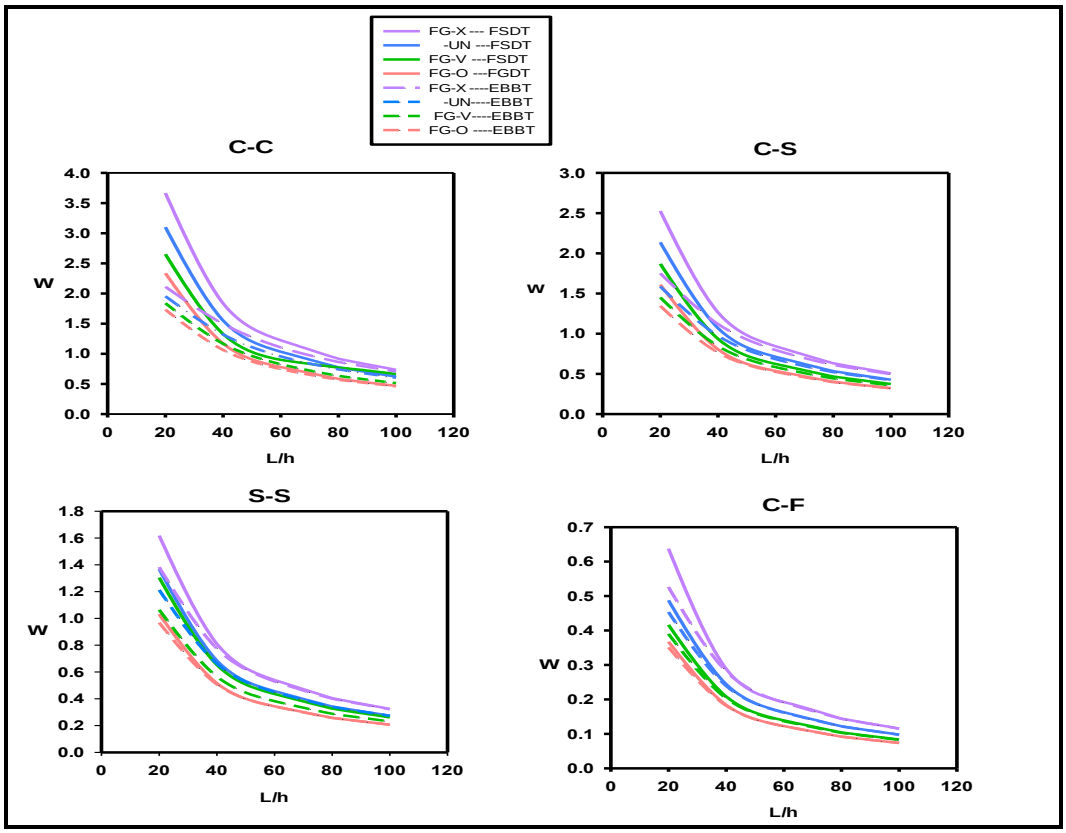

Figure 4. 22: shows The dimensionless frequency of the FG-SWCNT microbeam with various boundary conditions, $h / l_m = 1$.

4.3.3.6: Effect of length material scale parameter l_m

Figure (4.21) and Table (4.18) show the effect of the length material parameter ratio on the dimensionless frequency regarding the boundary condition and volume fraction of SWCNT. The frequencies for microbeams with all boundary conditions decrease as the ratio increases, and the frequencies increase as the volume fraction of SWCNTs increases. The highest frequency can be obtained when the parameter of material length equals thickness $h/lm = 1$, the type of boundary condition is clamped-clamped, and the volume fraction($\mathrm{Vcnt} = 0.28$). is the largest.

CHAPTER FIVE: CONCLUSION AND FUTURE WORKS

5.1: Conclusion

A thesis presented a study on the non-dimensional natural frequency and transverse deflection of three different models represented via the first shear deformation beam theory (FSDT) and Euler beam theory (EBT) along with the modified couple stress theory (MCST). It is possible to draw the following conclusions:

1. In the FG-microbeam vibration analysis, the material length scale, as opposed to the classical beam theory ($lm = 0$), is a good parameter on the prediction size effect via modified couple stress theory.
2. the FG-X CNTRC polymer microbeam is determined to be the strongest beam, with the smallest transverse deflection and the highest natural frequency when compared to –UD, FG-V, and FG-O.
3. The natural frequencies of microbeams of even porosity distribution (FGM-I) is lower than uneven porosity distribution (FGM-II) those of microbeams.
4. Increasing the power-law index decreases the stiffness of the FG microbeam, resulting in an increase in deflections and a drop in natural frequencies.
5. Increasing the volume fraction of porosity leads to a decrease in the flexural strength, natural frequency.
6. Increasing the volume fraction of SWCNT leads to an increase in the modulus of elasticity and natural frequency.
7. When shear deformation effects are included, deflections increase

5.2 Future Projects :

In the future, this thesis could investigate several characteristics of FG micro-beams with modified couple stress. As a consequence, the FG micro-beam subjects require additional investigation. are presented at some point.

- Static, free, buckling analysis and dynamic stability of Bi-directional of functionally graded single-walled carbon nanotube referenced polymer micro-beams utilizing modified couple stress theory.
- Experimental analysis of static, buckling analysis, and free vibration of functionally graded single-walled carbon nanotube referenced polymer micro-beams utilizing modified couple stress theory can be studied in the future to compare the experimental results in conjunction with theoretical results.
- The present thesis can be extended to study static and free vibration of other structural elements such as FG micro-plates and,micro-shells.

[1] B. Saleh, J. Jiang, R. Fathi, T. Al-hababi, Q. Xu, L. Wang, D. Song, A. Ma, 30 Years of functionally graded materials: An overview of manufacturing methods, Applications and Future Challenges, Composites. Part B Eng. 201 (2020) 108376. https://doi.org/10.1016/j.compositesb.2020.108376.

[2] S.K. Bohidar, R. Sharma, P.R. Mishra, Functionally Graded Materials: A Critical Review, International Journal of Research 1 (2014) 289–301. https://journals.pen2print.org/index.php/ijr/article/view/378#.XO0ZqXktAjs.mendeley.

[3] I.M. El-Galy, B.I. Saleh, M.H. Ahmed, Functionally graded materials classifications and development trends from industrial point of view, SN International Journal of Engineering and Applied Sciences (IJEAS), 1 (2019) 1–23. https://doi.org/10.1007/s42452-019-1413-4.

[4] Y. Li, Z. Feng, L. Hao, L. Huang, C. Xin, Y. Wang, E. Bilotti, K. Essa, H. Zhang, Z. Li, F. Yan, T. Peijs, A Review on Functionally Graded Materials and Structures via Additive Manufacturing: From Multi-Scale Design to Versatile Functional Properties, Applied Materials Today. 5 (2020). https://doi.org/10.1002/admt.201900981.

[5] M. Naebe, K. Shirvanimoghaddam, Functionally graded materials: A review of fabrication and properties, Applied Materials Today. 5 (2016) 223–245. https://doi.org/10.1016/j.apmt.2016.10.001.

[6] S. Amir, Z. Soleimani-Javid, E. Arshid, Size-dependent free vibration of sandwich micro beam with porous core subjected to

thermal load based on SSDBT, ZAMM Zeitschrift Fur Angew. Z Angew Math Mech.. 99 (2019) 1–21. https://doi.org/10.1002/zamm.201800334.

[7] F. Ebrahimi, M. Zia, Large amplitude nonlinear vibration analysis of functionally graded Timoshenko beams with porosities, Acta Astronautica. 116 (2015) 117–125. https://doi.org/10.1016/j.actaastro.2015.06.014.

[8] Y.L. Lei, The Dynamic Mechanical Analysis of FG Beams with Different Boundary Conditions by DSC The Dynamic Mechanical Analysis of FG Beams with Different Boundary Conditions by DSC Thesis submitted as a requirement for the degree of The University of New South Wal, (2020).

[9] T.T. Tran, Q.H. Pham, T. Nguyen-Thoi, Static and free vibration analyses of functionally graded porous variable-thickness plates using an edge-based smoothed finite element method, Defence Technology. (2020). https://doi.org/10.1016/j.dt.2020.06.001.

[10] D. Chen, J. Yang, S. Kitipornchai, Free and forced vibrations of shear deformable functionally graded porous beams, International journal of mechanical. Sci. 108–109 (2016) 14–22. https://doi.org/10.1016/j.ijmecsci.2016.01.025.

[11] N. Wattanasakulpong, A. Chaikittiratana, Flexural vibration of imperfect functionally graded beams based on Timoshenko beam theory: Chebyshev collocation method, Meccanica. 50 (2015) 1331–1342. https://doi.org/10.1007/s11012-014-0094-8.

[12] S. Iijima, Growth of carbon nanotubes, Materials Science and Engineering: B, 19 (1993) 172–180.

[13] H.B. Khaniki, M.H. Ghayesh, A review on the mechanics of carbon

nanotube strengthened deformable ,Engineering Structures.. 220 (2020) 110711. https://doi.org/10.1016/j.engstruct.2020.110711.

[14] H.S. Shen, Nonlinear bending of functionally graded carbon nanotube-reinforced composite plates in thermal environments, Composite Structures. 91 (2009) 9–19. https://doi.org/10.1016/j.compstruct.2009.04.026.

[15] M.H. Yas, M. Heshmati, Dynamic analysis of functionally graded nanocomposite beams reinforced by randomly oriented carbon nanotube under the action of moving load, Applied Mathematical Modelling. 36 (2012) 1371–1394. https://doi.org/10.1016/j.apm.2011.08.037.

[16] A. Kausar, I. Rafique, B. Muhammad, Review of Applications of Polymer/Carbon Nanotubes and Epoxy/CNT Composites, Polymer-Plastics Technology and Engineering. 55 (2016) 1167–1191. https://doi.org/10.1080/03602559.2016.1163588.

[17] H. Rokni, A.S. Milani, R.J. Seethaler, Size-dependent vibration behavior of functionally graded CNT-Reinforced polymer microcantilevers: Modeling and optimization, European Journal of Mechanics - A/Solids. 49 (2015) 26–34. https://doi.org/10.1016/j.euromechsol.2014.06.004.

[18] R. Kadoli, K. Akhtar, N. Ganesan, Static analysis of functionally graded beams using higher order shear deformation theory, Applied Mathematical Modelling. 32 (2008) 2509–2525. https://doi.org/10.1016/j.apm.2007.09.015.

[19] M.Simsik, Static Analysis of a Functionally Graded Beam under a Uniformly Distributed Load by Ritz Method,International Journal of Engineering and Applied Sciences. 1 (2009) 1–11.

[20] H.T. Thai, T.P. Vo, Bending and free vibration of functionally graded beams using various higher-order shear deformation beam theories, International Journal of Mechanical Sciences. 62 (2012) 57–66. https://doi.org/10.1016/j.ijmecsci.2012.05.014.

[21] T.P. Vo, H.T. Thai, T.K. Nguyen, F. Inam, J. Lee, Static behaviour of functionally graded sandwich beams using a quasi-3D theory, Composite. Part B Engeneering. 68 (2015) 59–74. https://doi.org/10.1016/j.compositesb.2014.08.030.

[22] L. long Jing, P. jian Ming, W. ping Zhang, L. rong Fu, Y. peng Cao, Static and free vibration analysis of functionally graded beams by combination Timoshenko theory and finite volume method, Composite Structures.138 (2016) 192–213. https://doi.org/10.1016/j.compstruct.2015.11.027.

[23] M. Şimşek, M. Al-shujairi, Static, free and forced vibration of functionally graded (FG) sandwich beams excited by two successive moving harmonic loads, Compositestructures. 108 (2017) 18–34. https://doi.org/10.1016/j.compositesb.2016.09.098.

[24] S.O.W. Khafaji, M.A. Al-Shujairi, M.J. Aubad, Transient analysis of transversely functionally graded Timoshenko beam (TFGTB) in conjunction with finite element method, Archive of Mechanical Engineering. 67 (2020) 1–23. https://doi.org/10.24425/ame.2020.131694.

[25] S.K. Park, X.L. Gao, Bernoulli-Euler beam model based on a modified couple stress theory, Journal of Micromechanics and Microengineering (JMM). 16 (2006) 2355–2359. https://doi.org/10.1088/0960-1317/16/11/015.

[26] H.M. Ma, X.L. Gao, J.N. Reddy, A microstructure-dependent

Timoshenko beam model based on a modified couple stress theory, Journal of Mechanics and Physics of Solids, 56 (2008) 3379–3391. https://doi.org/10.1016/j.jmps.2008.09.007.

[27] M. Şimşek, J.N. Reddy, Bending and vibration of functionally graded microbeams using a new higher order beam theory and the modified couple stress theory, International Journal of Engineering Science 64 (2013) 37–53. https://doi.org/10.1016/j.ijengsci.2012.12.002.

[28] M. Şimşek, T. Kocatürk, Ş.D. Akbaş, Static bending of a functionally graded microscale Timoshenko beam based on the modified couple stress theory, Composite Structures, 95 (2013) 740–747. https://doi.org/10.1016/j.compstruct.2012.08.036.

[29] M. Şimşek, J.N. Reddy, A unified higher order beam theory for buckling of a functionally graded microbeam embedded in elastic medium using modified couple stress theory, Composite Structures,101 (2013) 47–58. https://doi.org/10.1016/j.compstruct.2013.01.017.

[30] M. Şimşek, Nonlinear static and free vibration analysis of microbeams based on the nonlinear elastic foundation using modified couple stress theory and He's variational method, Composite Structures, 112 (2014) 264–272. https://doi.org/10.1016/j.compstruct.2014.02.010.

[31] M. Aydın, H.H. Yurtcu, J.N. Reddy, Size-dependent vibration of a microplate under the action of a moving load based on the modified couple stress theory, Archive of Mechanical Engineering. 226 (2015) 3807–3822. https://doi.org/10.1007/s00707-015-1437-9.

[32] D. Chen, J. Yang, S. Kitipornchai, Elastic buckling and static

bending of shear deformable functionally graded porous beam, Composite Structures. 133 (2015) 54–61. https://doi.org/10.1016/j.compstruct.2015.07.052.

[33] Y.S. Al Rjoub, A.G. Hamad, Free vibration of functionally Euler-Bernoulli and Timoshenko graded porous beams using the transfer matrix method, KSCE Journal of Civil Engineering. 21 (2017) 792–806. https://doi.org/10.1007/s12205-016-0149-6.

[34] N. Shafiei, A. Mousavi, M. Ghadiri, On size-dependent nonlinear vibration of porous and imperfect functionally graded tapered microbeams, International Journal of Engineering Science. 106 (2016) 42–56. https://doi.org/10.1016/j.ijengsci.2016.05.007.

[35] M. Şimşek, M. Aydın, Size-dependent forced vibration of an imperfect functionally graded (FG) microplate with porosities subjected to a moving load using the modified couple stress theory, Composite Structure. 160 (2017) 408–421. https://doi.org/10.1016/j.compstruct.2016.10.034.

[36] N. Fouda, T. El-midany, A.M. Sadoun, Bending, buckling and vibration of a functionally graded porous beam using finite elements, J. Applied and Computational Mechanics. 3 (2017) 274–282. https://doi.org/10.22055/jacm.2017.21924.1121.

[37] A. Bachiri, A. Mahmoudi, M. Bourada, S. Benyoucef, Bending and Free vibration of imperfect FGM beam resting on elastic foundation . Congrès National sur les Energies et Matériaux (CNEM), (2019).

[38] H.S. Shen, C.L. Zhang, Thermal buckling and postbuckling behavior of functionally graded carbon nanotube-reinforced composite plates, Materials & Design, 31 (2010) 3403–3411. https://doi.org/10.1016/j.matdes.2010.01.048.

[39] L.L. Ke, J. Yang, S. Kitipornchai, Nonlinear free vibration of functionally graded carbon nanotube-reinforced composite beams, Composite Structures. 92 (2010) 676–683. https://doi.org/10.1016/j.compstruct.2009.09.024.

[40] M.H. Yas, N. Samadi, Free vibrations and buckling analysis of carbon nanotube-reinforced composite Timoshenko beams on elastic foundation, International Journal of Pressure Vessels and Piping, 98 (2012) 119–128. https://doi.org/10.1016/j.ijpvp.2012.07.012.

[41] M. Heshmati, M.H. Yas, Free vibration analysis of functionally graded CNT-reinforced nanocomposite beam using Eshelby-Mori-Tanaka approach, Journal of Mechanical Science and Technology. 27 (2013) 3403–3408. https://doi.org/10.1007/s12206-013-0862-8.

[42] F. Lin, Y. Xiang, Vibration of carbon nanotube reinforced composite beams based on the first and third order beam theories, Applied Mathematical Modelling. 38 (2014) 3741–3754. https://doi.org/10.1016/j.apm.2014.02.008.

[43] A. Pourasghar, S. Kamarian, Dynamic stability analysis of functionally graded nanocomposite non-uniform column reinforced by carbon nanotube, Journal of Vibration and Control. 21 (2015) 2499–2508. https://doi.org/10.1177/1077546313513625.

[44] S. Khilari, S. Kochar, R. Sanvordenker, B. Thomas, Free vibration analysis of carbon nanotube reinforced composite Timoshenko beam, Progress in Industrial Ecology, an International Journal. 12 (2018) 78–92. https://doi.org/10.1504/PIE.2018.095873.

[45] T. Vo-Duy, V. Ho-Huu, T. Nguyen-Thoi, Free vibration analysis of laminated FG-CNT reinforced composite beams using finite

element method, Frontiers of Structural and Civil Engineering. 13 (2019) 324–336. https://doi.org/10.1007/s11709-018-0466-6.

[46] M. Talebitooti, M. Fadaee, A magnetostrictive active vibration control approach for rotating functionally graded carbon nanotube-reinforced sandwich composite beam, Smart Materials and Structures. 28 (2019). https://doi.org/10.1088/1361-665X/ab1e1f.

[47] M. Fadaee, M. Talebitooti, Active vibration control of carbon nanotube-reinforced composite beam submerged in fluid using magnetostrictive layers, Mechanics Based Design Structure and Machines 0 (2020) 1–18. https://doi.org/10.1080/15397734.2020.1728546.

[48] P. Amatachaya, W. Srimuang, Comparative heat transfer characteristics of a fl at two-phase closed thermosyphon (FTPCT) and a conventional two-phase closed thermosyphon (CTPCT) ☆, Int. Commun. Heat Mass Transf. 37 (2010) 293–298. https://doi.org/10.1016/j.icheatmasstransfer.2009.11.004.

[49] P. Kumar, J. Srinivas, Free vibration, bending and buckling of a FG-CNT reinforced composite beam Comparative analysis with hybrid laminated composite beam, Multidiscipline Modeling in Materials and Structures. 13 (2017) 590–611. https://doi.org/10.1108/MMMS-05-2017-0032.

[50] N. Wattanasakulpong, V. Ungbhakorn, Analytical solutions for bending, buckling and vibration responses of carbon nanotube-reinforced composite beams resting on elastic foundation, Computational Materials Science. 71 (2013) 201–208. https://doi.org/10.1016/j.commatsci.2013.01.028.

[51] M. Şimşek, Fundamental frequency analysis of functionally graded

beams by using different higher-order beam theories, https://www.sciencedirect.com/journal/nuclear-engineering-and-design. 240 (2010) 697–705. https://doi.org/10.1016/j.nucengdes.2009.12.013.

[52] G.M. Kolvik, Higher Order Shear Deformation Plate Theory, Faculty of Mathematics and Natural Sciences University of Oslo. (2012).

[53] F. Yang, A.C.M. Chong, D.C.C. Lam, P. Tong, Couple stress based strain gradient theory for elasticity International Journal of Solids and Structures 39- 2731–2743,(2002)

[54] R. D. Mindlin, Influence of Couple-stresses on Stress Concentrations Main, the William M. Murray Lecture, (1962).

APPENDIX A

VIRTUAL STRAIN AND KINETIC ENERGY

A.1 Euler- Bernoulli beam theory (EBBT)

The strain energy (E_s) for the microbeam can be written to describe a deformed isotropic linear of elastic material.

$$
\begin{aligned}
E_s &= \frac{1}{2}\int_0^L\int_0^w\int_{-h/2}^{h/2}\left(\sigma_{xx}\varepsilon_{xx}+2\sigma_{xz}\varepsilon_{xz}+2m_{xy}\,\chi_{xy}\right)dz\,dy\,dx \\
&= \frac{1}{2}\int_0^L\int_0^w\int_{-h/2}^{h/2}\left(E\,\varepsilon_{xx}{}^2+\underbrace{2\sigma_{xz}\varepsilon_{xz}}_{=0}+2l_m^2A_{xz}\,\chi^2{}_{xy}\right)dz\,dy\,dx \\
&= \frac{1}{2}\int_0^L\int_0^w\int_{-h/2}^{h/2}\left(E\,(\frac{\partial u}{\partial x}-z\,\frac{\partial^2 w}{\partial x^2})^2+2l_m^2A_{xz}\,(-\frac{1}{2}\,\frac{\partial^2 w}{\partial^2 x})^2\right)dz\,dy\,dx \\
&= \frac{1}{2}\int_0^L\left(A_{xx}\left(\frac{\partial u}{\partial x}\right)^2-2B_{xx}\left(\frac{\partial u}{\partial x}\right)\left(\frac{\partial^2 w}{\partial x^2}\right)+D_{xx}\left(\frac{\partial^2 w}{\partial x^2}\right)^2+l_m^2A_{xz}\left(\frac{\partial^2 w}{\partial x^2}\right)^2\right)dx
\end{aligned}
\qquad \ldots\ldots \text{(A1.a)}
$$

The first variation of the strain field of Euler- Bernoulli beam theory in the microbeam can be obtained in terms of the displacement as follows:

$$
\delta\int_0^t E_S\,dt=\int_0^t\int_0^L\left[\begin{array}{l}\underbrace{A_{xx}\left(\frac{\partial u}{\partial x}\frac{\partial\delta u}{\partial x}\right)}_{1}\underbrace{-B_{xx}\left(\frac{\partial u}{\partial x}\right)\left(\frac{\partial^2\delta w}{\partial x^2}\right)}_{2}\underbrace{-B_{xx}\left(\frac{\partial^2 w}{\partial x^2}\right)\left(\frac{\partial\delta u}{\partial x}\right)}_{3}\\ \underbrace{+\left(D_{xx}+l_m^2A_{xz}\right)\left(\frac{\partial^2 w}{\partial x^2}\frac{\partial^2\delta w}{\partial x^2}\right)}_{4}\end{array}\right]dx\,dt \qquad \text{.... (A1.b)}
$$

$$
\delta\int_0^t E_{S)1}dt=\int_0^t(\int_0^L A_{xx}\left(\frac{\partial u}{\partial x}\frac{\partial\delta u}{\partial x}\right)dx)dt=\int_0^t\left(A_{xx}\,\frac{\partial u}{\partial x}\delta u\Big|_0^L-\int_0^L A_{xx}\,\frac{\partial^2 u}{\partial x^2}\delta u\right)dt
$$

$$\delta\int_0^t E_{S)2}\,dt = \int_0^t (-\int_0^L B_{xx}\left(\frac{\partial u}{\partial x}\right)\left(\frac{\partial^2 \delta w}{\partial x^2}\right)dx)dt =$$

$$\int_0^t \left(-B_{xx}\frac{\partial u}{\partial x}\frac{\partial \delta w}{\partial x}\Big|_0^L + \int_0^L B_{xx}\frac{\partial^2 u}{\partial x^2}\frac{\partial \delta w}{\partial x}dx - B_{xx}\frac{\partial^2 u}{\partial x^2}\delta w\,|_0^L + \int_0^L B_{xx}\frac{\partial^3 u}{\partial x^3}\delta w\;dx \right)dt$$

$$\delta\int_0^t E_{S)3}dt = -\int_0^t (B_{xx}\left(\frac{\partial^2 w}{\partial x^2}\right)\left(\frac{\partial \delta u}{\partial x}\right)dx)dt = \int_0^t \left(-B_{xx}\frac{\partial^2 w}{\partial x^2}\delta u|_0^L + \int_0^L B_{xx}\frac{\partial^3 w}{\partial x^3}\delta u\,dx \right)dt$$

$$\delta\int_0^t E_{S)4}dt = \int_0^t\int_0^L \left(D_{xx} + l_m^2 A_{xz}\right)\left(\frac{\partial^2 w}{\partial x^2}\frac{\partial^2 \delta w}{\partial x^2}\right)dx\,dt$$

$$= \int_0^t \left(\begin{array}{l} \left(D_{xx} + l_m^2 A_{xz}\right)\dfrac{\partial^2 w}{\partial x^2}\dfrac{\partial \delta w}{\partial x}\Big|_0^L - \left(D_{xx} + l_m^2 A_{xz}\right)\displaystyle\int_0^L \frac{\partial^3 w}{\partial x^3}\frac{\partial \delta w}{\partial x}dx \\ + \quad \left(D_{xx} + l_m^2 A_{xz}\right)\dfrac{\partial^3 w}{\partial x^3}\delta w\,|_0^L + \displaystyle\int_0^L \left(D_{xx} + l_m^2 A_{xz}\right)\frac{\partial^4 w}{\partial x^4}\delta w\,|_0^L\,dx \end{array} \right)dt$$

The kinetic energy (E_K) of Euler- Bernoulli beam theory in the microbeam can be written :

$$E_k = \frac{1}{2}\int_0^L\int_0^A \rho(z)\left(\left(\frac{\partial u_x}{\partial t}\right)^2 + \left(\frac{\partial u_z}{\partial t}\right)^2\right)dA\,dx$$

$$E_k = \frac{1}{2}\int_0^L\int_0^A \rho(z)\left(\left(\frac{\partial u}{\partial t} - z\,\frac{\partial^2 w}{\partial t\,\partial x}\right)^2 + \left(\frac{\partial u_z}{\partial t}\right)^2\right)dA\,dx \qquad \ldots(A1.c)$$

$$E_k = \frac{1}{2}\int_0^L\int_0^A \rho(z)\left(\left(\left(\frac{\partial u_z}{\partial t}\right)^2 + \left(2z\,\frac{\partial u}{\partial t}\frac{\partial^2 w}{\partial t\,\partial x}\right) + \left(z\,\frac{\partial^2 w}{\partial t\,\partial x}\right)^2\right) + \left(\frac{\partial w}{\partial t}\right)^2\right)dA\,dx$$

The first variation of the kinetic energy (δE_K) of Euler- Bernoulli beam theory in the FG microbeam can be obtained in terms of the displacement can be written as:

$$\delta\int_0^L\int_0^t E_k\,dtdx = \int_0^L\int_0^t \left(\begin{array}{l} \underbrace{I_A\left(\frac{\partial u}{\partial t}\frac{\partial \delta u}{\partial t}\right)}_{1} + \underbrace{I_A\left(\frac{\partial w}{\partial t}\frac{\partial \delta w}{\partial t}\right)}_{2} - \underbrace{I_B\left(\frac{\partial u}{\partial t}\frac{\partial^2 \delta w}{\partial x\,\partial t}\right)}_{3} - \\ \underbrace{I_B\left(\frac{\partial^2 \delta w}{\partial x\,\partial t}\frac{\partial \delta u}{\partial t}\right)}_{4} + \underbrace{I_D\left(\frac{\partial^2 w}{\partial x\,\partial t}\frac{\partial^2 \delta w}{\partial x\,\partial t}\right)}_{5} \end{array} \right) dtdx \qquad ..(A1.d)$$

The equation (A1.d) is simplified by integrating by part :

$$\delta E_k)_1 = \int_0^t\int_0^L I_A\left(\frac{\partial u}{\partial t}\frac{\partial \delta u}{\partial t}\right)dxdt = \int_0^L\left(I_A\frac{\partial u}{\partial t}\delta u\Big|_0^t - \int_0^t I_A\frac{\partial^2 u}{\partial t^2}\delta u\;dt\right)dx$$

$$\delta E_k)_2 = \int_0^t\int_0^L I_A\left(\frac{\partial w}{\partial t}\frac{\partial \delta w}{\partial t}\right)dxdt = \int_0^L\left(I_A\frac{\partial w}{\partial t}\delta w\Big|_0^t - \int_0^t I_A\frac{\partial^2 w}{\partial t^2}\delta w\;dt\right)dx$$

$$\delta E_k)_3 = \int_0^t\int_0^L -I_B\left(\frac{\partial u}{\partial t}\frac{\partial^2 \delta w}{\partial x\,\partial t}\right)dxdt = \int_0^L\left(+I_B\frac{\partial u}{\partial t}\frac{\partial \delta w}{\partial x}\Big|_0^t - \int_0^t I_B\frac{\partial^2 u}{\partial t^2}\frac{\partial \delta w}{\partial x}dt\right)$$

$$\left(-I_B\frac{\partial^2 u}{\partial t^2}\delta w\Big|_0^t + \int_0^t I_B\frac{\partial^3 u}{\partial t^3}\delta w\;dt\right)dx$$

$$\delta E_k)_4 = \int_0^t\int_0^L -I_B\left(\frac{\partial^2 w}{\partial x\,\partial t}\frac{\partial \delta u}{\partial t}\right)dxdt = \int_0^L\left(-I_B\frac{\partial^2 w}{\partial x\,\partial t}\delta u\Big|_0^t + \int_0^t I_B\frac{\partial^3 w}{\partial x\,\partial^2 t}\delta u\;dt\right)dx$$

$$\delta E_k)_5 = \int_0^t\int_0^L I_D\left(\frac{\partial^2 w}{\partial x\,\partial t}\frac{\partial \delta^2 w}{\partial x\,\partial t}\right)dxdt = \int_0^L\left(I_D\frac{\partial^2 w}{\partial x\,\partial t}\delta u\Big|_0^t - \int_0^t I_D\frac{\partial^3 w}{\partial x\,\partial^2 t}\delta u\;dt\right)dx$$

The first variation of the internal strain energy of Euler- Bernoulli beam theory in terms of the internal stresses are defined as:

$$\delta\int_0^t E_S\;dt = \int_0^t\int_0^L \left[\underbrace{N\left(\frac{\partial u}{\partial x}\frac{\partial \delta u}{\partial x}\right)}_{\delta E_S)1} - \underbrace{\left(M + Y_{xy}\right)\left(\frac{\partial^2 w}{\partial x^2}\frac{\partial^2 \delta w}{\partial x^2}\right)}_{\delta E_S)2} \right] dx\;dt \qquad \ldots.(A1.e)$$

The equation for the internal stresses (A1.e) is simplified by integrating by part as:

$$\delta E_{S)1} = \int_0^L N\left(\frac{\partial u}{\partial x}\frac{\partial \delta u}{\partial x}\right)dx = N\,\frac{\partial u}{\partial x}\delta u\Big|_0^L - \int_0^L N\,\frac{\partial^2 u}{\partial x^2}\delta u dx$$

$$\delta E_{S)2} = \int_0^L \left(M + Y_{xy}\right)\left(\frac{\partial^2 w}{\partial x^2}\frac{\partial^2 \delta w}{\partial x^2}\right)dx = \left(M + Y_{xy}\right)\frac{\partial^2 w}{\partial x^2}\frac{\partial \delta w}{\partial x}\Big|_0^L - \left(M + Y_{xy}\right)\int_0^L \frac{\partial^3 w}{\partial x^3}\frac{\partial \delta w}{\partial x}dx$$

$$+\left(M + Y_{xy}\right)\frac{\partial^3 w}{\partial x^3}\delta w\Big|_0^L + \int_0^L \left(M + Y_{xy}\right)\frac{\partial^4 w}{\partial x^4}\delta w\; dx$$

A.2-First order shear deformation beam theory (FSDBT)

The strain energy (Es) of the FG micro beam according to First shear deformation theory (FSDT) can be written as:

$$E_s = \frac{1}{2}\int_0^L\int_0^w\int_{-h/2}^{h/2}\left(E\,\varepsilon_{xx}^{\;2} + 2\sigma_{xz}\varepsilon_{xz} + 2l_m^2 A_{xz}\;\chi^2{}_{xy}\right)dz\,dy\,dx$$

$$= \frac{1}{2}\int_0^L\int_0^w\int_{-h/2}^{h/2}\left(E\,\varepsilon_{xx}^{\;2} + 4ks\;A_{xz}\;\varepsilon_{xz}^{\;2} + 2l_m^2 A_{xz}\;\chi^2{}_{xy}\right)dz\,dy\,dx$$

$$= \frac{1}{2}\int_0^L\int_0^w\int_{-h/2}^{h/2}\left(\begin{array}{l} E\left(\frac{\partial u}{\partial x}\right)^2 - 2E\,z\left(\frac{\partial u}{\partial x}\right)\left(\frac{\partial \phi}{\partial x}\right) + E\,z^2\left(\frac{\partial \phi}{\partial x}\right)^2 + k_s A_{xz}\phi^2 - 2k_s A_{xz}\phi\left(\frac{\partial w}{\partial x}\right) \\ +k_s A_{xz}\left(\frac{\partial w}{\partial x}\right)^2 + \frac{1}{4}l_m^2 A_{xz}\left(\frac{\partial \phi}{\partial x}\right)^2 + \frac{1}{2}l_m^2 A_{xz}\left(\frac{\partial^2 w}{\partial x^2}\right)\left(\frac{\partial \phi}{\partial x}\right) + \frac{1}{4}l_m^2 A_{xz}\left(\frac{\partial^2 w}{\partial x^2}\right)^2 \end{array}\right)dz\,dy\,dx$$

$$= \frac{1}{2}\int_0^L\left[\begin{array}{l} A_{xx}\left(\frac{\partial u}{\partial x}\right)^2 - 2B_{xx}\left(\frac{\partial u}{\partial x}\right)\left(\frac{\partial \phi}{\partial x}\right) + D_{xx}\left(\frac{\partial \phi}{\partial x}\right)^2 + k_s A_{xz}\phi^2 - 2k_s A_{xz}\phi\left(\frac{\partial w}{\partial x}\right) \\ +k_s A_{xz}\left(\frac{\partial w}{\partial x}\right)^2 + \frac{1}{4}l_m^2 A_{xz}\left(\frac{\partial \phi}{\partial x}\right)^2 + \frac{1}{2}l_m^2 A_{xz}\left(\frac{\partial^2 w}{\partial x^2}\right)\left(\frac{\partial \phi}{\partial x}\right) + \frac{1}{4}l_m^2 A_{xz}\left(\frac{\partial^2 w}{\partial x^2}\right)^2 \end{array}\right]dx$$

…(A2.a)

$$\delta E_S = \int_0^L \left[\begin{array}{l} \underbrace{A_{xx}\left(\frac{\partial u}{\partial x}\frac{\partial \delta u}{\partial x}\right)}_{\delta Es\,1} - \underbrace{B_{xx}\left(\frac{\partial u}{\partial x}\frac{\partial \delta \phi}{\partial x}\right)}_{\delta Es\,2} - \underbrace{B_{xx}\left(\frac{\partial \phi}{\partial x}\frac{\partial \delta u}{\partial x}\right)}_{\delta Es\,3} + \underbrace{(D_{xx}+\frac{1}{4}l_m^2 A_{xz})\left(\frac{\partial \phi}{\partial x}\frac{\partial \delta \phi}{\partial x}\right)}_{\delta Es\,4} \\ + \underbrace{k_s A_{xz}\phi\delta\phi}_{\delta Es\,5} - \underbrace{k_s A_{xz}\left(\phi\frac{\partial \delta w}{\partial x}\right)}_{\delta Es\,6} + \underbrace{k_s A_{xz}\left(\frac{\partial w}{\partial x}\delta\phi\right)}_{\delta Es\,7} + \underbrace{k_s A_{xz}\left(\frac{\partial w}{\partial x}\frac{\partial \delta w}{\partial x}\right)}_{\delta Es\,8} \\ + \underbrace{\frac{1}{2}l_m^2 A_{xz}\left(\frac{\partial \phi}{\partial x}\frac{\partial \delta^2 w}{\partial x^2}\right)}_{\delta Es\,9} + \underbrace{\frac{1}{2}l_m^2 A_{xz}\left(\frac{\partial^2 w}{\partial x^2}\frac{\partial \delta \phi}{\partial x}\right)}_{\delta Es\,10} + \underbrace{\frac{1}{4}l_m^2 A_{xz}\left(\frac{\partial^2 w}{\partial x^2}\frac{\partial \delta^2 w}{\partial x^2}\right)}_{\delta Es\,11} \end{array} \right] dx$$

$$\delta\int_0^t E_{S)1}dt = \int_0^t \left(\int_0^L A_{xx}\left(\frac{\partial u}{\partial x}\frac{\partial \delta u}{\partial x}\right)dx\right)dt = \int_0^t \left(A_{xx}\frac{\partial u}{\partial x}\delta u\Big|_0^L - \int_0^L A_{xx}\frac{\partial^2 u}{\partial x^2}\delta u\right)dt$$

$$\delta\int_0^t E_{S)2}dt = \int_0^t \left(\int_0^L -B_{xx}\left(\frac{\partial u}{\partial x}\frac{\partial \delta \phi}{\partial x}\right)dx\right)dt = \int_0^t \left(-B_{xx}\frac{\partial u}{\partial x}\delta\phi\Big|_0^L + \int_0^L B_{xx}\frac{\partial^2 u}{\partial x^2}\delta\phi\right)dt$$

$$\delta\int_0^t E_{S)3}dt = \int_0^t \left(\int_0^L -B_{xx}\left(\frac{\partial u}{\partial x}\frac{\partial \delta \phi}{\partial x}\right)dx\right)dt = \int_0^t \left(-B_{xx}\frac{\partial \phi}{\partial x}\delta u\Big|_0^L + \int_0^L B_{xx}\frac{\partial^2 \phi}{\partial x^2}\delta u\right)dt$$

$$\delta\int_0^t E_{S)4}dt = \int_0^t \left(\int_0^L (D_{xx}+\frac{1}{4}l_m^2 A_{xz})\left(\frac{\partial \phi}{\partial x}\frac{\partial \delta \phi}{\partial x}\right)dx\right)dt = \int_0^t (D_{xx}+\frac{1}{4}l_m^2 A_{xz})\left(\frac{\partial \phi}{\partial x}\delta\phi\Big|_0^L - \int_0^L \frac{\partial^2 \phi}{\partial x^2}\delta\phi dx\right)dt$$

$$\delta\int_0^t E_{S)5}dt = \int_0^t \left(\int_0^L k_s A_{xz}\phi\delta\phi\,dx\right)dt$$

$$\delta\int_0^t E_{S)6}dt = \int_0^t \left(\int_0^L -k_s A_{xz}\left(\phi\frac{\partial \delta w}{\partial x}\right)dx\right)dt = \int_0^t \left(-k_s A_{xz}\,\phi\,\delta w\Big|_0^L + \int_0^L k_s A_{xz}\frac{\partial \phi}{\partial x}\delta w\right)dt$$

$$\delta\int_0^t E_{S)7}dt = \int_0^t \left(\int_0^L -k_s A_{xz}\left(\frac{\partial w}{\partial x}\delta\phi\right)dx\right)dt$$

$$\delta\int_0^t E_{S)8}dt = \int_0^t \left(\int_0^L -ksA_{xz}\left(\frac{\partial w}{\partial x}\frac{\partial \delta^2 w}{\partial x^2}\right)dx\right)dt = +ksA_{xz}\int_0^t \left(\frac{\partial w}{\partial x}\delta w\Big|_0^L - \int_0^L \frac{\partial \delta^2 w}{\partial x^2}\delta w\;dx\right)dt$$

$$\delta\int_0^t E_{S)9}dt = \int_0^t \left(\int_0^L \frac{1}{4}l_m^2 A_{xz}\left(\frac{\partial \phi}{\partial x}\frac{\partial \delta^2 w}{\partial x^2}\right)dx\right)dt = \frac{1}{4}l_m^2 A_{xz}\int_0^t \left(\frac{\partial \phi}{\partial x}\frac{\partial \delta w}{\partial x}\Big|_0^L - \frac{\partial^2 \phi}{\partial x^2}\delta w\Big|_0^L + \int_0^L \frac{\partial^3 \phi}{\partial x^3}\delta w\;dx\right)dt$$

$$\delta\int_0^t E_{S)10}dt = \int_0^t \left(\frac{1}{4}l_m^2 A_{xz}\left(\frac{\partial^2 w}{\partial x^2}\frac{\partial \delta \phi}{\partial x}\right)dx\right)dt = \int_0^t \left(\frac{1}{4}l_m^2 A_{xz}\frac{\partial^2 w}{\partial x^2}\delta\phi\Big|_0^L - \int_0^L \frac{1}{4}l_m^2 A_{xz}\frac{\partial^3 w}{\partial x^3}\delta\phi\,dx\right)dt$$

$$\delta\int_0^t E_{S)11}dt = \int_0^t \int_0^L \frac{1}{4}l_m^2 A_{xz}\left(\frac{\partial^2 w}{\partial x^2}\frac{\partial^2 \delta w}{\partial x^2}\right)dx\,dt = \int_0^t \left(\begin{array}{l} \frac{1}{4}l_m^2 A_{xz}\frac{\partial^2 w}{\partial x^2}\frac{\partial \delta w}{\partial x}\Big|_0^L - \frac{1}{4}l_m^2 A_{xz}\frac{\partial^3 w}{\partial x^3}\delta w\Big|_0^L \\ + \int_0^L \frac{1}{4}l_m^2 A_{xz}\frac{\partial^4 w}{\partial x^4}\delta w\;dx \end{array} \right)dt$$

…(A2.b)

The kinetic energy (E_K) of the FG micro beam according to First shear deformation theory (FSDT) can be written as:

$$
\begin{aligned}
E_k &= \frac{1}{2}\int_0^t\int_0^L\int_0^w\int_{-h/2}^{h/2}\rho(z)\left(\left(\frac{\partial u}{\partial t}\right)^2+\left(\frac{\partial w}{\partial t}\right)^2\right)dz\,dy\,dx\,dt \\
&= \frac{1}{2}\int_0^t\int_0^L\int_0^w\int_{-h/2}^{h/2}\rho(z)\left(\left(\frac{\partial (u-z\,\phi)}{\partial t}\right)^2+\left(\frac{\partial w}{\partial t}\right)^2\right)dz\,dy\,dx\,dt \\
&= \frac{1}{2}\int_0^t\int_0^L\int_0^w\int_{-h/2}^{h/2}\begin{pmatrix}\rho(z)\left(\frac{\partial u}{\partial t}\right)^2+\rho(z)\left(\frac{\partial w}{\partial t}\right)^2 \\ -2\rho(z)z\left(\frac{\partial u}{\partial t}\right)\left(\frac{\partial \phi}{\partial t}\right)+\rho(z)z^2\left(\frac{\partial \phi}{\partial t}\right)^2\end{pmatrix}dz\,dy\,dx\,dt \\
&= \frac{1}{2}\int_0^t\int_0^L\int_0^L\left[I_A\left(\frac{\partial u}{\partial t}\right)^2+I_A\left(\frac{\partial w}{\partial t}\right)^2-2I_B\left(\frac{\partial u}{\partial t}\right)\left(\frac{\partial \phi}{\partial t}\right)+I_D\left(\frac{\partial \phi}{\partial t}\right)^2\right]dx\,dt
\end{aligned}
\tag{A2.c}
$$

Where $\rho(z)$ the material density of FG-micro beam

$$
\delta\int_0^t E_k\,dt = \int_0^t\int_0^L\left[\begin{matrix}\underbrace{I_A\left(\frac{\partial u}{\partial t}\frac{\partial \delta u}{\partial t}\right)}_{\delta E_{k1}}+\underbrace{I_A\left(\frac{\partial w}{\partial t}\frac{\partial \delta w}{\partial t}\right)}_{\delta E_{k2}}-\underbrace{I_B\left(\frac{\partial u}{\partial t}\frac{\partial \delta \phi}{\partial t}\right)}_{\delta E_{k3}} \\ \underbrace{-I_B\left(\frac{\partial \phi}{\partial t}\frac{\partial \delta u}{\partial t}\right)}_{\delta E_{k4}}+\underbrace{I_D\left(\frac{\partial \phi}{\partial t}\frac{\partial \delta \phi}{\partial t}\right)}_{\delta E_{k5}}\end{matrix}\right]dx\,dt
$$

The equation for the first variation of kinetic energy is simplified by integrating by part

$$\delta E_k)1 = \int_0^t \int_0^L I_A \left(\frac{\partial u}{\partial t} \frac{\partial \delta u}{\partial t} \right) dx dt = \int_0^L \left(I_A \frac{\partial u}{\partial t} \delta u \Big|_0^t - \int_0^t I_A \frac{\partial^2 u}{\partial t^2} \delta u \; dt \right) dx$$

$$\delta E_k)2 = \int_0^t \int_0^L I_A \left(\frac{\partial w}{\partial t} \frac{\partial \delta w}{\partial t} \right) dx dt = \int_0^L \left(I_A \frac{\partial w}{\partial t} \delta w \Big|_0^t - \int_0^t I_A \frac{\partial^2 w}{\partial t^2} \delta w \; dt \right) dx$$

$$\delta E_k)3 = \int_0^t \int_0^L -I_B \left(\frac{\partial u}{\partial t} \frac{\partial \delta \phi}{\partial t} \right) dx dt = \int_0^L \left(-I_B \frac{\partial u}{\partial t} \delta \phi \Big|_0^t + \int_0^t I_B \frac{\partial^2 u}{\partial t^2} \delta \phi \, dt \right) dx$$

$$\delta E_k)4 = \int_0^t \int_0^L -I_B \left(\frac{\partial \phi}{\partial t} \frac{\partial \delta u}{\partial t} \right) dx dt = \int_0^L \left(-I_B \frac{\partial \phi}{\partial t} \delta u \Big|_0^t + \int_0^t I_B \frac{\partial^2 \phi}{\partial t^2} \delta u \; dt \right) dx$$

$$\delta E_k)5 = \int_0^t \int_0^L I_D \left(\frac{\partial \phi}{\partial t} \frac{\partial \delta \phi}{\partial t} \right) dx dt = \int_0^L \left(I_D \frac{\partial \phi}{\partial t} \delta \phi \Big|_0^t - \int_0^t I_D \frac{\partial^2 \phi}{\partial t^2} \delta \phi \, dt \right) dx$$

…..(A2.d)

الخلاصة

المواد المتدرجة وظيفيًا هي فئة جديدة واعدة من الهياكل المجهرية. تتغير الخصائص الميكانيكية للهياكل المجهرية المتدرجة وظيفيًا اعتمادًا على تغيير في البعد المكاني للهيكل. التطورات الحديثة في تقنيات التصنيع ، مثل تعدين المساحيق ،جعلت من الممكن تكييف الخصائص الميكانيكية للهياكل على نطاق صغير عن طريق تصنيعها من خليط وظيفي متعدد الطبقات من مادتين أو أكثر.

تم تبسيط المعادلات الحاكمة وشروط الحدود من خلال مبدأ هاملتون ، ونظرية عتبة أويلر برنولي ، ونظرية تشوه القص من الدرجة الأولى . يتم الحل عدديًا بطريقة مضاعفات لاغرانج. تم الاعتماد على برنامج ماتلاب في ايجاد النتائج. تمت دراسة الخواص الميكانيكية للهياكل المتدرجة وظيفيًا من خلال طريقة الخليط الحاكم وتقنية موري تاناكا. هناك عدة عوامل تؤثر على النماذج الثلاثة للتدريج الوظيفي لعتبة بحجم الماكرو، وهي: مؤشر القاعدة العامة للمزائج ، وكسر حجم المسامية ، أنواع توزيع المسامية (FGM-I ، و FGM-II) ، وكسر حجم انابيب النانو الكربون ، وأنواع توزيعات التدريج وظيفيًا لأنابيب النانوية الكربونية وهي (FG-V), (FG-X) ,(UD),و(FG-O) ،نسبة نحافة العتبة وشروط الحدية المختلفة. بشكل عام ، عند استخدام مفهوم التدريج الوظيفي في تصميم هيكل المواد المركبة ذات الحجم الصغير ، فقد أظهر تحسنًا في الأداء الميكانيكي . النقاط التالية التي تم التوصل إليها من دراسة النماذج الثلاثة على النحو التالي: عند زيادة مؤشر القاعدة العامة للمزائج سيقلل من صلابة الحزمة الدقيقة المتدرجة وظيفيًا المكونة من السيراميك والمعدن مما يؤدي إلى زيادة الانحراف وتقليل التردد الطبيعي. في حين أن الانحراف والتردد الطبيعي للنموذج الثاني لمواد المسامية المتدرجة وظيفيًا لهما سلوك مختلف يعتمد على مؤشر القاعدة العامة للمزائج.الحد الأقصى للتردد الطبيعي الذي تم الحصول عليه للنموذج الثالث من عتية البوليمربحجم الماكرو ذات الأنابيب النانوية الكربونية المتدرجة وظيفيًا هي ٢٨%. علاوة على ذلك ، فإن العتبة الدقيقة من الأنابيب النانوية الكربونية المتدرجة وظيفيًا نوع (FG-X) لها أقصى تردد طبيعي ، في حين (FG-O) لديها أدنى تردد طبيعي. إن نظرية المطورة للاجهادات المتداخلة (MCST) قادرة على التنبؤ بأصغر انحناء سكوني وأكبر اهتزاز حر للعتبة الدقيقة المتدرج وظيفيًا اعتمادًا على معلمة مقياس طول المادة عند مقارنتها بالتنبؤ بنظرية الشعاع الكلاسيكي (CBT).كانت النتائج المقارنة مع الدراسات السابقة مقبولة. يمكن استخدام نتائج هذا التحقيق لتصميم وتحسين الآلات الدقيقة والأنظمة الدقيقة .

جمهورية العراق
وزارة التعليم العالي والبحث العلمي
جامعة بابل / كلية الهندسة
قسم الهندسة الميكانيكية

التحليل السكوني والاهتزاز الحر لمواد متدرجة وظيفيا باستخدام النظرية المطورة للاجهادات المتداخلة

رسالة

مقدمة إلى جامعة بابل / كلية الهندسة وهي جزء من متطلبات نيل شهادة الماجستير في الهندسة/ الهندسة الميكانيكية/ التطبيقي

أعدت من قبل
دعاء محمد رضا محسن

بأشراف

أ.م.د. محمد علي صيهود

١٤٤٢ هـ ٢٠٢١ م